Optical control of transport properties of 2D Dirac materials

Kevin Tanguy Elian Dini

Faculty of Physical Sciences
University of Iceland
2018

OPTICAL CONTROL OF TRANSPORT PROPERTIES OF 2D DIRAC MATERIALS

Kevin Tanguy Elian Dini

180 ECTS thesis submitted in partial fulfillment of a
PhD Scientiarum degree in Physics

Advisors
Ivan Shelykh, Oleg Kibis

Faculty Representative
Oddur Ingólfsson

PhD committee
Viðar Guðmundsson
Andrei Manolescu
Hafliði Gislason

Opponents
Polina Kuzhir
André Xuereb

Faculty of Physical Sciences
School of Engineering and Natural Sciences
University of Iceland
Reykjavik, 09 2018

Optical control of transport properties of 2D Dirac materials
Band Engineering of 2D Dirac materials
180 ECTS thesis submitted in partial fulfillment of a PhD degree in Physics

Faculty of Physical Sciences
School of Engineering and Natural Sciences
University of Iceland
Dunhagi 3
IS-107, Reykjavik, Reykjavik
Iceland
Telephone : 525 4000

Bibliographic information :
Kevin Tanguy Elian Dini, 2018, Optical control of transport properties of 2D Dirac materials, PhD thesis, Faculty of Physical Sciences, University of Iceland.

ISBN 978-9935-9320-8-2
Printing : Háskólaprent, Fálkagata 2, 107 Reykjavík
Reykjavik, Iceland, 09 2018

To my family

Abstract

Light matter coupling is a field that has rapidly grown in the past decades to become one of the most important interdisciplinary research subject. It combines the phenomena of condensed matter and quantum optics and brings a new panel of unique effects. Therefore, studying the combination of what is best in both those fields may lead to breakthroughs and deeper understanding. In this manuscript, we theoretically investigate the influence of a polarized electromagnetic field on one of the most famous and unique type of two dimensional materials : Dirac materials.

To do so, we first study the influence of this so called 'dressing' field, on the simplest of those materials, one graphene monolayer. Then we slightly complicate the problem and move to gapped Dirac systems such as Transition metal Dichalchogenides and graphene grown on a Boron Nitride substrate or massive electrons in a Dirac like system such as in Bilayer graphene. Finally we look for a way to control all optically the dynamics of electrons in graphene and to use the valley index as a selection parameter. In order to perform this theoretical work, we slightly study two tools for time dependent study of periodic systems : the Floquet-Magnus framework for time periodic system and the Gaussian wave packet simulation for Dirac systems.

Utdrattur

Víxlverkun milli ljóss og efnis er umræðuefni innan eðlisfræðinnar sem hefur stækkað ört undanfarna áratugi og orðið að einu mikilvægasta rannsóknarsviði. Sviðið blandar saman áhrifum úr þéttefnisfræði og skammtaljósfræði og hefur sína einstöku eiginleika. Með því að skoða hvaða eiginleika þessara tveggja sviða er best að setja saman, getur leitt til nýjunga og betri skilnings. Í þessari ritgerð, rannsökum við fræilega hvaða áhrif skautað rafsegulsvið hefur á einu þekktasta klasa tvíviðra kerfi : Dirac efni.

Til að ná markmiðinu, skoðum við fyrst áhrif svokallaðs klæðningarsviðs á einfaldasta efninu, einu lagi af grafíni. Síðan er fariði flóknari kerfi sem eru Dirac efni með orkugeil eins og hliðarmálma-díkalkógeníðar (e. transition metal dichalcogenides) og grafín sem hefur vaxið á undirlagi úr bóron-nítriði eða rafeindir sem hafa massa í tveggja laga grafíni. Loks skoðum við aðferð til að stýra eiginleikum rafeindir með ljósi í grafíni og að sía rafeindir þar eftir dalavísi þeirra. Til þess að framkvæma þessa vinnu, er notast við tvö verkfæri til að meðhöndla kerfi sem eru lotubundin í tíma. Eitt er Floquet-Magnus formalisminn og hitt er hermun rafeinda í Dirac kerfum með Gaussískum bylgjupókkum.

Acknowledgements

I would like, first of all, to thank my scientific supervisor Pr. Ivan Shelykh for his constant support and for advising me through the different projects I worked on during my PhD. I would like to also thank him for introducing me to all those amazing people all around the world that I really liked to work with.

It was a pleasure to work with all those people, I thank Skender, Ksenia, Kristinn, Vanik, Kristin and Helgi for those amazing times in Iceland both in the office and outside. The years I spent there are among the best of my life and I thank all of them for that.

The few months I spent in Singapore were also absolutely amazing thank to Tim, Tania, Anastasia and all the people I got to know there. I really liked working there and I thank Nanyang Technogical University for its hospitality.

I would like to also thank ITMO University in Saint-Pertersburg for its hospitality. The time spent there was really nice and the collaborations went very well thanks to the professionalism of their staff.

On a more professional note I especially thank Ivan Iorsh (ITMO University) for cooperation, great advising and his will to share his large knowledge of the field. A large part of the work could not have been performed without his help. I would also like to thank Pr. Oleg Kibis (Novosibirsk State Technical University) for our collaborations and for taking time to teach me the rigour that is necessary to every scientist.

I of course thank University of Iceland and all its staff for providing me a stable support and everything that was needed to perform work successfully.

The opportunity they gave me to teach tutorials allowed me to discover something that now became a passion.

Finally I would like to thank my family for their love and support.

Contents

1. Introduction

1.1. Electron gas systems

The study of the flow of charged particles, or electric current, has lead in the past centuries to huge technological improvements especially in the field of information transmission and energy transport and conversion. At the macroscopic scale, the simplest devices we could think about are the light bulb and the telegraph, which during the XIXth century were part of the most advanced technological devices. The transit from the macroscopic scale to the microscopic one, lead to the development of different ways to precisely control the flow of electrons and to the electronic technological revolution.

The basis of this phenomena, is the the displacement of charged particles, generally electrons, through a conductive medium. These displacements are dictated by the electromagnetic force, the intrinsic characteristic of this interaction make the charged particles move from a higher electric potential to a lower one, independently to the material they are moving in.

The understanding of the electronic structure of solids mostly comes from the observation of their crystallographic symmetry groups and from the study of the constituent atoms orbitals. Band theory, which is a direct consequence of the existence of the atomic orbitals, tells that electrons in solids form energy bands of quantum states that they occupy. The structure of this bands give solids their electronic properties i.e. their classification as a metal, semiconductor or insulator and the charge carriers dynamics inside them.

Several theoretical, numerical and experimental techniques have been developed in order to find the band structure of all kinds of crystalline solids ($k \cdot p$ theory, Density Functional Theory, Quantum oscillation experiments, photoemission spectroscopy). Using those tools, the band structure of a large number of solids has been calculated, such as semiconductors with a Zinc Blende crystal structure such as GaN. We display, as an example, a simplified version of its band structure at 300K in fig 1.

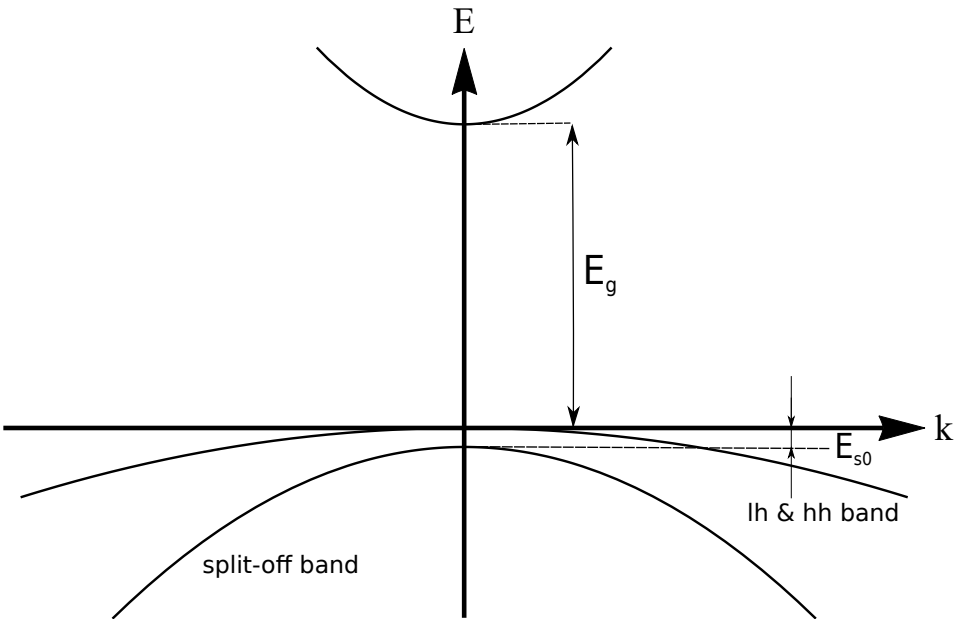

Figure 1.1 – The band structure of a direct gap semiconductor, here with a Zinc Blende crystal structure. In the case of GaN the band gap E_g is 3.2 eV and the heavy and light holes effective masses are the very close. The s-type conduction band lies above the Fermi energy, while the valence band has a triple subband structure due to the mixing of the three p-orbital states.

In intrinsic semiconductors, the Fermi level lies in the gap between the conduction and the valence bands. Due to spin-orbit interaction, the valence band splits into three subbands, the two holes bands and the split-off band. The two holes subbands contain light-holes (lh) and heavy-holes (hh) and are degenerated at the center of the Brillouin zone (Γ point). Since the

maximum of the valence band and the minimum of the conduction band are situated at the same wave vector value, GaN is defined as a direct gap semiconductor.

In order to understand how those band will be filled depending on the parameters of the system, we need to introduce the Fermi-Dirac distribution, which define the occupation probability of fermions, depending on the energy of the particle and on the temperature:

$$f(E) = \frac{1}{e^{(E-\mu)/k_B T} + 1}, \tag{1.1}$$

where E is the energy of the electron, μ is the chemical potential, k_B is the Boltzmann constant and T is the temperature.

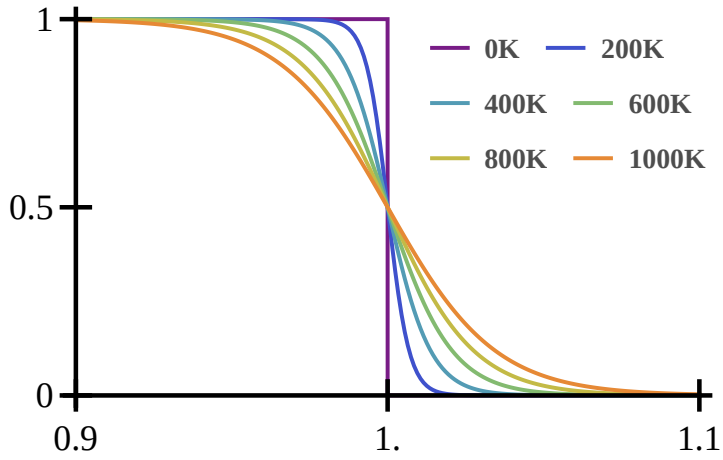

Figure 1.2 – Fermi-Dirac distribution for different temperatures

At equilibrium, for $T = 0$, all the states up to the Fermi energy $E_F = \mu$ are filled while those above are empty. Since the distribution (1.1) is P-symmetric, if an electron flows in one direction, there will be an electron with the same properties propagation in the opposite direction. Therefore, no electric current is flowing in the present case. For temperatures different from zero, the occupation probability becomes non zero above the Fermi energy. In the case of semiconductors, where E_F lies between the conduction and the valence band (see 1.1), the electrons can use the little excess of energy to

get thermally excited from the valence to the conduction band. Under the application of an external electric field, they will accelerate and create an electric current. After the transition of the electron from the valence band to the conduction band, one negative charge is missing in the valence band. The common conceptual way to study the behavior of any system with a nearly full band, is to study how it behaves when possessing the missing particles. Therefore an absence of an electron in a former fully occupied band is called an electron hole, or hole. Consequently, they have a net positive charge and are accelerated in the opposite direction of the electrons. In the case of insulators, the band gap is so large that the temperature necessary to create a thermal transition is to high to be considered as a moderate temperature. Therefore there is no possible transition between the valence band and the conduction band and no current can appear.

Near the band edges, one good approximation is to consider the dispersion of both electrons and holes parabolic. Therefore, the electron and hole are considered free but with masses different from the vacuum ones and not necessarily isotropic. The new masses are called effective masses and are defined as tensors. For this reason, near the band edge, electrons in solids are usually called free electron gases or free hole gases. Before we try to understand why the technology of two dimensional electronic systems might be revolutionized by the discovery of graphene, we are going to make a geometrical classification of systems of different dimensionality based on the de Broglie wavelength of electrons, $\lambda = h/p$, where h is the Planck constant and p the momentum of the electron.

The most common form of metals, semiconductors and insulators in nature is the bulk one. In this case electrons are unconfined and free to move in the 3 spatial directions. The most opposite geometry is the quantum dot, where they are confined in box with lateral size smaller than the electron wavelength. The two last possibilities are obviously the 1 and 2 dimension confinement, respectively the quantum well and the quantum wire. Managing to obtain any dimensionality using a given material is a very important

and active field both in scientific research and industry. Materials which can be patterned to fit in any dimensionality are quite rare and usually have amazing properties.

1.2. Graphene

1.2.1 General properties

Silicon based transistors drive the modern computing revolution. The size of transistors has consistently been decreasing allowing more transistors to be packed onto a single chip thereby increasing computers power. According the Moore's law, the improvement rate is doubling the number of transistor on a chip every two years. The economic reason for such a phenomenal rate is the $1 trillion computer market driven by a worldwide demand for faster and more affordable computers. The physical reason behind the growth rate is the ability of engineers and scientists to fashion silicon into smaller and more efficient computer circuitry. The most recent Intel processor has a transistor with a channel length of 10 nm with high expectations of dividing this size by two around 2020, we here have an example of true nanotechnology. But this incredible speed of technological improvement, will at some point reach some fundamental limit and an alternative to silicon will have to be found. A potential one is carbon bases structures which show superior electrical, mechanical and thermal properties to silicon.

In Mendeleev periodic table, carbon and silicon are direct neighbours, they both have 4 valence electrons. But the distribution of the energies those electrons is way tighter in graphene than silicon, making easier the mixing of their wavefunctions and therefore their hybridization. In carbon, these valence electrons give rise to 2s, $2p_x$, $2p_y$, and $2p_z$ orbitals while the 2 inner shell electrons belong to a spherically symmetric 1s orbital that is tightly bound and has an energy far from the Fermi energy of carbon. For this reason, only the electrons in the 2s and 2p orbitals contribute to the solid-state properties of graphite. This unique ability to hybridize sets

carbon apart from other elements and allows carbon to form 0D, 1D, 2D, and 3D structures.

Graphene, a 2D allotrope of carbon, is made out of carbon atoms arranged on a honeycomb structure made out of hexagons (see Figure 1.3), and can be thought as composed of benzene rings stripped out from their hydrogene atoms. Fullrene, a 0D carbon structure based on graphene, can be obtained with the introduction of pentagons, and hence can be thought as wrapped up graphene. Carbon nanotubes can be obtained by rolling a graphene monolayer along one direction and reconecting the carbon bonds, they can therefore be considered as 1D objects. Graphite, a 3D allotrope of graphene, was known and used way before the beginning of the history of modern science, for writing and drawing for example. Its property to leave a mark on a solid surface when scratched on it, comes from the fact that graphite is made of a large number of graphene monolayers that are weakly coupled to each others by van der Waals forces. Although graphene is the base on which all those allotropes are built and has been produced many many times during the history of mankind it has been isolated only recently [1]. One may wonder why such a simple material has not been deeply studied in the past. The first reason is that no one expected graphene to exist in the free state and secondly, no experimental tools existed to find a one atom thick flake left among the pencil debris covering the macroscopic area of the experiment. Graphene was eventually spotted due to the subtle optical effect in creates on top of a very special type of substrate [1]. To summarise, graphene is extremely easy to make but not so easy to detect.

The electronic properties of graphene are strongly related to its unique structural flexibility. The sp^2 hybridization between one s-orbital and two p-orbitals leads to a triangular planar structure with formation of σ-bond between atoms which are separated by 1.42 Å. Those σ-bonds are responsible for the robustness of the lattice structure in all dimensions. The unaffected π-orbital, which is perpendicular to the planar structure can bind covalently with neighbouring carbon atoms, leading to the formation of a π-band. Since

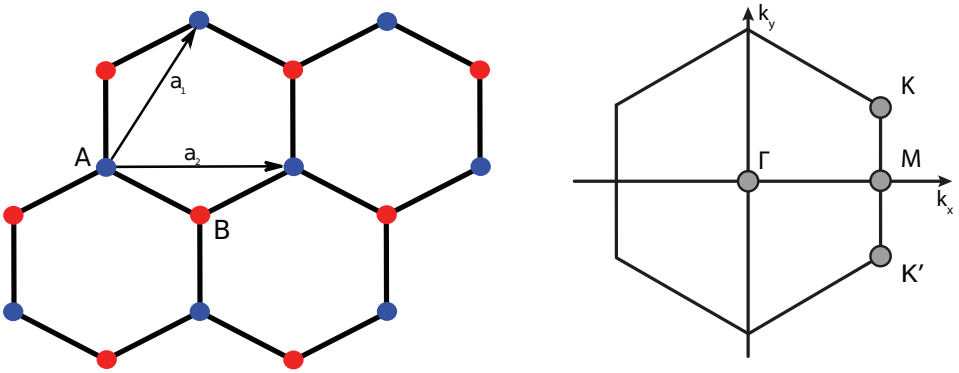

Figure 1.3 – (Left) Lattice structure of graphene made out of two interpenetrating triangular lattices; (Right) Corresponding Brillouin zone. The Dirac cones are located at the K and K' corners.

each p-orbital has one extra electron and according to the Pauli principle, the π-band is half filled.

One of the most interesting aspects of graphene, is that its low energy excitations are massless, chiral, Dirac fermions. This particular dispersion, that is only valid at low energy, i.e., close to the Dirac points that we will define later, mimics the physics of quantum electrodynamics (QED) for massless fermions, except that in graphene the Dirac fermions move at a speed v_F that is 300 times lower than the speed of light c. Hence, many of the unusual properties of the QED, may appear in graphene, but at much smaller speeds. One of the most interesting feature of Dirac fermions is their insensitivity to external electrostatic potentials due to the so-called Klein paradox, i.e., Dirac fermions can be transferred through a classically forbidden region with a probability one [2]. We will discuss in detail this phenomenon further in the thesis. The control of graphene properties has been and continue to be extended in new directions allowing for creation of graphene based systems and hopefully in the near future graphene will be the next step in the never ending search of the components for electronics.

1.2.2 Elementary electronic properties of graphene

Graphene is an allotrope of carbon consisting of a single layer of carbon atoms arranged in an honey comb lattice as shown in Figure 1.3. The structure is not a Bravais lattice, but can be seen as a triangular lattice with a basis of two atoms per unit cell. The lattice vectors can be written as:

$$\mathbf{a_1} = \frac{\sqrt{3}a}{2}\left(\sqrt{3}, 1\right), \qquad \mathbf{a_2} = \frac{\sqrt{3}a}{2}\left(\sqrt{3}, -1\right) \tag{1.2}$$

where $a \approx 1.48$ Åis the inter atom distance. The reciprocal lattice vectors can be written as:

$$\mathbf{b_1} = \frac{2\pi}{3a}\left(1, \sqrt{3}\right), \qquad \mathbf{b_2} = \frac{2\pi}{3a}\left(1, -\sqrt{3}\right) \tag{1.3}$$

Two particular points in the reciprocal space of graphene, at the corners of the Brillouin zone (BZ), give to graphene its unique properties. We will call them Dirac points, and detail later why they are called like this. Their position in the momentum space can be expressed as :

$$\mathbf{K} = \left(\frac{2\pi}{3a}, \frac{2\pi}{3\sqrt{3}a}\right), \qquad \mathbf{K'} = \left(\frac{2\pi}{3a}, -\frac{2\pi}{3\sqrt{3}a}\right) \tag{1.4}$$

In order to use the tight binding approach we need to define the nearest neighbours vectors :

$$\delta_\mathbf{1} = \frac{a}{2}\left(1, \sqrt{3}\right), \qquad \delta_\mathbf{2} = \frac{a}{2}\left(1, -\sqrt{3}\right), \qquad \delta_\mathbf{3} = -a\,(1, 0) \tag{1.5}$$

The tight binding Hamiltonian, considering that electrons can only hop to the nearest neighbours can be written has :

$$\widehat{H}_{TB} = -t \sum_{\langle i,j \rangle, \sigma} a^{\dagger}_{\sigma,i} b_{\sigma,j} + h.c. \tag{1.6}$$

where $a^{\dagger}_{\sigma,i}$ $\left(a^{\dagger}_{\sigma,i}\right)$ annihilates (creates) an electron with spin σ on the site $\mathbf{R_i}$ on the sublattice A (the definition is equivalent for the sublattice B), t (approximatively 2.8 eV) is the nearest neighbour hopping energy. This Hamiltonian can be expressed in the continuum limit as [3, 4]:

$$\widehat{H} = \begin{pmatrix} 0 & -tg^{*}(\mathbf{k}) \\ -tg(\mathbf{k}) & 0 \end{pmatrix} \tag{1.7}$$

where :

$$g(\mathbf{k}) = \sum_{j} \exp\left(i\boldsymbol{\delta_j} \cdot \mathbf{k}\right). \tag{1.8}$$

And with the associate eigenenergies :

$$\begin{aligned} E_{\pm}(\mathbf{k}) &= \pm t\sqrt{3 + f(\mathbf{k})} \\ f(\mathbf{k}) &= 2\cos\left(\sqrt{3}k_y a\right) + 4\cos\left(\frac{\sqrt{3}}{2}k_y a\right)\cos\left(\frac{3}{2}k_x a\right) \end{aligned} \tag{1.9}$$

where the plus sign design the upper (π) and the minus sign the lower (π^*). From the dispersion (Eq.1.9, Figure 1.4), we can see that there are indeed 6 special point, corresponding to the 6 corners of the Brillouin zone (see Figure 1.3), and they can be sorted in two categories of so called Dirac points that we will now denote as K and K' as defined previously. In the same figure we show a zoom of the band structure close to one of the Dirac points. The Hamiltonian and the dispersion close to this area can be obtained by

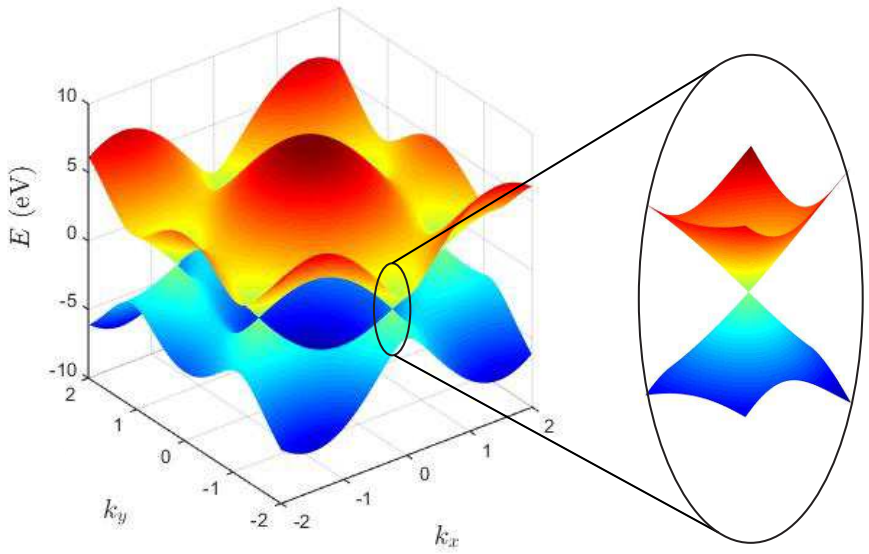

Figure 1.4 – (Left) Energy spectrum (Right) Zoom close to one of the Dirac points.

performing the Taylor expansion of (1.7) and (1.9) close to K (or K') as : $k = K + q$ with $|q| \ll |K|$:

$$\widehat{H} = \hbar v_F \mathbf{k} \cdot \widehat{\boldsymbol{\sigma}} \tag{1.10}$$
$$E_{\pm} = \pm \hbar v_F q$$

where v_F represent the Fermi velocity which can be expressed as $v_F = 3ta/2\hbar$ with the value $v_F \approx 10^6 m/s$ [5,6].

If there is a difference between the electrons potential in sublattices A and B, a band gap is opened at the Dirac points. The gap can be obtained by many methods. For exemple, growing a graphene monolayer on a substrate with a different lattice constant will induce a lattice mismatch[7,8]. Also, a method commonly used is to stretch the graphene monolayer to obtain the same result [9, 10]. The new Hamiltonian close to the Dirac points can be expressed as :

$$\widehat{H} = \begin{pmatrix} \Delta_g/2 & \hbar v_f \left(\xi k_x - i k_y\right) \\ \hbar v_f \left(\xi k_x + i k_y\right) & -\Delta_g/2 \end{pmatrix} \tag{1.11}$$

where Δ_g is the energy splitting between the two sublattices and xi is the valley index. The eigenvalues of such Hamiltonian can be expressed as :

$$E_{\pm} = \pm \sqrt{(\hbar v_F k)^2 + \left(\frac{\Delta_g}{2}\right)^2}. \tag{1.12}$$

A graphene band gap can also be obtained by applying a mono chromatic laser field in the mid infra red range to the sheet [11,12]. This effect will be developed in details later in this thesis.

1.2.3 Dirac Fermions

We now consider the Hamiltonian (1.6) and consider the Fourier transform of the electron operators:

$$a_n = \frac{1}{\sqrt{N}} \sum_k e^{-i\mathbf{k}\cdot\mathbf{R_n}} a\left(k\right) \tag{1.13}$$

where N is the number of unit cells. Therefore, using this expression a,d taking into account the contributions from both valleys, one can obtain a simple expression for low energies i.e. close to the Dirac points:

$$a_n \approx e^{-i\mathbf{k}\cdot\mathbf{R_n}} a_{1,n} + e^{-i\mathbf{k}\cdot\mathbf{R_n}} a_{2,n} \tag{1.14}$$

where the index $i = 1$ ($i = 2$) refers to the K (K') valley. In order to obtain a valid, simple expression for the Hamiltonian (1.6), we will use this representation of the electron operator. After some algebra, one may obtain:

$$\hat{H} = -iv_F \int \left(\hat{\mathbf{\Psi}}_1^\dagger \boldsymbol{\sigma} \nabla \hat{\Psi}_1 + \hat{\mathbf{\Psi}}_2^\dagger \boldsymbol{\sigma}^* \nabla \hat{\mathbf{\Psi}}_2 \right) dxdy \tag{1.15}$$

where $\boldsymbol{\sigma} = (\sigma_x, \sigma_y), \boldsymbol{\sigma}^* = (\sigma_x, -\sigma_y)$ and $\hat{\mathbf{\Psi}}_i = (a_i, b_i)$. One can see that (1.15) is composed of two Dirac-like Hamiltonians, one around K and the other around K'. Therefore, we can write, in terms of the first quantization, in the vicinity of the Dirac points:

$$v_F \boldsymbol{\sigma} \cdot \mathbf{k} \psi_K = E_K \psi_K, \qquad v_F \boldsymbol{\sigma}^* \cdot \mathbf{k} \psi_{K'} = E_{K'} \psi_{K'}. \tag{1.16}$$

The Hamiltonian (1.16) is, from a formal point of view, exactly that of an ultra-relativistic (or massless) particle of spin 1/2, with the velocity of light c replaced by the Fermi velocity v_F, which is 300 time smaller. Furthermore, the "left-handed" particle described by (1.16) (close to the K point) is not equivalent to its counterpart in the K' valley, corresponding to a "right-handed" particle. The eigenfunction, in the vicinity of the Dirac points, can be expressed as :

$$\psi_{\pm,K} = \frac{1}{\sqrt{2}} \begin{pmatrix} e^{-i\theta_k/2} \\ \pm e^{i\theta_k/2} \end{pmatrix}, \qquad \psi_{\pm,K'} = \frac{1}{\sqrt{2}} \begin{pmatrix} e^{i\theta_k/2} \\ \pm e^{-i\theta_k/2}, \end{pmatrix} \tag{1.17}$$

where the plus minus sign correspond to the two eigenenergies $E = \pm \hbar v_F k$ and $\theta = \arctan(q_y/q_x)$. Since the two valleys are linked by the time reversal symmetry, if the origin of the reciprocal space becomes the M point (see 1.3), the time-reversal symmetry operation becomes equivalent to a reflexion operation along the k_x axis.

1.2.4 Klein Tunnelling

As shortly discussed in the introduction, Klein tunneling is one of the most peculiar and interesting properties of Dirac fermions. In order to properly understand it, we will now study the scattering of chiral electrons in two dimensions by a square potential barrier in a single valley. Figure 1.5 describe the problem studied. In this part as in the totality of this thesis, we assume that there is no inter-valley scattering. First using a simple gauge transformation we rewrite (1.17):

$$\psi_{\pm,K} = \frac{1}{\sqrt{2}} \begin{pmatrix} 1 \\ \pm e^{i\theta_k} \end{pmatrix} \tag{1.18}$$

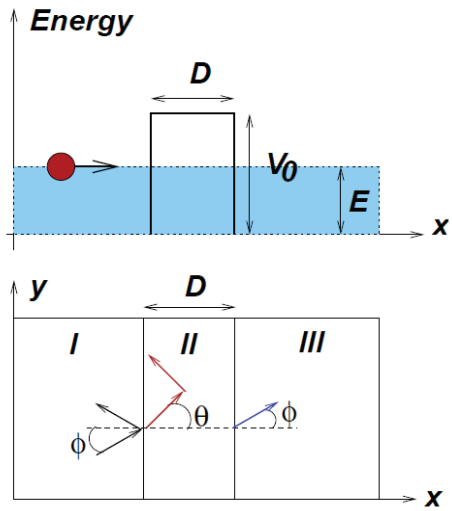

Figure 1.5 – (Top) Schematic picture of the scattering of Dirac electrons by a square potential (Bottom) Top view of the 2D problem. This figure is taken from [3].

The simplest way to solve this problem i.e. find the ratio of electron which are transmitted, is to write the wave function of the Dirac fermion in each region, write the wave function continuity at the edge of each region, and then solve the system of equations obtained for the transmission coefficient.

The wavefunction in the different regions can be decomposed in an incident wave and reflected one. In region one, we obtain:

$$\psi_I = \frac{1}{\sqrt{2}} \begin{pmatrix} 1 \\ se^{i\phi} \end{pmatrix} e^{i(k_x x + k_y y)} + \frac{r}{\sqrt{2}} \begin{pmatrix} 1 \\ se^{i(\pi-\phi)} \end{pmatrix} e^{i(-k_x x + k_y y)} \tag{1.19}$$

where $\phi = \arctan(k_y/k_x)$. In region II we have:

$$\psi_{II} = \frac{a}{\sqrt{2}} \begin{pmatrix} 1 \\ s'e^{i\theta} \end{pmatrix} e^{i(q_x x + k_y y)} + \frac{b}{\sqrt{2}} \begin{pmatrix} 1 \\ s'e^{i(\pi-\theta)} \end{pmatrix} e^{i(-q_x x + k_y y)} \tag{1.20}$$

with $\theta = \arctan(q_x/k_y)$ and q_x defined by:

$$q_x = \sqrt{(V_0 - E)^2 - k_y^2} \tag{1.21}$$

And in region III, only the transmitted wave is present:

$$\psi_{III} = \frac{t}{\sqrt{2}} \begin{pmatrix} 1 \\ se^{i\phi} \end{pmatrix} e^{i(k_x x + k_y y)} \tag{1.22}$$

with $s = \text{sign}(E)$ and $s = \text{sign}(E - V_0)$. The wave function continuity can be written as : $\psi_I(0, y) = \psi_{II}(0, y)$ and $\psi_{II}(D, y) = \psi_{III}(D, y)$. Unlike the Schrodinger equation we only need to match the wavefunction but not its derivative. Therefore, solving those equations for t, one can express the transmission coefficient $T(\phi) = tt^*$, first in the general case then in the special case of high potential barrier ($|V_0| \gg E$):

$$T(\phi) = \frac{\cos^2(\phi)}{\left(\cos(Dq_x)\cos(\phi)\cos(\theta)\right)^2 + \sin^2(Dq_x)\left(1 - ss'\sin(\phi)\sin(\theta)\right)} \tag{1.23}$$

$$T(\phi) = \frac{\cos^2(\phi)}{1 - \cos^2(Dq_x)\sin^2(\phi)} \tag{1.24}$$

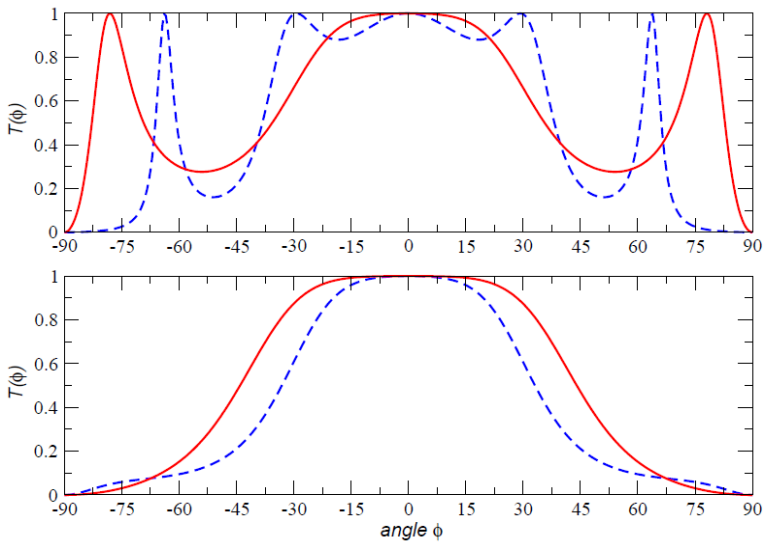

Figure 1.6 – Angular bahavior of the transmition coefficient for two values of V_0: $V_0 = 200meV$ dashed line and $V_0 = 285meV$ solid line. The other parameters are $D = 110nm$ (top), $D = 50nm$ (bottom), $E = 80meV$, $\lambda = 50nm$. This figure is taken from [3].

A way to explain this effect, is through the conservation of the pseudo-spin [13]. An electron which is described by Eq. (1.16), carries a pseudo-spin one half, related to its freedom to be either on sublattice A or B. This new degree of freedom is encoded in the fact that the electron wavefunction is a bispinor and the Hamiltonian is a 2x2 matrix in the sublattice space. We therefore define the chirality operator (or helicity) as:

$$\widehat{C} = \frac{\widehat{\mathbf{k}} \cdot \widehat{\boldsymbol{\sigma}}}{k} \tag{1.25}$$

Its eigenvalues are $C = \pm 1$. When there are no potentials, it commutes with Hamiltonian and therefore is a conserved quantity. The chirality oper-

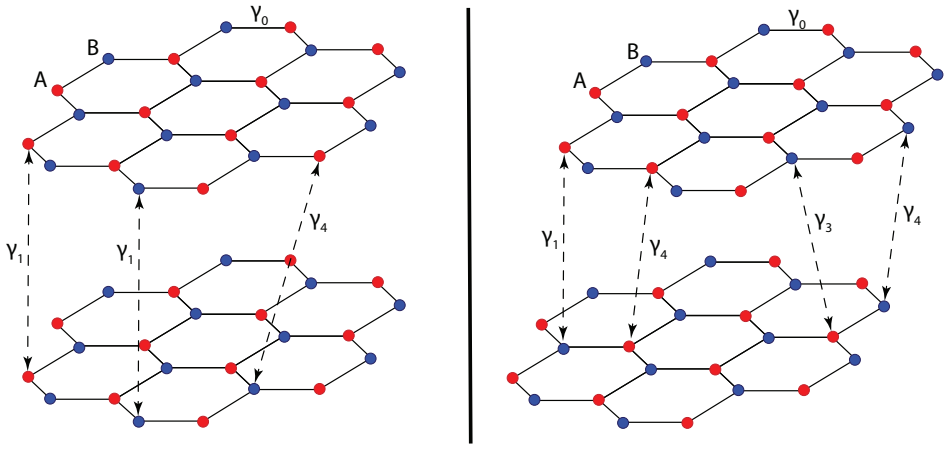

Figure 1.7 – Side view of (left) AA stacking and (right) Bernal stacking bilayer graphene with various hopping parameters

ator can therefore be diagonalized using the same eigenvector as the Hamiltonian, we therefore obtain:

$$\widehat{C}\,|\boldsymbol{k},\pm\rangle = \pm\,|\boldsymbol{k},\pm\rangle\,. \tag{1.26}$$

Therefore, in the case of the simple Dirac Hamiltonian, chirality C is just the band index.

If the electron tries the backscatter on the square potential, due to conservation of chirality it has to also reverse its pseudo-spin. However, the potential does not act on the sublattice space, and therefore cannot reverse the pseudospin. Backscattering is therefore impossible.

1.2.5 Bilayer graphene

Naturally, one may wonder what would be the properties of two stacked graphene monolayers and what would be the main differences with the single monolayer system. As one would expect the two different cases have many similarities such as high conductivity at room temperature and mechanical stiffness and flexibility. Therefore bilayer graphene as monolayer graphene

has potential for future applications in many areas. The main difference lies in the low-energy band structure. Like monolayer there is no band gap between the conduction band and the valence band, but the low energy dispersion is quadratic rather than linear. This means that electrons in bilayer graphene behave like massive chiral particles. In this part we will study why does this property appear and what are the consequences on the dispersion.

The tight-binding Hamiltonian (1.6) can be extended to stacks with a finite number of graphene layers. The simplest case is bilayer graphene [14, 15]. Bilayer graphene can exist in two forms, the Bernal-stacked one [16], where atoms of one sublattice lie directly over the center of a hexagon in the lower graphene sheet or less commonly in the AA form in which the two layers are exactly aligned. It is also possible to obtain twisted layers where one is rotated relative to the other [17]. The most common bilayer structures are shown in Figure 1.8. In this manuscript we will focus our attention on Bernal stacking bilayer graphene.

Using the same tight-binding approach as for (1.6), and not considering the spin dependence, we write the Hamiltonian associated to this problem [3]

$$\begin{aligned}\widehat{H}_{AB} = &-\gamma_0 \sum_{m,\langle i,j\rangle} \left(a^\dagger_{m,i} b_{m,j} + h.c.\right) - \gamma_1 \sum_j \left(a^\dagger_{1,j} a_{2,j} + h.c.\right) \\ &- \gamma_3 \sum_j \left(a^\dagger_{1,j} b_{2,j} + a^\dagger_{2,j} b_{1,j} + h.c.\right) - \gamma_4 \sum_j \left(b^\dagger_{1,j} b_{2,j} + h.c.\right)\end{aligned} \tag{1.27}$$

where $a_{m,i}$ ($b_{m,i}$) create an electron annihilates an electron on the sublattice A (B) on the layer $m = 1, 2$. We here use the graphite notation for the hopping parameters: $\gamma_0 = t$ is the in-plane hopping energy, γ_1 is the hopping energy between atom A_1 and A_2, γ_3 between A_1 (A_2) and B_2 (B_1) and γ_4 between B_1 and B_2.

In the continuum limit, by expanding on momentum around the K points

as previously for monolayer graphene, Hamiltonian (1.28) can be expressed on the basis $\Psi = (\Psi_{A_1}, \Psi_{B_1}, \Psi_{A_2}, \Psi_{B_2})$ as [14]:

$$\widehat{H}_{AB} = \begin{pmatrix} \epsilon_{A_1} & v_F\pi^\dagger & -v_4\pi^\dagger & v_3\pi \\ v_F\pi & \epsilon_{B_1} & \gamma_1 & -v_4\pi^\dagger \\ -v_4\pi & \gamma_1 & \epsilon_{A_2} & v_F\pi^\dagger \\ v_3\pi^\dagger & -v_4\pi & v_F\pi & \epsilon_{B_2} \end{pmatrix} \tag{1.28}$$

where $v_i = \frac{\sqrt{3a\gamma_i}}{2\hbar}$ and $\pi = \xi p_x + ip_y$. In order to only keep the bands relevant for energies close to the Fermi level, we need to eliminate orbitals related to the dimer sites and obtain a two-band Hamiltonian for low energies. Using the procedure described in [14] we write a two bands Hamiltonian on the basis (Ψ_{A_1}, Ψ_{B_2}) under the condition that intra and inter layer hoppings are larger than the other energies [15] :

$$\widehat{H}_{AB} = \widehat{H}_0 + \widehat{H}_\omega + \widehat{H}_4 \tag{1.29}$$

$$\widehat{H}_0 = -\frac{1}{2m}\begin{pmatrix} 0 & \left(\pi^\dagger\right)^2 \\ \pi^2 & 0 \end{pmatrix} \tag{1.30}$$

$$\widehat{H}_\omega = v_3\begin{pmatrix} 0 & \pi \\ \pi^\dagger & 0 \end{pmatrix} - \frac{v_3 a}{4\sqrt{3}\hbar}\begin{pmatrix} 0 & \left(\pi^\dagger\right)^2 \\ \pi^2 & 0 \end{pmatrix} \tag{1.31}$$

$$\widehat{H}_4 = \frac{2v_F v_4}{\gamma_1}\begin{pmatrix} \pi^\dagger\pi & 0 \\ 0 & \pi\pi^\dagger \end{pmatrix} \tag{1.32}$$

where $m = \gamma_1/2v_F^2$ is the effective mass given to the electron due to hopping between the non-dimer sites and the dimer sites.

Here we assume that the on-site energies are equal on both layer and both sublattices. We will now shortly describe the influence of each term in order to properly understand the electronic properties of the system.

The Hamiltonian H_0 describes massive chiral electrons. It dominates at low energies, so that the other terms can be considered as perturbations of

it. For example, the term $\pi^2/2m$ accounts for an effective hopping between the non-dimer sites A_1, B_2 via the dimer sites B_1, A_2 consisting of a hop from A_1 to B_1 (contributing a factor $v\pi$), followed by a transition between B_1, A_2 dimer sites (giving an effective mass to the electrons), and a hop from A_2 to B_2 (a second factor of $v\pi$). The solutions are massive chiral electrons, with parabolic dispersion $E = \pm p^2/2m$.

Outside of the low-energies conditions, when the momentum is far from the K-point, there is a triangular perturbation of the circular iso-energetic lines known as triangular warping, effect which also appear in graphene (by taking into account the second nearest neighbours in the tight binding calculation) and in graphite. It occurs because the band structure follows the crystal lattice symmetry which is described by $f(k)$ defined in (1.9) [18]. In bilayer graphene, the triangular warping arises due to the γ_3 hopping, i.e. hopping between the sites A_1 and B_2. This effect is described by $\widehat{H}_\omega$. The second half of it arises from the Taylor expansion of $f(k)$ and has dependence in square of the momentum. Therefore since the coefficient is of a comparable order with $\widehat{H}_0$ this term will slightly modify the effective mass of the chiral electron. The first half has a more important impact on the dispersion, it causes triangular warping of the iso-energetic lines. For energies lower than 1 meV, the topology of the Fermi surface changes drastically, a Lifshitz transition occurs, creating 4 pockets, one central one and three leg pockets. This effect will be discussed in more details in the second part of this manuscript.

The last term of the Hamiltonian, $\widehat{H}_4$, describes interlayer coupling of dimer and non dimer sites. Due to this term electron-holes assymetry occurs in the band structure as it can be obviously seen by studying the energy dispersion associated to $\widehat{H}_0 + \widehat{H}_4$. This effect will not be studied further in this manuscript but has been added for consistency.

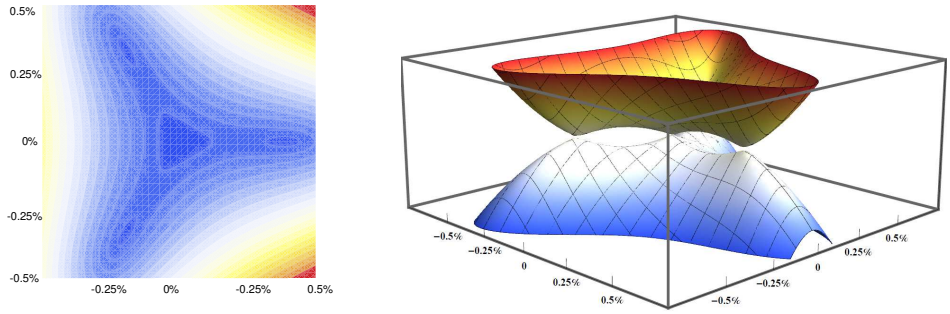

Figure 1.8 – (left) Isoenergetic lines of the low energy spectrum of bilayer graphene. (right) 3 dimensional plot of the low energy spectrum. The axis unit is the percentage of the Brillouin zone.

1.3. Light-Matter Interaction

Due to the laws of conservation of energy and momentum, the absorption of a photon, belonging to an incident electromagnetic field, by a free electron is impossible. These processes are appreciable only if the scattering-induced washing of electron energy, is comparable with the photon energy $\hbar\omega$. In the frame work of classical physics, a charged particle interacts with radiation or any external electromagnetic field a as described by Newton's second low of motion:

$$\frac{\partial}{\partial t}\mathbf{p} = e\mathbf{E} + \frac{e}{c}\mathbf{v} \times \mathbf{H} \tag{1.33}$$

where $\mathbf{E}$ and $\mathbf{H}$ are respectively externaly applied electric and magnetic fields. Introducing a phenomenological relaxation time and neglectic the contribution of the magnetic component of the electromagnetic field irradiating a 2D electronic system, we can express the time derivative of the momentum as:

$$\frac{\partial}{\partial t}\mathbf{p} = -\frac{\mathbf{p}}{\tau} + e\mathbf{E}_{/\!/}(t) \tag{1.34}$$

where $\mathbf{E}_{/\!/}(t)$ is the inplane component of the electric field. Any out of

the plane component would be irrelevant since it would not contribute to accelerate electrons in a purely 2D system. Assuming that the momentum has the same oscillation frequency as the field, $\frac{\partial}{\partial t}\mathbf{p} = -i\omega\mathbf{p}$, one can write the expression linking the momentum to the electric field:

$$\mathbf{p} = \frac{e\mathbf{E}_{/\!/}(t)}{\frac{1}{\tau} - i\omega} \tag{1.35}$$

Using the well known equations of classical electro dynamics, $\mathbf{j}(t) = ne\mathbf{v} = \sigma\mathbf{E}_{/\!/}$, one obtain:

$$\frac{\sigma(\omega)}{\sigma_0} = \frac{1 + i\omega\tau}{1 + \omega^2\tau^2} \tag{1.36}$$

The absorption coefficient coming from the intrasubband scattering of free carriers can be expressed as :

$$\alpha(\omega) = \frac{\sigma_0}{\epsilon_0 c\eta_r}\frac{1}{1 + \omega^2\tau^2} \tag{1.37}$$

where η_r is the refractive index of the medium. In the low frequency limit, $\omega\tau \ll 1$ one obtain:

$$\alpha(\omega) = \frac{\sigma_0}{\epsilon_0 c\eta_r} \tag{1.38}$$

whereas in the high frequency one, $\omega\tau \gg 1$ the absorption coefficient behaves as ω^{-2}, and can be considered as negligible:

$$\alpha(\omega) = \frac{\sigma_0}{\epsilon_0 c\eta_r\omega^2\tau^2}. \tag{1.39}$$

In order to calculate the inter and intra band transitions, the calculation

can no longer be performed in a classical way, quantum formalism must be used. The electric and magnetic components of an electromagnetic field can be expressed depending on the vector potential $\mathbf{A}$ and the scalar potential ϕ in the following form [19]

$$\mathbf{E} = -\nabla\phi - \frac{\partial \mathbf{A}}{\partial t} \tag{1.40}$$

$$\mathbf{B} = \nabla \times \mathbf{A} \tag{1.41}$$

In quantum mechanics, the interaction between a fermion and an electromagnetic field is usually described in the framework of the minimal coupling. In Cartesian coordinates, the Lagrangian of a non-relativistic particle in an EM field can be expressed as :

$$\mathcal{L} = \frac{1}{2}m\sum_i \dot{x}_i^2 + q\sum_i \dot{x}_i A_i - e\phi \tag{1.42}$$

In the framework of Lagrangian physics, the generalized momenta is given by :

$$p_i = \frac{\partial \mathcal{L}}{\partial \dot{x}_i} = m\dot{x}_i + qA_i \tag{1.43}$$

The velocities can therefore be expressed as:

$$\dot{x}_i = \frac{p_i - qA_i}{m} \tag{1.44}$$

In the end, considering the scalar potential to be zero, the description of the fermion-photon coupling can be done by performing the canonical transformation:

$$p_i \rightarrow p_i - qA_i. \tag{1.45}$$

Considering the simplest model i.e. infinite quantum well, the photons of the EM field, can be absorbed when an electron jumps from the valence band to the conduction band. In the case of a weak EM field, the Hamiltonian can be split into an unperturbed part H_0 and a time dependent perturbation part $H_D(t)$:

$$\hat{H} = \hat{H}_0 + \hat{H}_D(t). \tag{1.46}$$

Let us consider first the case of a two dimensional electron gas under submitted to a spatially homogeneous EM field, where bare electrons can be described by a simple free particle Hamiltonian. Neglecting the second order in A, the electron-photon coupling term can be expressed as:

$$\hat{H}_D(t) = \frac{e}{2m}\mathbf{A}\cdot\mathbf{p} \tag{1.47}$$

The Fermi's golden rule describes the transition rate, from one energy eigenstate to another one affected by a weak perturbation:

$$P_{i,f} = \frac{2\pi}{\hbar}\left|\langle f\left|H_D(t)\right|i\rangle\right|^2\rho \tag{1.48}$$

where ρ is the density of final states. This expression can be used in our case for transition from the valence band to the conduction band with one photon, of frequency ω, absorption :

$$P_{v,c} = \frac{2\pi}{\hbar}\left|\langle c\left|H_D(t)\right|v\rangle\right|^2\delta\left(E_c - E_v - \hbar\omega\right) \tag{1.49}$$

where E_c and E_v are respectively the energy of levels c and v.

1.4. Electromagnetically dressed graphene

In the previous parts of this manuscript, we looked into the basic properties of bare two dimensional systems and considered the effect of an external EM field on the electronic properties of two dimensional systems. We will now use this knowledge to study the electronic properties of graphene under an electromagnetic field in the high frequency limit and get some strong basis in order to later create in-situ light tuned systems that may bring some insight on how to create new electronic devices using Dirac systems.

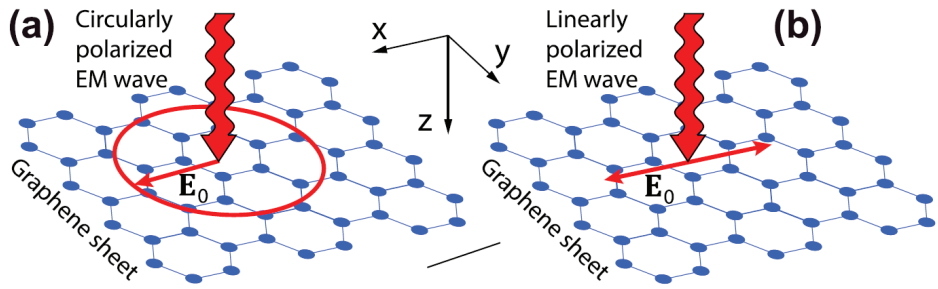

Figure 1.9 – A graphene sheet dressed by (a) circularly polarized electromagnetic wave with the amplitude E_0 and frequency ω and (b) linearly polarized one. Figure is taken from [12]

We here consider a monolayer of graphene, lying in the xy-plane, illuminated by a continuous wave with frequency ω (see Figure 1.9). Electronic properties of graphene mostly depend on the band parameter close to the band edge i.e. the Dirac points. Therefore, for clarity purposes, the following description will be performed close to the Dirac point, at low energies. The bare system is described by the Hamiltonian (1.9). If $\mathbf{A}_\omega(t)$ is time periodic vector potential of the laser field then using the minimal coupling approach, the following substitution on (1.9) is performed [3]

$$\mathbf{k} \to \mathbf{k} - \frac{e}{\hbar}\mathbf{A}_{\omega}(t). \tag{1.50}$$

Therefore the single electron time dependent Hamiltonian can be expressed as :

$$\widehat{H} = \hbar v_F \left(\mathbf{k} - \frac{e}{\hbar}\mathbf{A}_{\omega}(t)\right) \cdot \widehat{\boldsymbol{\sigma}}. \tag{1.51}$$

In the following we consider the case where the absorption coefficient is almost zero. In order for this assumption to be realistic, we need to set the frequency of the EM field to be much larger than the energy difference between the graphene bands close to the Fermi Level. Electrons under the influence of such field will be called "dressed electrons" in this thesis. Of course this allows for photoexcitations of electrons to the states far above the Fermi level, but at this energies, electrons thermalize very quickly by the emission of optical phonons to the lowest empty states available in the conduction band and raise the Fermi level. Therefore, those transition will be, as an approximation, neglected.

We will now solve the Schrodinger equation associated to (1.51) in order to obtain the spectrum of the dressed electron and the associated wave functions. Also in order to study the influence of the dressing field polarization, we will study separately the case of linear and circular polarizations.

For the case of circularly polarized electromagnetic wave, the vector potential $\mathbf{A} = (A_x, A_y)$ is defined as :

$$\mathbf{A} = \frac{E_0}{\omega}(\cos\omega t, \sin\omega t) \tag{1.52}$$

where E_0 is the amplitude of the wave and ω is the wave frequency. Then the Hamiltonian (1.51) can be expressed as the sum of the bare system

Hamiltonian and a field associated perturbation:

$$\widehat{H} = \widehat{H}_0 + \widehat{H}_P \tag{1.53}$$

where:

$$\widehat{H}_0 = \hbar v_F \mathbf{k} \cdot \boldsymbol{\sigma} \tag{1.54}$$

and

$$\widehat{H}_P = -\frac{v_F e E_0}{\omega} \left(\cos \omega t \hat{\sigma}_x + \sin \omega t \hat{\sigma}_y\right). \tag{1.55}$$

The non-stationary Schrodinger equation associated to (1.55) describes the time evolution of electronic states at the Dirac point i.e. for $k = 0$. In order to solve this equation we choose to use an ansatz of the form :

$$\Psi_P = e^{-i\alpha t/\hbar} \left(A\Phi_1(\boldsymbol{r})\, e^{-i\omega t/2} + B\Phi_2(\boldsymbol{r})\, e^{i\omega t/2}\right), \tag{1.56}$$

where $\Phi_{1,2}$ are the basic functions of the 2×2 matrix Hamiltonian (1.51) and A, B and α are sought parameters. Replacing into the associated Schrodinger equation we obtain the following equation:

$$\begin{pmatrix} \alpha + \frac{\hbar\omega}{2} & \frac{veE_0}{\omega} \\ \frac{veE_0}{\omega} & \alpha - \frac{\hbar\omega}{2} \end{pmatrix} \begin{pmatrix} A \\ B \end{pmatrix} = \begin{pmatrix} 0 \\ 0 \end{pmatrix} \tag{1.57}$$

The conditions for the solutions to not be trivial are :

$$\alpha = \pm\Omega = \pm\sqrt{\left(\frac{\hbar\omega}{2}\right)^2 + W_0^2} \tag{1.58}$$

where $W_0 = \frac{veE_0}{\omega}$ is the kinetic energy of the rotational electron motion induced by the circularly polarized field.

Therefore replacing into (1.56) and performing some simple analytics and under the normalization condition $|A| + |B|^2 = 1$, we obtain the following set of solutions:

$$\Psi_P^{\pm} = e^{\pm i\Omega t/\hbar}\left(\sqrt{\frac{2\Omega \pm \hbar\omega}{4\Omega}}\Phi_1(\boldsymbol{r})\, e^{-i\omega t/2} \pm \frac{e}{|e|}\sqrt{\frac{2\Omega \mp \hbar\omega}{4\Omega}}\Phi_2(\boldsymbol{r})\, e^{i\omega t/2}\right). \tag{1.59}$$

Those two wave function describe exactly the system at the Dirac point and provide a complete basis for any time t, using them we can now solve the Schrodinger equation associated to (1.51). We again write the solution in the form of an Ansatz writen as an expansion on the basis just previously defined:

$$\Psi_k = \Xi_+(t)\,\Psi_P^+ + \Xi_-(t)\,\Psi_P^-. \tag{1.60}$$

Substituting this expression into the Schrodinger equation associated to the full Hamiltonian (1.51), we obtain a system of two quite complicated differential equation. We now assume that the kinetic energy associated to the rotational electronic motion is small compared to the photon energy, which is equivalent to consider a not too strong electron-photon coupling:

$$W_0 \ll \hbar\omega. \tag{1.61}$$

In the end the system of equations can be expressed as:

$$i\dot{\Xi}_1(t) = -v_F \frac{e}{|e|}\left(\frac{W_0}{\hbar\omega}\left(k_x\cos\omega t + k_y \sin\omega t\right)\Xi_1(t) - \left(k_x - ik_y\right)e^{-i(\Omega-\hbar\omega)t/\hbar}\Xi_2(t)\right) \tag{1.62}$$

$$i\dot{\Xi}_2(t) = -v_F \frac{e}{|e|}\left(\frac{W_0}{\hbar\omega}\left(k_x\cos\omega t + k_y \sin\omega t\right)\Xi_2(t) + \left(k_x + ik_y\right)e^{i(\Omega-\hbar\omega)t/\hbar}\Xi_1(t)\right)$$

Solving this system of equations, we finally arrive to an approximate solution for the energy spectrum:

$$E_k = \pm\sqrt{\left(\frac{\Delta_g}{2}\right)^2 + \left(J_0\left(\frac{2v_F eE_0}{\hbar\omega^2}\right)\hbar v_F k\right)^2} \tag{1.63}$$

where Δ_g is the gap which open due to the EM field, and can be expressed as:

$$\Delta_g = \sqrt{(\hbar\omega)^2 + \left(\frac{2v_F eE_0}{\omega}\right)^2} - \hbar\omega \tag{1.64}$$

In the end we obtain an expression for the energy spectrum of both valance and conduction bands (the $\pm$ differentiating them). The main consequence of the field in this polarization case is the opening of a band gap at the Dirac points. One may notice that we chose to not keep the valley index in our calculations. To be rigorous, the valley index actually change the final expression, showing an valley dependent effect i.e. the gap is positive in K valley and negative in K'. But effectively, in our system, no valley dependent effect can be observed since the effective dispersion is the same in both valleys. We will see later in this manuscript that in already gapped Dirac systems (gapped graphene, transition metal dichalchognides etc) valley dependence is important and will need to be taken into account.

For the case of linear polarization, the vector potential $\boldsymbol{A} = (A_x, A_x)$ can be written as:

$$\boldsymbol{A} = \frac{E_0}{\omega}(\cos\omega t, 0) \tag{1.65}$$

Since the procedure is quite similar to the one in the circular case, we will just write the results here, details can be found in [12].

The energy spectrum of the dressed electrons can be expressed as:

$$E_k = \pm\hbar v_F \sqrt{k_x^2 + J_0^2\left(\frac{2v_F e E_0}{\hbar\omega^2}\right) k_y^2} \tag{1.66}$$

where J_0 is the Bessel function of the first kind. In order for is expression to be relevant, as in the circular polarization case, the non absorbative field condition must be verified i.e. $E_k \ll \hbar\omega$. We see here that the linearly polarized light modifies the electronic dispersion in an anisotropic way. Indeed the Fermi velocity is decreased in one direction while it is kept unchanged in the perpendicular one.

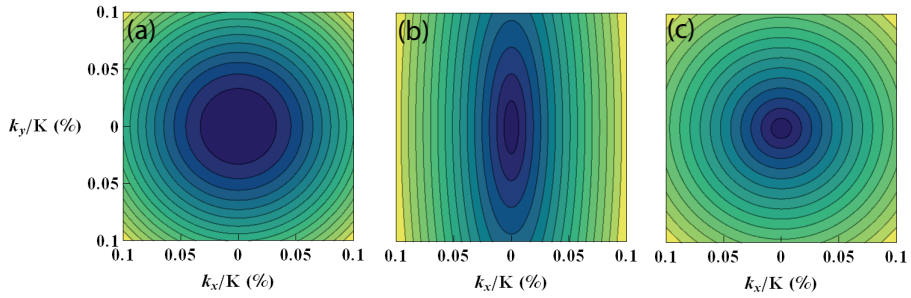

Figure 1.10 – Isoenergy plot of dressed electrons in dressed graphene with different polarizations, depending on the distance from the center of the Brillouin zone: (a) circularly polarized dressing field; (b) dressing field polarized along the x axis; (c) bare graphene for reference.

We have here shown that the band properties of electrons in graphene can be tuned using a electromagnetic dressing field. Particularly, a circular polarized, which can be understood as a superposition of two perpendicular

linearly polarized beams, combine two effects which are direct consequences of the dynamical Stark effect. It first modifies isotropically the Fermi velocity. One should note that as we have just seen in the case of linearly polarized light, the Fermi velocity is modified in only one direction. Second, it opens a direct band gap which is proportional to the intensity of the dressing beam. As we saw before, graphene possesses two different kind of low energy points. But since the initial dispersion is gapless, it is impossible here to make the difference between them easily. In the second half of this manuscript we will study the influence of a dressing field on gapped Dirac system and will moreover use the elliptical polarisation as a true tuning parameter.

1.5. Floquet-Magnus expansion

In this section, the dynamics of a particle in a 2D system under the influence of a potential periodic in time is studied. For most of the time-dependent problems, the solutions can only be attained numerically. However, in the case of a potential period small compared to the other time scales of the system, the motion of the particle can be split in two part: a "slow" motion and "fast" motion. This simplification comes from the fact that the particle does not have the time to react to the potential before its sign changes. Therefore, the influence of the potential on the particle dynamics is minimal (sometimes even negligible). Thus we will consider here the limit of high frequencies of the driving potential.

Even-though the existence of a time-independent Hamiltonian describing a the slow part of the dynamical problem, seems to contradict the fact that the time dependent dynamics do not possess a constant of motion, it should be stressed that this "effective" Hamiltonian depends on coordinates which describes the "slow" part of motion. This coordinate is not the exact position of the particle. The real motion of the particle consists in rapid motion around the trajectory of the slow motion. Moreover, at high frequencies, the real motion and the slow motion of the particle are almost identical.

Therefore, some condition of applicability of the following theory need to be carefully defined and verified when applied to quantum systems.

We here consider a quantum system, described by an Hamiltonian periodic in time with period T:

$$\widehat{H}(t+T) = \widehat{H}(t). \tag{1.67}$$

Such systems can be treated using the Floquet formalism [20–24]. The symmetry with respect to discrete time translation implies the solution of the Schrodinger equation associated are linear combinations of functions of the form:

$$\psi_\lambda = e^{-i(\lambda t/\hbar)} u_\lambda(x, \omega t) \tag{1.68}$$

where u_λ are periodic with respect to ωt with period 2π. The states u_λ are the quasistates or the Floquet states, and λ are the associated energies or quasienergies. We now define the Floquet Hamiltonian, which has for eigenstates u_λ:

$$\widehat{H}_F = -i\hbar\frac{\partial}{\partial t} + \widehat{H}. \tag{1.69}$$

The structure of the wave function (1.68) describes perfectly the separation between the "slow" part, $e^{-i(\lambda t/\hbar)}$, given that $0 \leq \lambda/\hbar \leq \omega$, and the "fast" part $u_\lambda(x, \omega t)$ which only depends on the fast time parameter ωt. We will now develop an equation of motion for the slow part of the dynamics.

The propagator can be expressed as [24]:

$$\widehat{U}(t) = \widehat{P}(t)\, e^{-it\widehat{K}/\hbar} \tag{1.70}$$

where $\widehat{K}$ is self-adjoint and $\widehat{P}$ is unitary and periodic with the period of

the Hamiltonian. $\widehat{K}$ is called the quasienergy Floquet operator and its exact calculation can be tricky since often its form must be guessed. Our objective now is to find a unitary gauge transformation such that in the new gauge, the initial Hamiltonian becomes time independent. The general form of this gauge transformation can be expressed as $e^{i\widehat{F}(t)}$ where $\widehat{F}(t)$ is an Hermitian operator, with the same period as $\widehat{H}$ [25].

Applying the gauge transformation to both sides of the Schrodinger equation associated to the initial Hamiltonian we obtain:

$$i\hbar\frac{\partial}{\partial t}e^{i\widehat{F}}\psi = e^{i\widehat{F}}\widehat{H}\psi + i\hbar\left(\frac{\partial}{\partial t}e^{i\widehat{F}}\right)\psi \tag{1.71}$$

In the new gauge, $\phi = e^{i\widehat{F}}\psi$ this equation can be expressed as:

$$i\hbar\frac{\partial}{\partial t}\phi = \widehat{G}\phi \tag{1.72}$$

where the Hamiltonian $\widehat{G}$, which is the effective Hamiltonian, can be written as :

$$\widehat{G} = e^{i\widehat{F}}\widehat{H}e^{-i\widehat{F}} + i\hbar\frac{\partial e^{i\widehat{F}}}{\partial t}e^{-i\widehat{F}} \tag{1.73}$$

Let us assume that an operator $\widehat{F}$ exists such that $\widehat{G}$ is time independent. Then the eigenfuntions of $\widehat{G}$, that we here call v_λ evolve according to :

$$\phi_\lambda = e^{-i(\lambda t/\hbar)}v_\lambda \tag{1.74}$$

which can be expressed in the original basis as :

$$\psi_\lambda(t) = e^{-i\widehat{F}}\phi_\lambda = e^{-i(\lambda t/\hbar)}e^{-i\widehat{F}}v_\lambda. \tag{1.75}$$

Since v_λ is time-independent, the function $e^{-i\widehat{F}}$, is periodic in time with the same period as $\widehat{H}$. Therefore, ψ_λ is a Floquet state with quasienergy λ.

According to what we just studied, we can say that in order to study a system described by a time periodic Hamiltonian, we need to split the dynamics in two parts: one slow part and one fast part. The fast part can be neglected in the case of high frequency potential. Then in order to obtain a time-independent description of the system, we need to find the right unitary transformation that will make the time dependence disappear in the new basis.

Unfortunately, it is often very difficult, sometimes even impossible, to give an exact analytical expression for the effective Hamiltonian $\widehat{G}$ and the associated unitary transformation. Therefore it is very convenient to build those operators simultaneously perturbatively, by expanding them in powers of the driving period $T = 2\pi/\omega$. The method consist in constructing the time-independent effective Hamiltonian by transferring all the non desired time dependent terms in the unitary transformation operator. Obviously one knows that some time dependence will always remain in the effective Hamiltonian, but it can be neglected if the frequency of the driving field is high enough.

We start by expanding the effective Hamiltonian and the associated unitary transformation [26, 27]

$$\widehat{G} = \sum_{n=0}^{\infty} \frac{1}{\omega^n}\widehat{G}^{(n)}, \widehat{F} = \sum_{n=1}^{\infty} \frac{1}{\omega^n}\widehat{F}^{(n)} \tag{1.76}$$

and the following expansions :

$$e^{i\widehat{F}}\widehat{G}e^{-i\widehat{F}} = \widehat{G} + i\left[\widehat{F},\widehat{G}\right] - \frac{1}{2}\left[\widehat{F},\left[\widehat{F},\widehat{G}\right]\right] + ... \tag{1.77}$$

$$\left(\frac{\partial e^{i\widehat{F}}}{\partial t}\right)e^{-i\widehat{F}} = i\frac{\partial\widehat{F}}{\partial t} - \frac{1}{2}\left[\widehat{F},\frac{\partial\widehat{F}}{\partial t}\right] - \frac{i}{6}\left[\widehat{F},\left[\widehat{F},\frac{\partial\widehat{F}}{\partial t}\right]\right] + ... \tag{1.78}$$

Under the conditions that we stated before, the initial Hamiltonian can be rewritten in the following form:

$$\widehat{H}(t) = \widehat{H}_0 + \widehat{V}(t) = \widehat{H}_0 + \sum_{j=0}^{\infty}\widehat{V}^{(j)}e^{ij\omega t} + \widehat{V}^{(-j)}e^{-ij\omega t} \tag{1.79}$$

where $\widehat{H}_0$ is the Hamiltonian associated to the bare system and $V(t)$ represent the driving potential. Using the expressions we just defined we can write the general expression, up to the second order, for the effective perturbative Hamiltonian of a system under a periodic high frequency potential :

$$\widehat{G} = \widehat{H}_0 + \frac{1}{\omega}\sum_{j=1}^{\infty}\frac{1}{j}\left[\widehat{V}^{(j)},\widehat{V}^{(-j)}\right] + \frac{1}{2\omega^2}\sum_{j=1}^{\infty}\frac{1}{j^2}\left(\left[\left[\widehat{V}^{(j)},\widehat{H}_0\right],\widehat{V}^{(-j)}\right] + h.c.\right) \tag{1.80}$$
$$+ \frac{1}{3\omega^2}\sum_{j,l=1}^{\infty}\frac{1}{jl}\left(\left[\widehat{V}^{(j)},\left[\widehat{V}^{(l)},\widehat{V}^{(-j-l)}\right]\right] + 2\left[\widehat{V}^{(j)},\left[\widehat{V}^{(-l)},\widehat{V}^{(l-j)}\right]\right] + h.c.\right)$$

and the associated gauge transformation:

$$\begin{aligned}\widehat{F} =&\frac{1}{i\omega}\sum_{j=1}^{\infty}\frac{1}{j}\left(\widehat{V}^{(j)}e^{ij\omega t}-\widehat{V}^{(-j)}e^{-ij\omega t}\right)+\frac{1}{i\omega^2}\sum_{j=1}^{\infty}\frac{1}{j^2}\left(\left[\widehat{V}^{(j)},\widehat{H}_0\right]e^{ij\omega t}-h.c.\right)\\&+\frac{1}{2i\omega^2}\sum_{j,l=1}\frac{1}{j\,(j+l)}\left(\left[\widehat{V}^{(j)},\widehat{V}^{(l)}\right]e^{i(j+l)\omega t}-h.c.\right)\\&+\frac{1}{2i\omega^2}\sum_{j\neq l=1}^{\infty}\frac{1}{j(j-l)}\left(\left[\widehat{V}^{(j)},\widehat{V}^{(-l)}\right]e^{i(j-l)\omega t}-h.c.\right)\end{aligned}\tag{1.81}$$

One may note that the only condition of applicability lies in the amplitude of the zeroth order term in the gauge transformation. This is in accordance with the calcualtions we performed exactly in the dressed graphene section. Since there are no other conditions than the time periodicity, any kind of time-periodic potential can be used either space homogeneous or strongly localised. This theory gives us a very powerful and generic tool to solve Floquet problems in the framework of perturbation theory, allowing us to free ourselves from the concern of finding the complex solutions to the exact problem. We will later use those expansions to study the influence of an external high-frequency electromagnetic field on gapped Dirac systems when the problem cannot be solved exactly and see how we can use those effects locally to create new electronic systems controlled by light.

1.6. Zitterbewegung effect and Wave Packet simulations

Zitterbewegung (trembling motion) was theoretically predicted by Schrodinger [28] after Dirac proposed his equation to describe the behavior of an electron in vacuum. The non-commutativity of the quantum velocity operator and the Dirac Hamiltonian make appear this peculiar effect even without the presence of any external field. A bit later, the scientific community understood that this phenomenon is due to interferences between the electrons in the positive energy state and with those in the negative one. The Zitterbewegung (ZB) is therefore an inner property of the Dirac Hamiltonian, occuring only because of the existence of bot positive and negative

energy states. But unfortunately, this effect has not been observed directly in vacuum, even though its direct consequences such as Darwin effect in the presence of an external field have been.

Finding ways to study this effect was a really hot topic in theoretical condensed matter physics a decade ago. Indeed, when dealing with semiconductors, one has to consider, even in the simplest cases, two energy branches or more and as we saw earlier in this thesis, depending on a simple renormalisation, the valence and the conduction band can be respectively considered as negative and positive energy branches for example. Therefore, the interferences between upper and lower energy states leads to a trembling motion even in the absence of external fields. Due to similarities in the theory between two interacting bands and the Dirac equation for electrons in vacuum, it is possible to adapt the existing theory developed in the framework of relativistic quantum theory for non-relativistic electrons in solids [29,30]. Most of the ZB studies for semiconductors have taken as a starting point plane electron waves or Gaussian wave packets [31,32].

Since, as we have shown before, graphene is described by a renormalized Dirac equation in the vicinity of the Dirac points, it is quite natural to think that graphene is an amazing tool to study the ZB effect. Many theoretical studies have been performed using plane waves representation [33,34]. One of the most important conclusion obtained by the community [35], is that the ZB is not an undamped effect, it can only be considered as a transient effect. Under the condition of a smoothly varying wave packet, the ZB oscillations will become negligible for large time scales. Therefore any stationary study become inaccurate and the study of the dynamics becomes necessary. With the emergence of many new technologies in the pulse laser frame in the last decade, using wave packets to study how the ZB effect evolves with time comes naturally. In this part we will give a short review of the behaviour of a Gaussian wave packet in graphene and in gapped graphene, taking into account the ZB effect. The main goal is not to understand all the details about this phenomenon but to have enough knowledge about the behaviour

of an electron wave packet in Dirac systems in order to have a good basis to understand the results that will be obtained later in this manuscript.

We found out before that in the stationary regime, the electron eigenstate in graphene can be expressed as (1.18). In this section, since we are concerned with the dynamics of electron wave packet, we rewrite the wave function as :

$$\phi\left(\mathbf{r},t\right)=\frac{1}{2\sqrt{2}\pi\hbar}\exp\left(i\mathbf{k}\cdot\mathbf{r}-iE_{s}t/\hbar\right)\begin{pmatrix}1\\ se^{i\phi}\end{pmatrix} \tag{1.82}$$

where s correspond to the band index and E is the associated eigenenergy.

Using the Green's function formalism, the evolution of an initial state $\psi_0\left(\mathbf{r},t\right)$ in the Schrodinger representation can be expressed as :

$$\psi_{m}\left(\mathbf{r},t\right)=\int G_{m,n}\left(\mathbf{r},\mathbf{r}',t\right)\psi_{n}\left(\mathbf{r}',0\right)d\mathbf{r}' \tag{1.83}$$

where m and n are the matrix indices, corresponding to the upper and lower components of $\psi\left(\mathbf{r},t\right)$. These components correspond to the probability of finding electrons at the sites of the sublattices A and B respectively. The Green's function expression is usually:

$$G_{m,n}\left(\mathbf{r},\mathbf{r}',t\right)=\hbar\sum_{s=\pm1}\int d\mathbf{k}\phi_{s,\mu}\left(\mathbf{r},t\right)\phi_{s,\mu}^{*}\left(\mathbf{r}',0\right). \tag{1.84}$$

Using expression (1.82) we now find:

$$G_{11}\left(\mathbf{r},\mathbf{r}',t\right)=G_{22}\left(\mathbf{r},\mathbf{r}',t\right)=\frac{\hbar}{\left(2\pi\hbar\right)^{2}}\int\exp\left(i\mathbf{k}\left(\mathbf{r}-\mathbf{r}'\right)\right)\cos\left(v_{F}kt\right)d\mathbf{k} \tag{1.85}$$

$$G_{21}\left(\mathbf{r},\mathbf{r}',t\right)=G_{12}^{*}\left(\mathbf{r},\mathbf{r}',t\right)=\frac{-i\hbar}{\left(2\pi\hbar\right)^{2}}\int\frac{k_x+ik_y}{k}\exp\left(i\mathbf{k}\left(\mathbf{r}-\mathbf{r}'\right)\right)\sin\left(v_F kt\right)d\mathbf{k} \tag{1.86}$$

where v_F is as before the Fermi velocity in graphene.

We consider a Gaussian shaped electron wave packet having the width d and a non-vanishing average momentum $\mathbf{k_0}$. The wave function of such wave packet in graphene can be expressed as:

$$\psi\left(\mathbf{r},0\right)=\frac{1}{d\sqrt{\pi}}\frac{1}{\sqrt{\left|c_1\right|^2+\left|c_2\right|^2}}\begin{pmatrix}c_1\\c_2\end{pmatrix}\exp\left(-\frac{r^2}{2d^2}+ik_0y\right) \tag{1.87}$$

where the coefficient c_i represent the initial pseudospin polarization. We suppose that d is much larger than the lattice constant of the graphene monolayer and therefore $\psi\left(\mathbf{r},0\right)$ is a smooth envelope function. Using the formalism we just developed we can express the time dependent wave function of the Gaussian wave packet as :

$$\psi_1\left(\mathbf{r},t\right)=\frac{1}{\sqrt{\left|c_1\right|^2+\left|c_2\right|^2}}\left(c_1\phi_1\left(\mathbf{r},t\right)-c_2\phi_2\left(-x,y,t\right)\right) \tag{1.88}$$

$$\psi_2\left(\mathbf{r},t\right)=\frac{1}{\sqrt{\left|c_1\right|^2+\left|c_2\right|^2}}\left(c_1\phi_1\left(\mathbf{r},t\right)+c_2\phi_2\left(\mathbf{r},t\right)\right) \tag{1.89}$$

where in the cylindrical coordinates basis:

$$\phi_1\left(\mathbf{r},t\right)=\frac{e^{-a^2/2}}{d\sqrt{\pi}}\int_0^\infty e^{-q^2/2}cos\left(qt\right)J_0\left(q\sqrt{r^2-a^2-2iay}\right)qdq \tag{1.90}$$

$$\phi_2(\mathbf{r},t) = \frac{e^{-a^2/2}}{d\sqrt{\pi}} \int_0^\infty e^{-q^2/2} \frac{x+a+iy}{\sqrt{r^2-a^2-2iay}} sin(qt)\, J_1\left(q\sqrt{r^2-a^2-2iay}\right) qdq \tag{1.91}$$

where J_0 and J_1 are Bessel functions and a is the dimensionless parameter $a = k_0 d$.

Now that the formalism in which the study of the dynamics of a Gaussian wave packet will be performed is properly defined, we will study the ZB effect and the influence of the initial pseudospin polarization. This will give us a good basis on which to relay for the study of the dynamics in non homogeneous Dirac systems.

Let us first consider the case when the lower component of the initial wave function is zero i.e. $c_1 = 1$ and $c_2 = 0$. The physical meaning of this initial condition is that the electron is at $t = 0$ located on the sublattice A. The dynamical wave function can be expressed using (1.88) and (1.89) as :

$$\Psi(\mathbf{r},t) = \begin{pmatrix} \phi_1(\mathbf{r},t) \\ \phi_2(\mathbf{r},t) \end{pmatrix} \tag{1.92}$$

In Figure (1.11) we represent the evolution of the total (sum of sublattices A and B) electron density for $d = 0.5\mu m$ and $a = 1$ at different times. One can see that the wave packet splits in two parts moving in opposite directions. The electron density is therefore symmetric with respect to y. Note that y is a particular direction since we introduce the initial wave vector along it (see (1.87)). As the time of the simulation increases, the width of both parts of the packet increase equally due to the effect of dispersion. Also the ZB effect can here be observed through the non conservation of the x symmetry. Indeed the total symmetry does not respect the x inversion symmetry due to oscillation of the packet along the x direction. We will not study deeper the properties of those oscillations since it is slightly outside of the framework

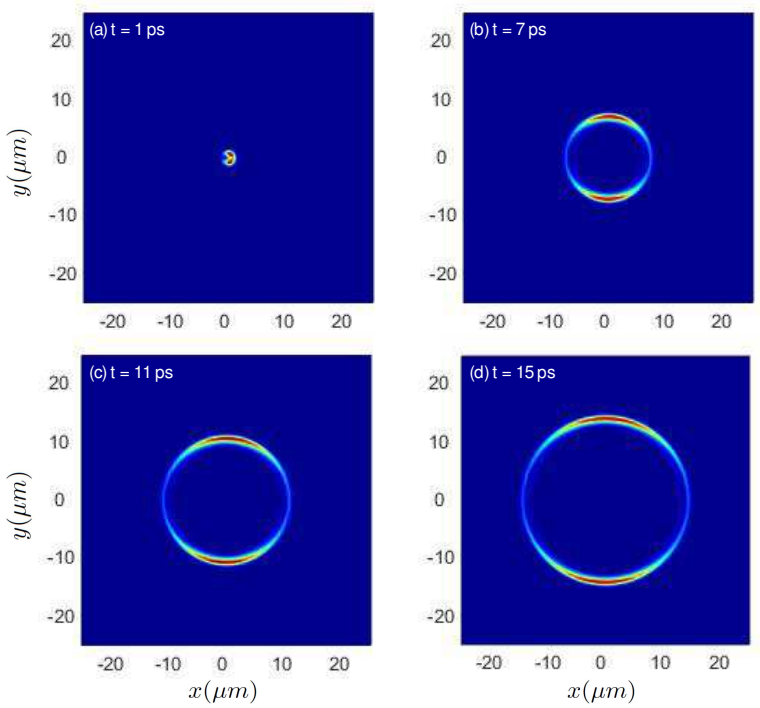

Figure 1.11 – Electron probability density for an initial wavepacket in the pseudospin configuration $c_1 = 1$ and $c_0 = 0$. The other parameters are $d = 0.5\mu m$ and $a = 1$.

of this thesis, the reader should just note that non expected break of the symmetry in the further simulations will most likely be due to ZB effect.

We now consider another initial pseudospin polarization, $c_1 = c_2 = 1$. Then as previously the dynamical wave function can be expressed as :

$$\Psi(\mathbf{r}, t) = \frac{1}{\sqrt{2}} \begin{pmatrix} \phi_1(\mathbf{r}, t) - \phi_2(-x, y, t) \\ \phi_1(\mathbf{r}, t) + \phi_2(\mathbf{r}, t) \end{pmatrix} \tag{1.93}$$

In Figure (1.12) we plot with the same parameters as previously the total electron density. One can see that one of the similarities with the previous case is that the wave packet splits in two part along y, therefore the symmetry along this axis is conserved. The density distribution along x clearly shows

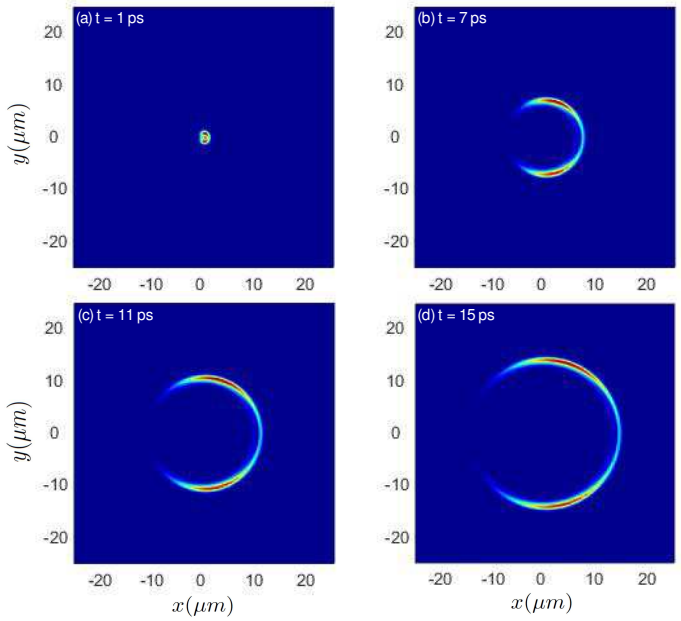

Figure 1.12 – Electron probability density for an initial wavepacket in the pseudospin configuration $c_1 = 1$ and $c_0 = 1$. The other parameters are $d = 0.5\mu m$ and $a = 1$.

that the maximum is displaced in the positive direction, meaning that the packet center moves along the x axis. This motion can be tuned using the initial parameters of the wave packet i.e. if the initial width of the wave packet is increased the velocity of motion of its center is decreased. It is not difficult to show that as in other two-band systems, the phenomenon of ZB in graphene is a result of an interference of states corresponding to positive and negative eigenenergies of Hamiltonian. For wide enough packet and at the moment when the ZB disappears, two split parts of initial wave packet move along y axis with opposite velocities. In this situation the subpackets moving in the positive and negative directions consist of the states with positive and negative energies correspondingly.

We will finally study the case where the initial pseudospin is defined as $c_1 = 1$ and $c_2 = i$. The dynamical wave function can be expressed as

$$\Psi(\mathbf{r},t) = \frac{1}{\sqrt{2}} \begin{pmatrix} \phi_1(\mathbf{r},t) - i\phi_2(-x,y,t) \\ i\phi_1(\mathbf{r},t) + \phi_2(\mathbf{r},t) \end{pmatrix} \tag{1.94}$$

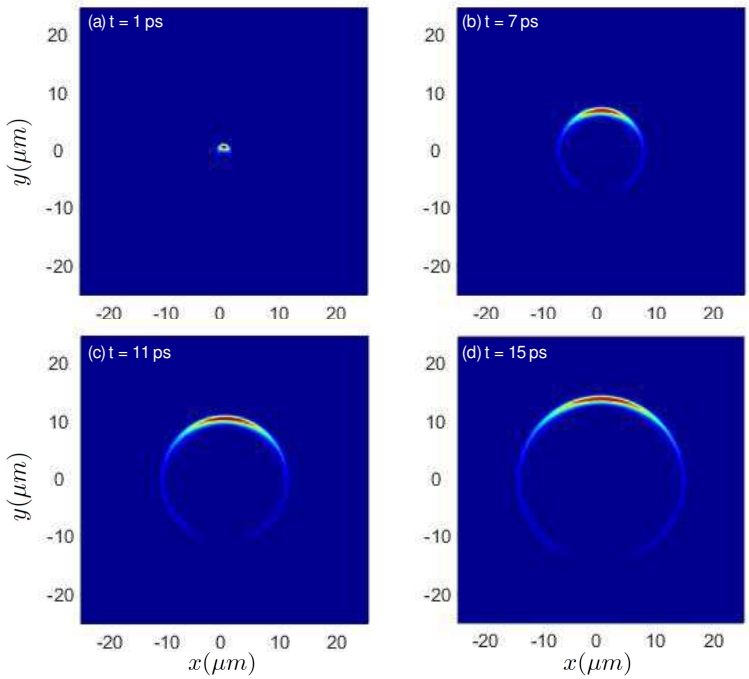

Figure 1.13 – Electron probability density for an initial wavepacket in the pseudospin configuration $c_1 = 1$ and $c_0 = i$. The other parameters are $d = 0.5\mu m$ and $a = 1$.

This case is quite different from the previous ones as we can see on Figure (1.13) plotted with the same parameters as previously. The wave packet here does not split into two parts. One can show by expressing (1.94) in its expanded form that the highly dominant contribution is the eigenenergy state corresponding to the propagation in the positive direction along y axis. Moreover in the case of wide initial packets, almost all the states belong to the positive branch of energy, the wave packet can therefore be considered as propagating along y axis and the ZB effect does not break any symmetry.

In light of all the possible initial conditions, the Gaussian wave packet

simulation in graphene is an excellent tool to study the ZB effect but not only. Using this basis we will perform, in the second part of this thesis simulations allowing us to see if the dynamics of the electrons, in more elaborated systems, actually fit with our predictions.

2. Optically induced Lifshitz transition in bilayer graphene

2.1. Introduction

In the last decades, the achievements in the laser technology and microwave techniques have made possible the control of various structures with a high-frequency electromagnetic field (dressing field), which is based on the Floquet theory of periodically driven quantum systems (Floquet engineering) [38–40, 143]. As a consequence, the study of condensed-matter structures strongly coupled to light has become an excited field of modern physics with the objective to find unique exploitable features. Particularly, electronic properties of various nanostructures coupled to a dressing field — including quantum wells [44–49], quantum rings [50–53], graphene [11, 12, 54–59, 141], topological insulators [60–63, 112], etc — are currently in the focus of attention. Developing this scientific trend in the present paper, we elaborated the theory to control the topology of the Fermi surface of bilayer graphene (BLG) with a dressing field.

BLG is the two-dimensional material consisting of two graphene monolayers, which excite enormous interest of the condensed-matter community during last years [113, 114]. In contrast to usual graphene monolayer with the linear (Dirac) electron dispersion [3, 66], the characteristic electronic properties of BLG are the massive chiral electrons and the so-called trigonal warping — the triangular perturbation of the circular iso-energetic lines near the band edge. As a consequence, the Fermi surface of BLG near the

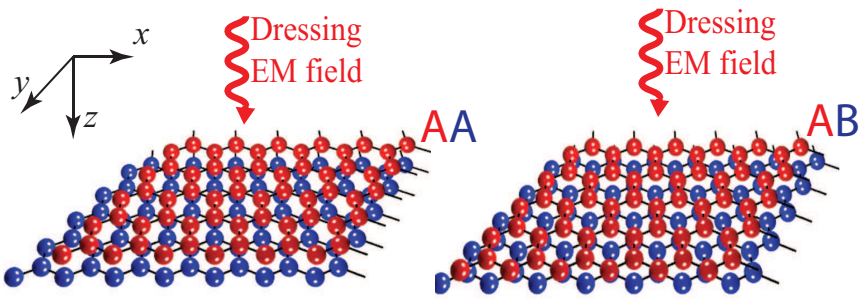

Figure 2.1 – (Color online) Sketch of the system under consideration: AA-stacked and AB-stacked bilayer graphene subjected to an electromagnetic wave (dressing EM field) propagating perpendicularly to the graphene plane.

band edge consists of several electron "pockets" which are very sensitive to external impacts. Particularly, the gate voltage or uniform mechanical stress crucially changes the structure of the pockets. This results in the Lifshitz phase transition — the abrupt change in the topology of the Fermi surface [115–118]. Although a strong electromagnetic field is actively studied in last years as a tool to control electronic properties of BLG — to induce the valley currents [119, 120], to create the Floquet topological insulator [121], to produce additional Dirac points [122], etc — the optical control of the Lifshitz transition in BLG still await for consideration. The present paper is aimed to fill partially this gap in the theory.

The paper is organized as follows. In Sec. II, we apply the conventional Floquet theory to derive the effective Hamiltonian describing stationary properties of electrons in irradiated BLG. In Sec. III, we discuss the dependence of renormalized electronic characteristics of the irradiated BLG on parameters of the dressing field. The last Sec. IV contain the Conclusion and Acknowledgments.

2.2. Model

There are the two different crystal structures of BLG, which are known as a AA-stacked and AB-stacked BLG [113, 114] (see Fig. 1). Since electronic properties of BLG strongly depends on the stacking geometry, let us consider these two structures successively. For the case of the AB-stacked BLG, its low-energy electronic states are described by the four-band Hamiltonian [113]

$$\hat{\mathcal{H}}'_{AB} = \begin{pmatrix} 0 & v_1\pi^\dagger & 0 & v_3\pi \\ v_1\pi & 0 & t_1 & 0 \\ 0 & t_1 & 0 & v_1\pi^\dagger \\ v_3\pi^\dagger & 0 & v_1\pi & 0 \end{pmatrix}, \tag{2.1}$$

where $\pi = \xi p_x + ip_y$, $p_{x,y}$ is the electron momentum in the BLG plane, $\xi = \pm 1$ is the valley index corresponding to the electron states in the two different K-points of the Brillouin zone, $K_\xi = (4\xi\pi/3a, 0)$, a is the interatomic distance, $v_{1,3} = \sqrt{3}at_{1,3}/2\hbar$ are the characteristic electron velocities, t_1 and t_3 are the characteristic energies of the interatomic electron hopping in the BLG plane and between the two graphene layers, correspondingly. Eliminating electron orbitals related to dimer sites, the Hamiltonian (2.1) can be reduced to the two-band effective Hamiltonian [113]

$$\hat{\mathcal{H}}_{AB} = -\alpha \begin{pmatrix} 0 & \left(\pi^\dagger\right)^2 \\ \pi^2 & 0 \end{pmatrix} + v_3 \begin{pmatrix} 0 & \pi \\ \pi^\dagger & 0 \end{pmatrix}, \tag{2.2}$$

where $\alpha = -1/2m - v_3 a/4\sqrt{3}\hbar$ and $m = t_1/2v_1^2$ is the effective electron mass. The effective Hamiltonian (2.2) describes the most interesting low-energy electronic properties of AB-stacked BLG — particularly, massive chiral electrons and trigonal warping [113, 123] — and, therefore, will be used by us in the following analysis. To describe the interaction between electrons in BLG and a dressing EM field within the conventional minimal coupling approach, we have to make the replacement, $\mathbf{p} \to \mathbf{p} - e\mathbf{A}$, in the

Hamiltonian (2.2), where $\mathbf{A} = (A_x, A_y)$ is the vector potential of the dressing field. Assuming the EM wave to be propagating perpendicularly to the BLG plane (see Fig. 1), the vector potential can be written as

$$\mathbf{A} = \frac{E_0}{\omega}(\cos\theta\cos\omega t, \sin\theta\sin\omega t), \tag{2.3}$$

where ω is the frequency of the EM wave, E_0 is the amplitude of the wave, and the angle θ defines the polarization of the EM wave: The angles $\theta = 0$ and $\theta = 0\pi/2$ correspond the two linear polarizations, whereas the angles $\theta = \pi/4$ and $\theta = -\pi/4$ correspond to the two circular polarizations. Then the time-dependent Hamiltonian (2.2) can be rewritten as

$$\hat{\mathcal{H}}_{AB}(t) = \hat{\mathcal{H}}_0 + \left[\sum_{n=1}^{\infty} \hat{V}_n e^{in\omega t} + \text{H.c.}\right], \tag{2.4}$$

where the time-independent part is

$$\hat{\mathcal{H}}_0 = \hat{\mathcal{H}}_{AB} - \frac{\alpha e^2 E_0^2}{2\omega^2}\begin{pmatrix} 0 & \cos 2\theta \\ \cos 2\theta & 0 \end{pmatrix}, \tag{2.5}$$

and the two first harmonics are

$$\begin{aligned}\hat{V}_1 = {} & \frac{\alpha|e|E_0\sqrt{2}}{\omega}\left[\begin{pmatrix} 0 & p_x\cos(\theta+\xi\pi/4) \\ -p_x\cos(\theta-\xi\pi/4) & 0 \end{pmatrix}\right. \\ & \left. + \begin{pmatrix} 0 & ip_y\sin(\theta-\xi\pi/4) \\ -ip_y\sin(\theta+\xi\pi/4) & 0 \end{pmatrix}\right] \\ & + \frac{v_3|e|E_0}{\sqrt{2}\omega}\begin{pmatrix} 0 & \sin(\theta+\xi\pi/4) \\ -\sin(\theta-\xi\pi/4) & 0 \end{pmatrix},\end{aligned} \tag{2.6}$$

$$\hat{V}_2 = -\frac{\alpha e^2 E_0^2}{2\omega^2}\begin{pmatrix} 0 & \sin^2(\theta-\xi\pi/4) \\ \sin^2(\theta+\xi\pi/4) & 0 \end{pmatrix}. \tag{2.7}$$

Applying the standard Floquet-Magnus approach [**?**,124,125] to renormalize the time-dependent Hamiltonian (2.4) and restricting the consideration by

the terms $\sim 1/\omega^2$, we arrive at the effective time-independent Hamiltonian

$$\begin{aligned}\hat{\mathcal{H}}_{\text{eff}} &= \hat{\mathcal{H}}_0 + \sum_{n=1}^{\infty} \frac{\left[\hat{V}_n, \hat{V}_n^{\dagger}\right]}{\hbar n\omega} \\ &+ \sum_{n=1}^{\infty} \frac{\left[\left[\hat{V}_n, \hat{\mathcal{H}}_0\right], \hat{V}_n^{\dagger}\right] + \text{H.c.}}{2(\hbar n\omega)^2}.\end{aligned} \tag{2.8}$$

To rewrite the Hamiltonian (3.48) in the dimensionless form, let us introduce the dimensionless electron momentum, $\mathbf{p} \to \mathbf{p}/(v_3/\alpha)$, and the dimensionless electron energy, $\varepsilon \to \varepsilon/(v_3^2/\alpha)$. Then the dimensionless Hamiltonian (3.48) depends only on the two dimensionless parameters, $\delta_1 = |e|E_0\alpha/v_3\omega$ and $\delta_2 = v_3^2/\alpha\hbar\omega$. Physically, the first of them is the ratio of the period-averaged momentum adsorbed by an electron from the dressing field, $|e|E_0/\omega$, and the characteristic trigonal-warping momentum, v_3/α. The second one is the ratio of the characteristic trigonal-warping energy, v_3^2/α, and the photon energy, $\hbar\omega$. If the dressing field is high-frequency enough, the both parameters, δ_1 and δ_2, are small. Correspondingly, we can write the Hamiltonian as an expansion on the the small parameter, $\delta_1\delta_2 \ll 1$. Then the dimensionless Hamiltonian (3.48) in the vicinity of the K_ξ-point ($p < 1$) reads

$$\hat{\mathcal{H}}_{\text{eff}} = \hat{\mathcal{H}}_{AB} + \mathbf{g}(\mathbf{p})\boldsymbol{\sigma}, \tag{2.9}$$

where $\boldsymbol{\sigma} = (\sigma_x, \sigma_y, \sigma_z)$ is the Pauli matrix vector, and $\mathbf{g}(\mathbf{p}) = (g_x, g_y, g_z)$ is the vector with the components

$$
\begin{aligned}
g_x &= (\delta_1\delta_2)^2[p_y^2[\cos^2\theta - 3 - 4\xi p_x(4\cos^2\theta - 1) - 4p^2\cos^2\theta] \\
&+ p_x^2(5 - 8\xi p_x + 4p^2)\sin^2\theta - \xi p_x \sin^2\theta] - \frac{\delta_1^2}{2}\cos 2\theta, \\
g_y &= \frac{(\delta_1\delta_2)^2}{2}[2p_y[\cos^2\theta + 2p^2(3 - 2\cos^2\theta)] \\
&+ 2\xi p_x p_y(2\cos^2\theta + 6 + 12\xi p_x \cos 2\theta + 4p^2)], \\
g_z &= \frac{\xi\delta_1^2\delta_2}{2}(1 - 4p^2)\sin 2\theta.
\end{aligned}
$$

As to the case of the AA-stacked BLG, its low-energy electronic states are described by the four-band Hamiltonian [114]

$$
\hat{\mathcal{H}}'_{AA} = \begin{pmatrix} 0 & v_0\pi^\dagger & t_1 & 0 \\ v_0\pi & 0 & 0 & t_1 \\ t_1 & 0 & 0 & v_0\pi^\dagger \\ 0 & t_1 & v_0\pi & 0 \end{pmatrix}, \tag{2.10}
$$

where t_1 is the interlayer hopping constant and v_0 is the electron velocity in monolayer graphene. Diagonalizing the Hamiltonian (2.10), we arrive at the electron energy spectrum,

$$
\varepsilon = \pm t_1 \pm v_0 p, \tag{2.11}
$$

which exhibits the two monolayer graphene dispersions, $\varepsilon = \pm v_0 p$, shifted with respect to each other by the twice interlayer hopping constant, $2t_1$. It should be stressed that the interlayer hopping direction of the AA-stacked BLG is orthogonal to the polarization vector of the normally incident dressing field. As a consequence, the dressing field does not affect the interlayer coupling in BLG and renormalizes electronic properties of each monolayer independently. Therefore, the effect of the dressing field on the AA-stacked

BLG can be reduced to the known problem of dressed graphene monolayer [12]. Since the electromagnetic dressing of graphene monolayer does not lead to the Lifshitz transition, we will focus the following analysis only on the AB-stacked BLG.

2.3. Results and Discussion

If the dressing field is linearly polarized along the x axis ($\theta = 0$), the Hamiltonian (2.9) reads

$$\begin{aligned}\hat{\mathcal{H}}_{\text{eff}} &= \sigma_x[\xi p_x + p_y^2[1-(\delta_1\delta_2)^2(2+12p_x+4p^2)] - \delta_1^2/2 \\ &- p_x^2] - \sigma_y[p_y(1-(\delta_1\delta_2)^2[1+2p^2]) + 2\xi p_x p_y \\ &\times (1-(\delta_1\delta_2)^2[4+6\xi p_x+4p^2])] + O(\delta_1^4\delta_2^4). \end{aligned} \tag{2.12}$$

Diagonalizing the Hamiltonian (2.12), we arrive at the energy spectrum of dressed electrons near the $K_\pm$ point, which is plotted in Fig. 2. In the absence of irradiation, the equi-energy map shows the four electron pockets near the $K_\pm$ point, which consist of one central pocket and three "leg" pockets (see Fig. 2a). These four pockets are positioned at the momenta $\mathbf{p} = 0$ and $\mathbf{p} = (\xi\cos(2n\pi/3), \sin(2n\pi/3))$, where $n = 0, 1, 2$. The dressing field distorts the pockets, shifting their position in the Brillouin zone (see Fig. 2b). Taking into account only the leading term of the Hamiltonian (2.12), we arrive at the equation,

$$(\delta_1^2/2 + p_x^2 - p_y^2 - \xi p_x)^2 + (p_y + 2\xi p_x p_y)^2 = 0,$$

describing the centers of the shifted pockets, p_x and p_y. This equation has the four solutions: The two ones correspond to the momenta $p_y = 0$ and $p_x = (\xi \pm \sqrt{1-2\delta_1^2})/2$, whereas the other two solutions are $\mathbf{p} = (-\xi/2, \pm\sqrt{2\delta_1^2+3}/2)$. It follows from this that the first two solutions approach each other with increasing the parameter δ_1 and merge at its critical value, $\delta_1' = 1/\sqrt{2}$. For $\delta_1 > \delta_1'$, the two electron pockets corresponding to

these merged solutions disappear (see Fig. 2c). It should be noted that the total valley Chern number, 2ξ, remains constant with the disappearance of the two pockets. Indeed, the central pocket of the bare bilayer graphene is characterized by the Chern number $-\xi$, whereas each of the three leg pockets has the Chern number ξ (see, e.g., Ref. 121). Under the influence of the dressing field, the central pocket "annihilates" with one of the leg pockets, which conserves the total Chern number. Since the "annihilation" of the two pockets changes the Fermi topology abruptly — from the quadruply-connected Fermi surface to the doubly-connected one — the Lifshitz transition takes place. It should be noted that it is similar to the Lifshitz transition in the strained bilayer graphene [115, 116]. Namely, the dressing field linearly polarized along the x axis effects on BLG similarly to an uniform strain applied along the same axis. As to experimental manifestation of the Lifshitz transition in bilayer graphene, it leads to the pronounced modification of the Landau levels in the presence of a magnetic field [115]. If the magnetic field, B, is weak enough, the inverse magnetic length, $\sqrt{\hbar/eB}$, is greater than the distance between the central electron pocket and the additional pockets pictured in Fig. 2 . In this case, electronic states in the different pockets are quantized by the magnetic field independently and the ground electronic state is 16-fold degenerated. As a consequence, the filling factor $\nu = 16$ appears in the quantum Hall conductance. After the Lifshitz transition, only two of four electron pockets survive. This lifts the additional degeneracy and the filling factor $\nu = 8$ will be observed in the Hall measurements. Thus, the Lifshitz transition leads to the possibility of optical control of quantum Hall effect, what can be observed in magnetotransport experiments.

In the case of circularly polarized dressing field ($\theta = \pi/4$), the effective Hamiltonian (2.9) reads

$$\hat{\mathcal{H}}_{\text{eff}} = \hat{\mathcal{H}}_{AB} + \frac{\xi\delta_1^2\delta_2}{2}(1 - 4p^2)\sigma_z + O(\delta_1^2\delta_2^2) \tag{2.13}$$

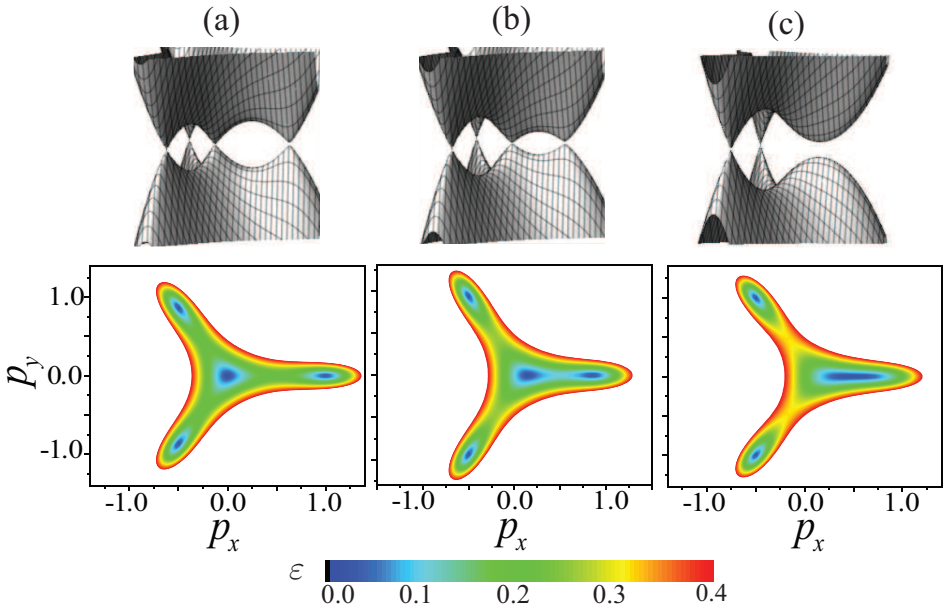

Figure 2.2 – (Color online) The three-dimensional plots of the electron energy spectrum of irradiated AB-stacked bilayer graphene, ε, near the band edge (top) and the corresponding equi-energy maps (bottom) for the linearly polarized dressing field with the photon energy $\hbar\omega = 25$ meV and different irradiation intensities, I: (a) $I = 0$ kW/cm^2, (b) $I = 10$ kW/cm^2, (c) $I = 45$ kW/cm^2.

and results in the dispersion equation,

$$\varepsilon^2 = \frac{\varepsilon_g^2}{4} + p^2(1-\varepsilon_g^2) - 2p^3\cos 3\phi + p^4(1+2\varepsilon_g^2), \tag{2.14}$$

where $\varepsilon_g = \sqrt{2}\delta_1^2\delta_2$ is the field-induced energy gap at the $K_\pm$ point. Opening the energy gap, the circularly polarized field effects on BLG similarly to the interlayer asymmetry induced by the gate voltage [116]. For the critical value of the energy gap, $\varepsilon_g = 1$, the term $\sim p^2$ in Eq. (2.14) vanishes and the electron dispersion is $\varepsilon = \pm\sqrt{0.25 - 2p^3\cos 3\phi}$, where ϕ is the polar angle in the BLG plane. At the Fermi energy $\varepsilon_F = 1/2$, this dispersion corresponds to the Fermi surface shown in Fig. 3a. The structure of the Fermi surface for different irradiation intensities, I, is shown in the phase diagram 3b. The critical point of the phase diagram — so-called monkey-saddle point [117] — corresponds to the critical energy gap, $\varepsilon_g = 1$. At this point, the Fermi surface is unstable with respect to small variations of both the Fermi energy and the irradiation intensity: It undergoes one of the four possible Lifshitz transitions depicted in Fig. 3b. Similarly to the case of linear polarization, the Lifshitz transition induced by the circularly polarized dressing field will manifest itself in magnetoconductance. Namely, the three separated pockets at the Fermi surface will lead to the filling factor $\nu = 12$ in the corresponding steps of quantum Hall conductivity. Moreover, it should be noted that the critical point pictured in Fig. 3b is characterized by the diverging density of states (DoS), which is similar to the conventional Van Hove singularity. Indeed, the density of states, ρ, in the vicinity of the critical point reads

$$\begin{aligned}\rho(\varepsilon) &= \frac{1}{(2\pi)^2}\int d^2\mathbf{p}\,\delta_1(\varepsilon - \sqrt{1/4 - 2p^2\cos 3\phi}) = \\ &= \frac{\sqrt{\varepsilon}}{9(2\pi)^2}\beta\left(\frac{1}{6},\frac{1}{2}\right)\left|\varepsilon^2 - \frac{1}{4}\right|^{-1/3},\end{aligned} \tag{2.15}$$

where $\beta(x,y)$ is the beta function (see the plot of the DoS in Fig. 3c). Since this DoS singularity leads to the instabilities of the system with respect to

arbitrary weak interactions [117], which can be observed experimentally.

It follows from the aforesaid that a dressing field can induce the Lifshitz transitions in BLG, which depend strongly on the field polarization. Though the Hamiltonians (2.12) and (2.13) were derived within the perturbation theory, the claimed phenomenon is qualitatively the same for any strength of the electron-field coupling. It should be stressed that the exact numerical solution of the Floquet-Magnus problem (2.4) leads to slightly shifted critical points of the Lifshitz transitions but does not affect their structure. As to experimental observation of the optically induced Lifshitz transition, a source of intense far-infrared radiation is required. Particularly, a source of the dressing field with the photon energy 25 meV must provide the output power of several mW in order to observe the effects pictured in Fig. 3. This output power has been reported for the quantum cascade lasers (see, e.g., Ref. 126) which look most appropriate for experimental observation of the discussed effects. It should be noted also that the absorption of the dressing field might provoke thermal fluctuations of electron gas. As a consequence, differentiation between different topological states can be complicated. In order to avoid this, an experimental set-up must include a high-efficient thermostat. Since the energy difference between different topological states pictured in Fig. 3 is of meV scale, the thermal fluctuations should be less than 1 K. Such a thermal stability can be provided by state-of-the-art experimental equipment. It should be noted also that the Fermi energy pictured in Fig. 3 can be modified experimentally by introducing doping on the sample. However, we have to take into account that an electromagnetic field can be considered as a dressing field within the conventional Floquet formalism if the collisional (Drude) absorption of the field by conduction electrons can be neglected (see, e.g., Refs. 46, 47). To neglect the Drude absorption of a high-frequency field in a doped sample, the well-known condition, $\omega\tau \gg 1$, should be satisfied. Since the doping of the sample decreases the mean free time of conduction electron, τ, the density of doping impurities should be small enough to satisfy this condition. Alternatively, the gate voltage can

be used to control the Fermi energy in bilayer graphene (see, e.g., Ref. 116).

2.4. Conclusion and acknowledgements

We demonstrated theoretically that a strong high-frequency electromagnetic field (dressing field) can be used as an effective tool to control topology of the Fermi surface of bilayer graphene (BLG). The discussed Lifshitz transition strongly depends on the polarization of the dressing field. Namely, the linearly polarized field can induce the Lifshitz transition from the quadruply-connected Fermi surface to the doubly-connected one, whereas the circularly polarized field induces the multicritical point, where the four different Fermi topologies may coexist. Physically, the linearly polarized field effects on BLG similarly to an uniform mechanical strain applied in the BLG plain along the polarization vector, whereas the circularly polarized field effects similarly to a gate voltage inducing the energy gap.

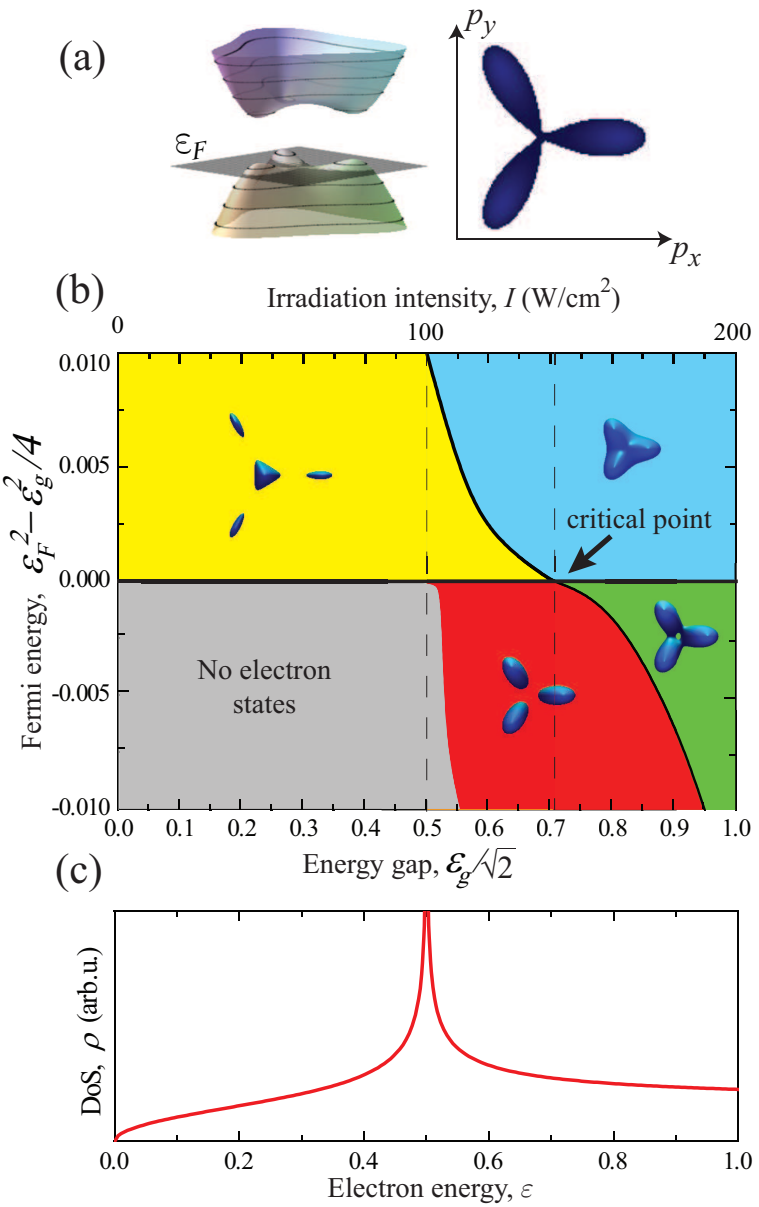

Figure 2.3 – (Color online) The electronic structure of irradiated AB-stacked bilayer graphene for the circularly polarized dressing field with the photon energy $\hbar\omega = 25$ meV: (a) Fermi surface at the monkey-saddle point; (b) Phase diagram of the Fermi surface topology; (c) Density of states spectrum near the monkey-saddle point.

3. All Optical control of band parameters of Gapped Dirac systems

3.1. Introduction

Advances in laser physics and microwave technique achieved in recent decades have made possible the use of high-frequency fields as tools of flexible control of various atomic and condensed-matter structures (so called "Floquet engineering" based on the Floquet theory of periodically driven quantum systems [**?**, 38–41]). As a consequence, the properties of electronic systems driven by oscillating fields are actively studied to exploit unique features of composite states of field and matter. Particularly, electron strongly coupled to electromagnetic field — also known as "electron dressed by field" (dressed electron) — has become a commonly used model in modern physics [42, 43]. Recently, the physical properties of dressed electrons were studied in various nanostructures, including quantum wells [44–49], quantum rings [50–53], graphene [11, 12, 54–59], and topological insulators [60–64].

The discovery of graphene — a monolayer of carbon atoms with linear (Dirac) dispersion of electrons [3, 65, 66] — initiated studies of the new class of artificial nanostructures known as Dirac materials. While graphene by itself is characterized by the gapless electron energy spectrum, many efforts have been dedicated towards fabrication Dirac materials with the band gap between the valence and conduction bands (gapped Dirac materials). The electron energy spectrum of the materials is parabolic near band edges but turns into the linear Dirac dispersion if the band gap vanishes. Therefore,

electronic properties of gapped Dirac materials substantially depend on the value of the gap and, consequently, are perspective for nanoelectronic applications [67–69]. Although dressed condensed-matter structures are in focus of attention for a long time, a consistent quantum theory of the gapped Dirac materials strongly coupled to light was not elaborated before. Since the electronic structure of Dirac materials differs crucially from conventional condensed-matter structures, the known theory of light-matter coupling cannot be directly applied to the gapped Dirac materials. Moreover, it should be noted that gapped Dirac materials are currently considered as a basis for new generation of optoelectronic devices. Therefore, their optical properties deserve special consideration. This motivated us to fill this gap in the theory. To solve this problem in the present study, we will focus on the two gapped Dirac materials pictured schematically in Fig. 1. First of them is the graphene layer grown on a hexagonal boron nitride substrate [70, 71], where the band gap can be tuned in the broad range with an external gate voltage [8] (see Fig. 1a). The second is a transition metal dichalchogenide (TMDC) which is a monolayer of atomically thin semiconductor of the type MX_2, where M is a transition metal atom (Mo, W, etc.) and X is a chalcogen atom (S, Se, or Te) [72, 73] (see Fig. 1b). The specific feature of the TMDC compounds is the giant spin-orbit coupling [74, 75] which is attractive for using in novel spintronic and valleytronic devices [76]. Formally, electronic properties of these materials near the band edge can be described by the same two-band Hamiltonian

$$\hat{\mathcal{H}} = \begin{pmatrix} \varepsilon^c_{\tau s} & \gamma(\tau k_x - i k_y) \\ \gamma(\tau k_x + i k_y) & \varepsilon^v_{\tau s} \end{pmatrix}, \tag{3.1}$$

where $\mathbf{k} = (k_x, k_y)$ is the electron wave vector in the layer plane, γ is the parameter describing electron dispersion,

$$\varepsilon^c_{\tau s} = \frac{\Delta_g}{2} + \frac{\tau s \Delta^c_{so}}{2} \tag{3.2}$$

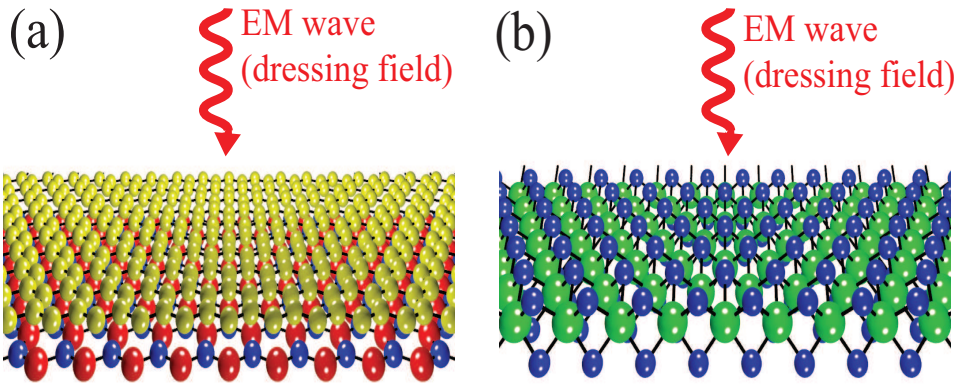

Figure 3.1 – (Color online) Sketch of the considered gapped Dirac materials subject to electromagnetic wave (dressing field): (a) Graphene grown on the substrate of hexagonal boron nitride; (b) Transition metal dichalcogenide monolayer MoS_2.

is the energy of the conduction band edge,

$$\varepsilon^{v}_{\tau s} = -\frac{\Delta_g}{2} - \frac{\tau s \Delta^{v}_{so}}{2} \tag{3.3}$$

is the energy of the valence band edge, Δ_g is the band gap between the conduction band and the valence band, $\Delta^{c,v}_{so}$ is the spin-orbit splitting of the conduction (valence) band, $s = \pm 1$ is the spin index describing the different spin orientations, and $\tau = \pm 1$ is the valley index which corresponds to the two valleys in the different points of the Brillouin zone (the K and K' valleys in graphene [3] and the K and $-K$ valleys in TMDC monolayers [75]). If $\Delta_g \neq 0$ and $\Delta^{c,v}_{so} \neq 0$, the Hamiltonian (3.4) describes TMDC monolayer [75]. In the case of zero spin-orbit splitting, $\Delta^{c,v}_{so} = 0$, the Hamiltonian (3.4) describes gapped graphene [70], whereas the case of $\Delta_g = \Delta^{c,v}_{so} = 0$ corresponds to usual gapless graphene [3]. It should be noted that the two-band Hamiltonian (3.1) describes successfully low-energy electron states near the band edge. As to omitted terms corresponding to the trigonal-

warping deformation of electron bands in monolayer graphene, they can be neglected if the Rashba spin-orbit coupling is stronger than the intrinsic spin-orbit coupling [77]. In the present paper, we elaborate the theory of electromagnetic dressing for electronic systems described by the low-energy Hamiltonian (3.1) and demonstrate that both the band gap and the spin splitting can be effectively controlled with the dressing field.

The paper is organized as follows. In the Section II, we apply the conventional Floquet theory to derive the effective Hamiltonian describing stationary properties of dressed electrons. In the Section III, we discuss the dependence of renormalized electronic characteristics of the dressed materials on parameters of the dressing field. The last two Sections contain conclusion and acknowledgements.

3.2. Model

Let us consider a gapped Dirac material with the Hamiltonian (3.1), which lies in the plane (x, y) at $z = 0$ and is subjected to an electromagnetic wave propagating along the z axis (see Fig. 1). The frequency of the wave, ω, is assumed to be far from all resonant frequencies of the electron system. Therefore, the electromagnetic wave cannot be absorbed by electrons near band edge and should be considered as a dressing field for the states around $\mathbf{k} = 0$. Considering the electron-field interaction within the minimal coupling approach, properties of dressed electrons can be described by the Hamiltonian

$$\begin{aligned}\hat{\mathcal{H}}(\mathbf{k}) &= \begin{pmatrix} 0 & |e|\gamma(\tau A_x - iA_y)/\hbar \\ |e|\gamma(\tau A_x + iA_y)/\hbar & 0 \end{pmatrix} \\ &+ \begin{pmatrix} \varepsilon^c_{\tau s} & \gamma(\tau k_x - ik_y) \\ \gamma(\tau k_x + ik_y) & \varepsilon^v_{\tau s} \end{pmatrix}, \end{aligned} \tag{3.4}$$

which can be easily obtained from the Hamiltonian of "bare" electrons (3.1) with the replacement $\mathbf{k} \to \mathbf{k} - (e/\hbar)\mathbf{A}$, where $\mathbf{A} = (A_x, A_y)$ is the vector po-

tential of the dressing field, and e is the electron charge. It should be noted that the quantum electrodynamics predicts the quadratic (in the vector potential) additions to the Hamiltonian (3.4) [78, 79]. To avoid complication of the model, we will assume that the considered dressing field is classically strong and can be described successfully with the minimal coupling. In what follows, we will show that the properties of dressed electrons strongly depend on the polarization of the dressing field. Therefore, we have to discuss the solution of the corresponding Schrödinger problem for different polarizations successively.

Linearly polarized dressing field.— Assuming the dressing field to be linearly polarized along the x axis, the vector potential can be written as

$$\mathbf{A} = \left(\frac{E_0}{\omega}\cos\omega t, 0\right), \tag{3.5}$$

where E_0 is the electric field amplitude, and ω is the wave frequency. Correspondingly, the Hamiltonian of the dressed electron system (3.4) can be rewritten formally as

$$\hat{\mathcal{H}}(\mathbf{k}) = \hat{\mathcal{H}}_0 + \hat{\mathcal{H}}_{\mathbf{k}}, \tag{3.6}$$

where

$$\hat{\mathcal{H}}_0 = \begin{pmatrix} 0 & \Omega\tau\hbar\omega/2 \\ \Omega\tau\hbar\omega/2 & 0 \end{pmatrix}\cos\omega t \tag{3.7}$$

is the Hamiltonian of electron-field interaction,

$$\hat{\mathcal{H}}_{\mathbf{k}} = \begin{pmatrix} \Delta_g/2 + \tau s\Delta_{so}^c/2 & \gamma(\tau k_x - ik_y) \\ \gamma(\tau k_x + ik_y) & -\Delta_g/2 - \tau s\Delta_{so}^v/2 \end{pmatrix} \tag{3.8}$$

is the Hamiltonian of "bare" electron, and

$$\Omega = \frac{2\gamma|e|E_0}{(\hbar\omega)^2} \tag{3.9}$$

is the dimensionless parameter describing the strength of electron coupling to the dressing field. The nonstationary Schrödinger equation with the Hamil-

tonian (3.7),

$$i\hbar\frac{\partial\psi_0}{\partial t} = \hat{\mathcal{H}}_0\psi_0, \tag{3.10}$$

describes the time evolution of electron states at the band edge ($\mathbf{k} = 0$). The two exact solutions of the Schrödinger problem (3.10) read as

$$\psi_0^{\pm} = \frac{1}{\sqrt{2}}\begin{pmatrix}1\\ \pm 1\end{pmatrix}\exp\left[\mp\frac{i\Omega\tau\sin\omega t}{2}\right]. \tag{3.11}$$

Since the two wave functions (3.11) form a complete basis at any fixed time t, we can seek solutions of the nonstationary Schrödinger equation with the full Hamiltonian (3.6) as an expansion

$$\psi_{\mathbf{k}} = a_1(t)\psi_0^{+} + a_2(t)\psi_0^{-}. \tag{3.12}$$

Substituting the expansion (3.12) into the Schrödinger equation,

$$i\hbar\frac{\partial\psi_{\mathbf{k}}}{\partial t} = \hat{\mathcal{H}}(\mathbf{k})\psi_{\mathbf{k}}, \tag{3.13}$$

we arrive at the expressions

$$\begin{aligned}
i\hbar\dot{a}_1(t) &= \left[\frac{\varepsilon^c_{\tau s}+\varepsilon^v_{\tau s}}{2} + \gamma\tau k_x\right]a_1(t)\\
&+ \left[\frac{\varepsilon^c_{\tau s}-\varepsilon^v_{\tau s}}{2} + i\gamma k_y\right]e^{i\Omega\tau\sin\omega t}a_2(t),\\
i\hbar\dot{a}_2(t) &= \left[\frac{\varepsilon^c_{\tau s}+\varepsilon^v_{\tau s}}{2} - \gamma\tau k_x\right]a_2(t)\\
&+ \left[\frac{\varepsilon^c_{\tau s}-\varepsilon^v_{\tau s}}{2} - i\gamma k_y\right]e^{-i\Omega\tau\sin\omega t}a_1(t).
\end{aligned} \tag{3.14}$$

It follows from the conventional Floquet theory of quantum systems driven by an oscillating field [**?**, 38, 39] that the sought wave function (3.12) must have the form $\Psi(\mathbf{r},t) = e^{-i\tilde{\varepsilon}(\mathbf{k})t/\hbar}\phi(\mathbf{r},t)$, where the function $\phi(\mathbf{r},t)$ periodically depends on time, $\phi(\mathbf{r},t) = \phi(\mathbf{r},t+2\pi/\omega)$, and $\tilde{\varepsilon}(\mathbf{k})$ is the quasi-energy of an electron. Since the quasi-energy (the energy of dressed electron) is the

physical quantity which plays the same role in quantum systems driven by an oscillating field as the usual energy in stationary ones, the present analysis of the Schrödinger problem (3.13) should be aimed to find the energy spectrum, $\tilde{\varepsilon}(\mathbf{k})$. It follows from the periodicity of the function $\phi(\mathbf{r},t)$ that one can seek the coefficients $a_{1,2}(t)$ in Eq. (3.12) as a Fourier expansion,

$$a_{1,2}(t) = e^{-i\tilde{\varepsilon}(\mathbf{k})t/\hbar} \sum_{n=-\infty}^{\infty} a_{1,2}^{(n)} e^{in\omega t}. \tag{3.15}$$

Substituting the expansion Eq. (3.15) into the Eqs. (3.14) and applying the Jacobi-Anger expansion,

$$e^{iz\sin\theta} = \sum_{n=-\infty}^{\infty} J_n(z) e^{in\theta},$$

one can rewrite the equations of quantum dynamics (3.14) in the time-independent form,

$$\sum_{n'=-\infty}^{\infty} \sum_{j=1}^{2} \mathcal{H}_{ij}^{(nn')} a_j^{(n')} = \tilde{\varepsilon}(\mathbf{k}) a_i^{(n)}, \tag{3.16}$$

where $J_n(z)$ is the Bessel function of the first kind, and $\mathcal{H}_{ij}^{(nn')}$ is the stationary Hamiltonian of dressed electron in the Floquet space with the matrix elements

$$\begin{aligned}
\mathcal{H}_{12}^{(nn')} &= \left[\frac{\varepsilon_{\tau s}^{c} - \varepsilon_{\tau s}^{v}}{2} + i\gamma k_y\right] J_{n'-n}(\Omega\tau), \\
\mathcal{H}_{21}^{(nn')} &= \left[\frac{\varepsilon_{\tau s}^{c} - \varepsilon_{\tau s}^{v}}{2} - i\gamma k_y\right] J_{n'-n}(\Omega\tau), \\
\mathcal{H}_{11}^{(nn')} &= \left[\frac{\varepsilon_{\tau s}^{c} + \varepsilon_{\tau s}^{v}}{2} + \gamma\tau k_x + n\hbar\omega\right] \delta_{nn'}, \\
\mathcal{H}_{22}^{(nn')} &= \left[\frac{\varepsilon_{\tau s}^{c} + \varepsilon_{\tau s}^{v}}{2} - \gamma\tau k_x + n\hbar\omega\right] \delta_{nn'},
\end{aligned} \tag{3.17}$$

where $\delta_{nn'}$ is the Kronecker delta. It should be noted that the Schrödinger equation (3.16) describes still exactly the initial Schrödinger problem (3.13). Next we will make some approximations.

In what follows, let us assume that the field frequency, ω, is high enough to satisfy the condition

$$\left| \frac{\mathcal{H}_{ij}^{(0n)}}{\mathcal{H}_{ii}^{(00)} - \mathcal{H}_{jj}^{(nn)}} \right| \ll 1 \tag{3.18}$$

for $n \neq 0$ and $i \neq j$. Mathematically, the condition (3.18) makes it possible to treat nondiagonal matrix elements of the Hamiltonian (3.17) with $n \neq n'$ as a small perturbation which can be omitted in the first-order approximation of the conventional perturbation theory for matrix Hamiltonians (see, e.g., Ref. 80). Since the condition (3.18) corresponds to an off-resonant field, the field can be neither absorbed nor emitted by the electrons. As a consequence, the main contribution to the Schrödinger equation (3.16) under the condition (3.18) stems from terms with $n, n' = 0$, which describe the elastic interaction between an electron and the field. Neglecting the small terms with $n, n' \neq 0$, the Schrödinger equation (3.16) can be rewritten in the simple form

$$\sum_{j=1}^{2} \mathcal{H}_{ij}^{(00)} a_j^{(0)} = \tilde{\varepsilon}(\mathbf{k}) a_i^{(0)}, \tag{3.19}$$

where $\mathcal{H}_{ij}^{(00)}$ is the 2×2 Hamiltonian with the matrix elements (3.17). Subjecting this Hamiltonian to the unitary transformation

$$U = \frac{1}{\sqrt{2}} \begin{pmatrix} 1 & 1 \\ 1 & -1 \end{pmatrix},$$

we arrive at the effective stationary Hamiltonian of electrons dressed by a linearly polarized field, $\hat{\mathcal{H}}_{\text{eff}} = U^{\dagger} \mathcal{H}^{(00)} U$, which is given by the matrix

$$\hat{\mathcal{H}}_{\text{eff}}(\mathbf{k}) = \begin{pmatrix} \widetilde{\Delta}_g/2 + \tau s \widetilde{\Delta}_{so}^{c}/2 & \tau \tilde{\gamma}_x k_x - i \tilde{\gamma}_y k_y \\ \tau \tilde{\gamma}_x k_x + i \tilde{\gamma}_y k_y & -\widetilde{\Delta}_g/2 - \tau s \widetilde{\Delta}_{so}^{v}/2 \end{pmatrix}, \tag{3.20}$$

where

$$\widetilde{\Delta}_g = \Delta_g J_0(\Omega) \tag{3.21}$$

is the effective band gap,

$$\widetilde{\Delta}^c_{so} = \frac{\Delta^c_{so} - \Delta^v_{so}}{2} + \frac{\Delta^c_{so} + \Delta^v_{so}}{2} J_0(\Omega) \tag{3.22}$$

is the effective spin splitting of the conduction band,

$$\widetilde{\Delta}^v_{so} = \frac{\Delta^v_{so} - \Delta^c_{so}}{2} + \frac{\Delta^c_{so} + \Delta^v_{so}}{2} J_0(\Omega) \tag{3.23}$$

is the effective spin splitting of the valence band, and

$$\tilde{\gamma}_x = \gamma, \quad \tilde{\gamma}_y = \gamma J_0(\Omega) \tag{3.24}$$

are the effective parameters of electron dispersion along the x, y axes. The eigenenergy of the effective Hamiltonian (3.20),

$$\begin{aligned} \tilde{\varepsilon}^{\pm}_{\tau s}(\mathbf{k}) &= \frac{\tau s(\widetilde{\Delta}^c_{so} - \widetilde{\Delta}^v_{so})}{4} \\ &\pm \sqrt{\left[\frac{2\widetilde{\Delta}_g + \tau s(\widetilde{\Delta}^c_{so} + \widetilde{\Delta}^v_{so})}{4}\right]^2 + \tilde{\gamma}_x^2 k_x^2 + \tilde{\gamma}_y^2 k_y^2}, \end{aligned} \tag{3.25}$$

is the sought energy spectrum of electrons dressed by the linearly polarized field. Mathematically, the unperturbed Hamiltonian (3.1) is equal to the effective Hamiltonian (3.20) with the formal replacements $\Delta_g \to \widetilde{\Delta}_g$, $\Delta^{c,v}_{so} \to \widetilde{\Delta}^{c,v}_{so}$, $\gamma_{x,y} \to \tilde{\gamma}_{x,y}$. Therefore, the behavior of a dressed electron is similar to the behavior of a "bare" electron with the renormalized band parameters (3.21)–(3.24). It should be noted that the effective Hamiltonian (3.20) is derived under the condition (3.18). Taking into account Eqs. (3.17), the condition (3.18) can be rewritten as $\gamma k, \Delta_g \ll \hbar\omega$. Therefore, the effective Hamiltonian is applicable to describe the dynamics of dressed electron near the band edge if the photon energy of the dressed field, $\hbar\omega$, substantially

exceeds the band gap, Δ_g.

Circularly polarized dressing field.— For the case of circularly polarized electromagnetic wave, the vector potential $\mathbf{A} = (A_x, A_y)$ can be written as

$$\mathbf{A} = \left(\frac{E_0}{\omega} \cos \xi\omega t, \frac{E_0}{\omega} \sin \xi\omega t \right), \tag{3.26}$$

where the different chirality indices $\xi = \pm 1$ correspond to the clockwice/counterclockwise circular polarizations. First of all, let us consider electron states at the wave vector $\mathbf{k} = 0$, where the Hamiltonian (3.4) can be written in the form

$$\hat{\mathcal{H}}(0) = \begin{pmatrix} \varepsilon^c_{\tau s} & -(\hbar\omega\Omega\tau/2)e^{-i\tau\xi\omega t} \\ -(\hbar\omega\Omega\tau/2)e^{i\tau\xi\omega t} & \varepsilon^v_{\tau s} \end{pmatrix}, \tag{3.27}$$

which is similar to the well-known Hamiltonian of magnetic resonance. The corresponding nonstationary Schrödinger equation,

$$i\hbar \frac{\partial \psi_{\tau s}(0)}{\partial t} = \hat{\mathcal{H}}(0)\psi_{\tau s}(0), \tag{3.28}$$

describes the time evolution of electron states at the wave vector $\mathbf{k} = 0$. Solutions of the equation (3.28) can be sought as

$$\psi^{\pm}_{\tau s}(0) = e^{-i\tilde{\varepsilon}^{\pm}_{\tau s}(0)t/\hbar} \begin{pmatrix} A_{\pm} e^{-i\tau\xi\omega t/2} \\ B_{\pm} e^{i\tau\xi\omega t/2} \end{pmatrix} e^{\pm i\tau\xi\omega t/2}, \tag{3.29}$$

where $\tilde{\varepsilon}^{\pm}_{\tau s}(0)$, $A_{\pm}$ and $B_{\pm}$ are the undefined constants. Substituting the wave function (3.29) into the Schrödinger equation (3.28) with the Hamiltonian (3.27), we arrive at the system of two algebraic equations,

$$\begin{aligned} A_{\pm} \left[\varepsilon^c_{\tau s} - \tau\xi \frac{\hbar\omega}{2}(1 \mp 1) - \tilde{\varepsilon}^{\pm}_{\tau s}(0) \right] - B_{\pm} \frac{\hbar\omega\Omega\tau}{2} = 0, \\ A_{\pm} \frac{\hbar\omega\Omega\tau}{2} - B_{\pm} \left[\varepsilon^v_{\tau s} + \tau\xi \frac{\hbar\omega}{2}(1 \pm 1) - \tilde{\varepsilon}^{\pm}_{\tau s}(0) \right] = 0, \end{aligned} \tag{3.30}$$

which can be easily solved. As a result, the two orthonormal exact solutions

of the Schrödinger problem (3.28) are

$$\begin{aligned}\psi^{\pm}_{\tau s}(0) &= e^{-i\tilde{\varepsilon}^{\pm}_{\tau s}(0)t/\hbar}e^{\pm i\tau\xi\omega t/2} \\ &\times \begin{pmatrix} \mp\left[\frac{\sqrt{\Omega^2+\delta^2}\pm|\delta|}{2\sqrt{\Omega^2+\delta^2}}\right]^{1/2} e^{-i\tau\xi\omega t/2} \\ \mathrm{sgn}(\delta)\left[\frac{\sqrt{\Omega^2+\delta^2}\mp|\delta|}{2\sqrt{\Omega^2+\delta^2}}\right]^{1/2} e^{i\tau\xi\omega t/2}\end{pmatrix},\end{aligned} \tag{3.31}$$

where

$$\tilde{\varepsilon}^{\pm}_{\tau s}(0) = \frac{\varepsilon^{c}_{\tau s}+\varepsilon^{v}_{\tau s}}{2} \pm \tau\xi\frac{\hbar\omega}{2} \pm \mathrm{sgn}(\delta)\frac{\hbar\omega}{2}\sqrt{\Omega^2+\delta^2} \tag{3.32}$$

is the quasienergy (energy of dressed electron in the conduction/valence band) at $\mathbf{k}=0$, and

$$\delta = \frac{\varepsilon^{c}_{\tau s}-\varepsilon^{v}_{\tau s}-\tau\xi\hbar\omega}{\hbar\omega}$$

is the resonance detuning assumed to be nonzero in order to avoid the field absorption near the band edge. Correspondingly, the effective stationary Hamiltonian of dressed electron states at $\mathbf{k}=0$ can be written in the basis (3.31) as

$$\hat{\mathcal{H}}_{\mathrm{eff}}(0) = \begin{pmatrix} \tilde{\varepsilon}^{+}_{\tau s}(0) & 0 \\ 0 & \tilde{\varepsilon}^{-}_{\tau s}(0)\end{pmatrix}. \tag{3.33}$$

In order to find the energy spectrum of dressed electron at the wave vector $\mathbf{k}\neq 0$, let us restrict the consideration by the case of $\Omega \ll 1$, which corresponds physically to high frequencies ω [see Eq. (3.9)]. Expanding the electron wave function, $\psi_{\tau s}(\mathbf{k})$, on the basis (3.31),

$$\psi_{\tau s}(\mathbf{k}) = a^{+}(t)e^{i\tilde{\varepsilon}^{+}_{\tau s}(0)t/\hbar}\psi^{+}_{\tau s}(0) + a^{-}(t)e^{i\tilde{\varepsilon}^{-}_{\tau s}(0)t/\hbar}\psi^{-}_{\tau s}(0), \tag{3.34}$$

and substituting the expansion (3.34) into the Schrödinger equation with the total Hamiltonian (3.4), we arrive at the system of equations

$$\begin{aligned} i\hbar\dot{a}^{+}(t) &\approx \tilde{\varepsilon}^{+}_{\tau s}(0)a^{+}(t) - \mathrm{sgn}(\delta)\gamma(\tau k_x - ik_y)a^{-}(t), \\ i\hbar\dot{a}^{-}(t) &\approx \tilde{\varepsilon}^{-}_{\tau s}(0)a^{-}(t) - \mathrm{sgn}(\delta)\gamma(\tau k_x + ik_y)a^{+}(t). \end{aligned} \tag{3.35}$$

The quantum dynamics equations (3.35) are equal to the stationary Schrödinger

equation,

$$i\hbar\frac{\partial}{\partial t}\begin{pmatrix}a^{+}(t)\\ a^{-}(t)\end{pmatrix}=\hat{\mathcal{H}}_{\text{eff}}(\mathbf{k})\begin{pmatrix}a^{+}(t)\\ a^{-}(t)\end{pmatrix},$$

where

$$\hat{\mathcal{H}}_{\text{eff}}(\mathbf{k})=\begin{pmatrix}\tilde{\varepsilon}^{+}_{\tau s}(0) & -\text{sgn}(\delta)\gamma(\tau k_x-ik_y)\\ -\text{sgn}(\delta)\gamma(\tau k_x+ik_y) & \tilde{\varepsilon}^{-}_{\tau s}(0)\end{pmatrix}. \tag{3.36}$$

is the effective stationary Hamiltonian of the considered system. The eigenenergy of the Hamiltonian,

$$\tilde{\varepsilon}^{\pm}_{\tau s}(\mathbf{k})=\frac{\tilde{\varepsilon}^{+}_{\tau s}(0)+\tilde{\varepsilon}^{-}_{\tau s}(0)}{2}\pm\sqrt{\left[\frac{\tilde{\varepsilon}^{+}_{\tau s}(0)-\tilde{\varepsilon}^{-}_{\tau s}(0)}{2}\right]^2+(\gamma k)^2}, \tag{3.37}$$

presents the sought energy spectrum of dressed electrons. If $\Delta_g=\Delta^{c,v}_{so}=0$, Eq. (3.37) exactly coincides with the known spectrum of electrons in gapless graphene irradiated by a circularly polarized light [12]. It follows from Eq. (3.37) that the renormalized band gap is

$$\begin{aligned}\widetilde{\Delta}_g&=\tau\xi\hbar\omega+\text{sgn}\left(\Delta_g-\tau\xi\hbar\omega\right)\hbar\omega\sqrt{\Omega^2+\left[\frac{\Delta_g-\tau\xi\hbar\omega}{\hbar\omega}\right]^2}\\ &\approx\tau\xi\hbar\omega-\sqrt{\Omega^2+1}\left(\tau\xi\hbar\omega-\frac{\Delta_g}{\Omega^2+1}\right),\end{aligned} \tag{3.38}$$

where the last equality holds under condition $\hbar\omega\gg\Delta_g$. The spin splittings in the conduction and valence bands can be written in simple form for the two limiting cases:

$$\widetilde{\Delta}^{c,v}_{so}=\pm\frac{\Delta^{c}_{so}-\Delta^{v}_{so}}{2}+\frac{\Delta^{c}_{so}+\Delta^{v}_{so}}{2\sqrt{1+\Omega^2}},\quad\hbar\omega\gg\Delta_g, \tag{3.39}$$

and

$$\widetilde{\Delta}_{so}^{c,v} = \pm\frac{\Delta_{so}^{c} - \Delta_{so}^{v}}{2} + \frac{\Delta_{so}^{c} + \Delta_{so}^{v}}{2}\left[1 - \frac{\Omega^2}{2}\frac{(\hbar\omega)^2}{\Delta_g^2}\right],$$
$$\hbar\omega \ll \Delta_g. \tag{3.40}$$

As expected, the renormalized band gap (3.38) and spin splittings (3.39)–(3.40) turn into their "bare" values, Δ_g and $\Delta_{so}^{c,v}$, if the dressing field is absent ($E_0 \to 0$).

Elliptically polarized dressing field.— Assuming the large axis of polarization ellipse to be oriented along the x axis, the vector potential of arbitrary polarized electromagnetic wave, $\mathbf{A} = (A_x, A_y)$, can be written as

$$\mathbf{A} = \frac{E_0}{\omega}\Big(\cos\omega t,\, \sin\theta\sin\omega t\Big), \tag{3.41}$$

where $\theta \in [-\pi/2, \pi/2]$ is the polarization phase: the polarization is linear for $\theta = 0$, circular for $\theta = \pm\pi/2$, and elliptical for other phases θ. Substituting the vector potential (3.41) into Eq. (3.4), we can write the total Hamiltonian (3.4) as

$$\hat{\mathcal{H}}(\mathbf{k}) = \hat{\mathcal{H}}_{\mathbf{k}} + \left(\hat{V}e^{i\omega t} + \hat{V}^{\dagger}e^{-i\omega t}\right), \tag{3.42}$$

where the Hamiltonian $\hat{\mathcal{H}}_{\mathbf{k}}$ is given by Eq. (3.8) and

$$\hat{V} = \frac{\hbar\omega\Omega}{4}\begin{pmatrix} 0 & \tau - \sin\theta \\ \tau + \sin\theta & 0 \end{pmatrix}. \tag{3.43}$$

is the operator of electron interaction with the dressing field (3.41). Generally, the effective stationary Hamiltonian of an electron driven by an oscillating field can be sought in the form [**?**]

$$\hat{\mathcal{H}}_{\text{eff}}(\mathbf{k}) = e^{i\hat{F}(t)}\hat{\mathcal{H}}(\mathbf{k})e^{-i\hat{F}(t)} + i\left(\frac{\partial e^{i\hat{F}(t)}}{\partial t}\right)e^{-i\hat{F}(t)}, \tag{3.44}$$

where $\hat{F}(t)$ is the anti-Hermitian operator which is periodical with the period of the oscillating field, $\hat{F}(t) = \hat{F}(t + 2\pi/\omega)$. In the particular case of weak electron-field coupling, $\Omega \ll 1$, this operator and the effective Hamiltonian (3.44) can be easily found as power series expansions,

$$\hat{F}(t) = \sum_{n=1}^{\infty} \frac{F^{(n)}(t)}{\omega^n}, \qquad \hat{\mathcal{H}}_{\text{eff}}(\mathbf{k}) = \sum_{n=0}^{\infty} \frac{\hat{\mathcal{H}}_{\text{eff}}^{(n)}(\mathbf{k})}{\omega^n}, \tag{3.45}$$

where $F^{(n)}(t) \sim \Omega^n$ (the Floquet-Magnus expansion [**?**]). Substituting the expansions (3.45) into Eq. (3.44) and restricting the accuracy by terms $\sim \Omega^2$, we arrive at the effective Hamiltonian

$$\hat{\mathcal{H}}_{\text{eff}}(\mathbf{k}) = \hat{\mathcal{H}}_{\mathbf{k}} + \frac{\left[\hat{V}, \hat{V}^{\dagger}\right]}{\hbar\omega} + \frac{[[\hat{V}, \hat{\mathcal{H}}_{\mathbf{k}}], \hat{V}^{\dagger}] + h.c.}{2(\hbar\omega)^2}. \tag{3.46}$$

Taking into account Eqs. (3.8) and (3.43), the effective stationary Hamiltonian (3.46) can be written as a matrix (3.20), where

$$\widetilde{\Delta}_g = \Delta_g \left[1 - \frac{\Omega^2}{4}(1 + \sin^2\theta)\right] - \frac{\tau\hbar\omega\Omega^2}{2}\sin\theta, \tag{3.47}$$

$$\begin{aligned} \widetilde{\Delta}_{so}^{c,v} &= \pm\frac{\Delta_{so}^c - \Delta_{so}^v}{2} + \frac{\Delta_{so}^c + \Delta_{so}^v}{2} \\ &\times \left[1 - \frac{\Omega^2}{4}\left(1 + \sin^2\theta\right)\right], \end{aligned} \tag{3.48}$$

$$\tilde{\gamma}_x = \gamma\left[1 - \frac{\Omega^2}{4}\sin^2\theta\right], \quad \tilde{\gamma}_y = \gamma\left[1 - \frac{\Omega^2}{4}\right] \tag{3.49}$$

are the band parameters renormalized by an elliptically polarized dressing field. Correspondingly, the eigenenergy of the effective Hamiltonian (3.46)

represents the sought energy spectrum of dressed electrons,

$$\tilde{\varepsilon}^{\pm}_{\tau s}(\mathbf{k}) = \frac{\tau s(\widetilde{\Delta}^{c}_{so} - \widetilde{\Delta}^{v}_{so})}{4} \pm \sqrt{\left[\frac{2\widetilde{\Delta}_g + \tau s(\widetilde{\Delta}^{c}_{so} + \widetilde{\Delta}^{v}_{so})}{4}\right]^2 + \tilde{\gamma}_x^2 k_x^2 + \tilde{\gamma}_y^2 k_y^2}, \tag{3.50}$$

with the renormalized band parameters (3.47)–(3.49). It should be stressed that the effective Hamiltonian (3.20) with the band parameters (3.47)–(3.49), which describes electrons dressed by an arbitrary polarized weak field, is derived under assumption of small coupling constant (3.9) and high frequency, ω. On the contrary, the effective Hamiltonian (3.20) with the band parameters (3.21)–(3.24 and the effective Hamiltonian (3.33) are suitable to describe electrons dressed by linearly and circularly polarized dressing fields of arbitrary intensity. As a consequence, the band parameters (3.21)–(3.24) and (3.38)–(3.39) turn into the band parameters (3.47)–(3.49) for $\Omega \ll 1$, $\hbar\omega \gg \Delta_g$, and $\theta = 0, \pm\pi/2$.

3.3. Results and Discussion

First of all, let us apply the developed theory to gapped graphene, assuming $\widetilde{\Delta}^{c,v}_{so} = 0$ in all derived expressions. The electron dispersion in gapped graphene, $\tilde{\varepsilon}(\mathbf{k})$, is plotted in Fig. 2 for the particular cases of linearly and circularly polarized dressing field. It the absence of the dressing field, the electron dispersion is isotropic in the graphene plane (see the solid lines in Figs. 2a and 2b). However, a linearly polarized field breaks the equivalence of the x, y axes [see Eq. (3.25)]. As a consequence, the anisotropy of the electron dispersion along the wave vectors k_x and k_y appears (see the dashed and dotted lines in Figs. 2a and 2b). In contrast to the linear polarization, a circularly polarized dressing field does not induce the in-plane anisotropy [see Eq. (3.37)]. However, the electron dispersion is substantially different for clockwise and counterclockwise polarizations (see the dashed and dotted

lines in Fig. 2c). Moreover, both linearly and circularly polarized field renormalizes the band gap (see Fig. 3). Mathematically, the dependence of the renormalized band gap, $|\widetilde{\Delta}_g|$, on the irradiation intensity, $I \sim E_0^2$, is given by Eqs. (3.21) and (3.38) [which are plotted in Fig. 3a] and Eq. (3.47) [which is plotted in Fig. 3b]. It should be noted that Eq. (3.38) correctly describes the gap for any off-resonant frequencies ω, whereas Eqs. (3.21) and (3.47) are derived under the condition $\hbar\omega \gg \Delta_g$ and, therefore, applicable only to small gaps. However, the gap can be gate-tunable in the broad range, $\Delta_g = 1 - 60$ meV [8, 70, 71]. Assuming the gap to be of meV scale and the field frequency to be in the terahertz range, we can easily satisfy this condition. It follows from Eqs. (3.21), (3.32) and (3.47) that the renormalized gap, $\widetilde{\Delta}_g$, crucially depends on the field polarization. Particularly, the clockwise/counterclockwise circularly polarized field (polarization indices $\xi = \pm 1$) differently interacts with electrons from different valleys of the Brillouin zone (valley indices $\tau = \pm 1$). Namely, for the case of $\tau\xi = -1$, the value of the gap monotonously increases with intensity (see the dashed line in Fig. 3a). On the contrary, for the case of $\tau\xi = 1$, the gap first decreases to zero and then starts to grow (see the solid line in Fig. 3a). This light-induced difference in the band gaps for the two different valleys is formally equivalent to the appearance of an effective magnetic field acting on the valley pseudospin and, therefore, can be potentially used in valleytronics applications. It should be noted that this optically-induced lifting of valley degeneracy has been observed for TMDC in the recent experiments [81] which are in reasonable agreement with the present theory. As to linearly polarized dressing field, it always quenches the band gap and can even turn it into zero (see the dotted line in Fig. 3a). Formally, the collapse of the band gap originates from zeros of the Bessel function in Eq. (3.21). Since the linearly and circularly polarized fields change the gap value oppositely, there are field polarizations which do not change the gap. The polarization phases, θ, corresponding to such polarizations are marked by the dashed lines in Fig. 3b.

Applying the elaborated theory to analyze the renormalized spin splitting

in TMDC monolayers, let us restrict the consideration by the most examined TMDC monolayer MoS_2. The dependence of the spin splitting on the dressing field is described by Eqs. (3.22)–(3.23) for the case of linearly polarized field, Eqs. (3.39)–(3.40) for the case of circularly polarized field, and Eq. (3.48) for an arbitrary polarized field. It follows from analysis of these expressions that the most pronounced renormalization of the splitting takes place for a circularly polarized field. The dependence of the renormalized spin splitting in the conduction band of MoS_2 monolayer, $|\widetilde{\Delta}^c_{so}|$, on the field intensity, $I \sim E_0^2$, is plotted in Fig. 4 for such a field. It is seen in Fig. 4 that the renormalized splitting depends on the product of the polarization and valley indices, $\tau\xi = \pm 1$, and can be turned into zero by a dressing field. Physically, the renormalization of both band gap and spin splitting is the result of mixing electron states from the valence and conduction bands by the field. Therefore, the renormalized band parameters strongly depends on the value of the "bare" band gap, Δ_g. In contrast to gapped graphene with band gaps of meV scale, TMDC monolayers have band gaps of eV scale [75]. As a consequence, the considered terahertz photons effect on the wide band gaps of TMDC very weakly (in contrast to the previously considered case of narrow-gapped graphene). Therefore, the main expected effect of the considered low-energy dressing field on electronic structure of TMDC is the renormalization of spin splitting. It follows from this also that the irradiation intensity which collapses the spin splitting in TMDCs monolayers (see Fig. 4) is really large than the intensity collapsing the band gap in gapped graphene (see Fig. 3a).

It should be noted that the similar optically-induced spin splitting was recently observed experimentally in GaAs [82]. However, the one-band energy spectrum of conduction electrons in GaAs differs crucially from the electron spectrum of gapped Dirac materials describing by the two-band Hamiltonian (3.1). Therefore, the known theory of optically-induced spin splitting for electrons with simple parabolic dispersion — including both the recent paper [82] and the classical article [83] — cannot by applied directly to the

materials under consideration. One has to take also into account that optical properties of TMDC are dominated by excitons [84, 85]. To avoid the influence of excitons on the discussed dressing-field effects, the photon energy, $\hbar\omega$, should be less than the binding exciton energy (which is typically of hundreds of meV in TMDC).

From viewpoint of experimental observability of the discussed phenomena, it should be noted that all dressing-field effects increase with increasing the intensity of the dressing field. However, an intense irradiation can melt a condensed-matter sample. To avoid the melting, it is reasonable to use narrow pulses of a strong dressing field. This well-known methodology has been elaborated long ago and commonly used to observe various dressing effects — particularly, modifications of energy spectrum of dressed electrons arisen from the optical Stark effect — in semiconductor structures (see, e.g., Refs. 86–88). Within this approach, giant dressing fields (up to GW/cm^2) can be applied to the structures. It should be noted also that we consider the electromagnetic wave as a purely dressing field which cannot be absorbed by electrons. This is correct under the condition $\omega\tau \ll 1$, where τ is the mean free time of electron (see, e.g., Ref. 46). The increasing of temperature decreases the time τ because of the strengthening of the electron-phonon scattering. Therefore, the temperature should be low enough to meet the aforementioned condition.

3.4. Conclusion

We showed that the electromagnetic dressing can be used as an effective tool to control various electronic properties of gapped Dirac materials, including the band gap in gapped graphene and the spin splitting in TMDC monolayers. Particularly, both the band gap and the spin splitting can be closed by a dressing field. It is demonstrated that the strong polarization dependence of the renormalized band parameters appears. Namely, a linearly polarized field decreases the band gap, whereas a circularly polarized field can both decrease and increase one. It is found also that a circularly

polarized field breaks equivalence of valleys in different points of the Brillouin zone, since the renormalized band parameters depend on the valley index. As a consequence, the elaborated theory creates a physical basis for novel electronic, spintronic and valleytronic devices operated by light.

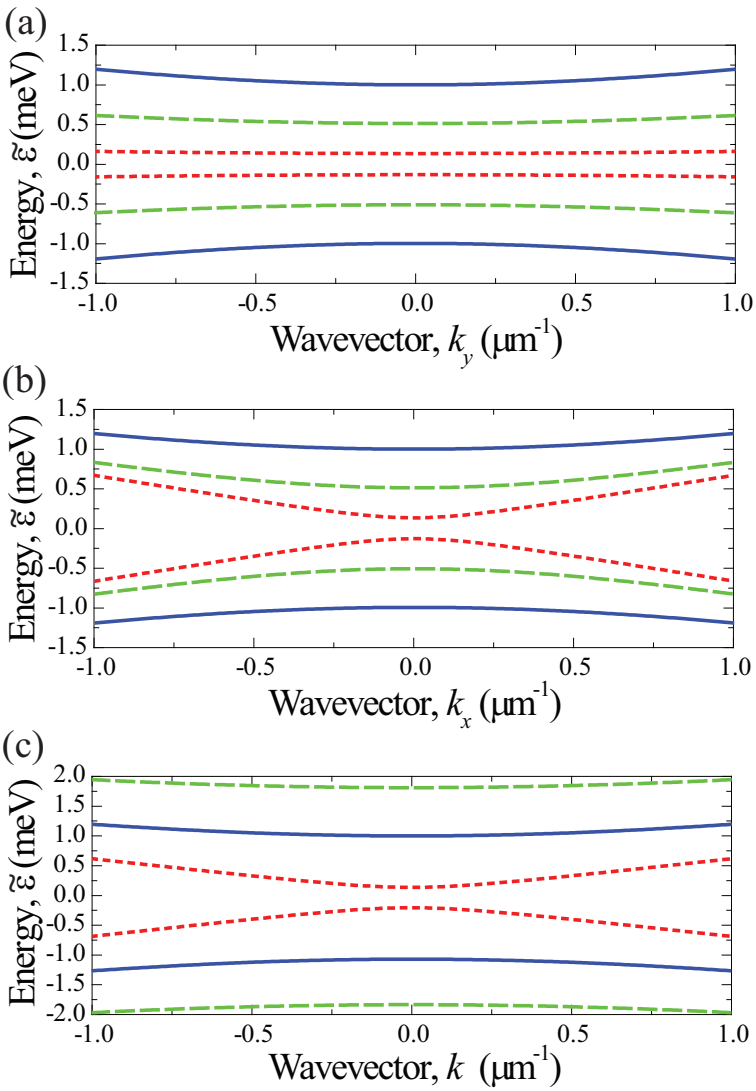

Figure 3.2 – (Color online) The energy spectrum of dressed electron, $\tilde{\varepsilon}(\mathbf{k})$, near the band edge of gapped graphene ($\Delta_g = 2$ meV, $\gamma/\hbar = 10^6$ m/s) irradiated by a dressing field with the photon energy $\hbar\omega = 10$ meV and the different intensities, I. In the parts (a) and (b): the dressing field is linearly polarized along the x axis; the irradiation intensities are $I = 0$ (solid lines), $I = 7.5$ kW/cm^2 (dashed lines), $I = 15$ kW/cm^2 (dotted lines). In the part (c): the dressing field is circularly polarized; the solid line describes the energy spectrum of "bare" electron ($I = 0$), whereas the dotted and dashed lines correspond to the different circular polarizations ($\tau\xi = -1$ and $\tau\xi = 1$, respectively) with the same irradiation intensity $I = 300$ W/cm^2.

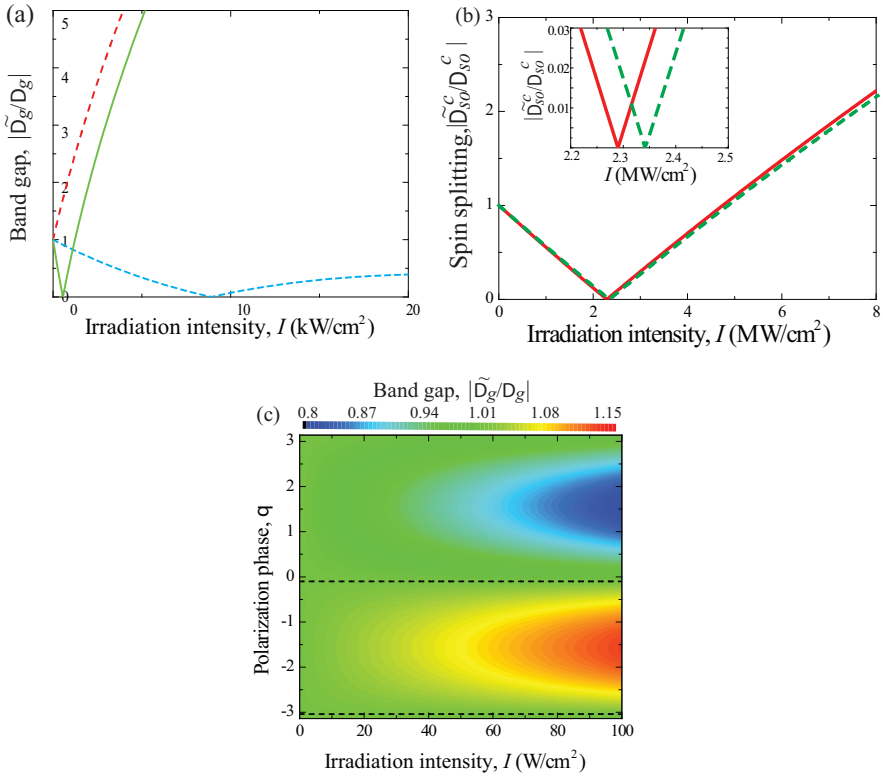

Figure 3.3 – (Color online) Dependence of the band gap in irradiated gapped graphene ($\Delta_g = 2$ meV, $\gamma/\hbar = 10^6$ m/s) on the irradiation intensity, I, and the polarization, θ, for the photon energy $\hbar\omega = 10$ meV. In the part (a): the dotted line corresponds to the linearly polarized dressing field, whereas the dashed and solid lines correspond to the different circular polarizations ($\tau\xi = -1$ and $\tau\xi = 1$, respectively). In the part (b): the dashed lines correspond to the polarizations, θ, which do not change the band gap.(c) Dependence of the spin-splitting on the irradiation intensity for the conduction band of a MoS_2 monolayer ($\Delta_g = 1.58$ eV, $\Delta^c_{so} = 3$ meV, $\Delta^v_{so} = 147$ meV, $\gamma/\hbar = 7.7 \times 10^5$ m/s) irradiated by a circularly polarized field with the photon energy $\hbar\omega = 10$ meV. The solid and dashed lines correspond to the different field polarizations ($\tau\xi = -1$ and $\tau\xi = 1$, respectively)

4. Optical Trapping of Electrons in graphene

Since the experimental discovery of graphene, its unique electronic properties continue to attract an increasing interest of the scientific community [1]. The spectrum of the electronic states around K and K' points in the Brillouin zone consists of a pair of touching Dirac cones, and thus mimics the dispersion of massless relativistic Fermions. This fact has dramatic consequences on the transport properties of graphene, one of which is Klein tunneling: the perfect transmission of gapless Dirac electrons through arbitrary potential barriers at normal incidence[2, 89].

Being extremely interesting from the point of view of fundamental physics, Klein tunneling nevertheless poses serious problems for a wide range of practical applications of graphene where confinement of electrons is necessary. To circumvent this obstacle, a variety of methods has been proposed. They include chemical functionalization [90,91], mechanical cutting of the graphene sheet into nanoribbons or nanodisks [92] and application of local strain resulting in the onset of an artificial gauge field [93,94]. Most of those methods, however, need irreversible modification of the graphene sheet and do not allow for a controllable tuning of the trapping parameters such as the strength of confinement.

In the present paper we explore an alternative way to achieve the trapping of massless Dirac electrons using fully optical means. Optical trapping is a standard way of the preparation of cold atom lattices (see e.g. Refs. [95, 96]

for the review) and the confinement of nanoparticles by optical tweezers (see e.g. Ref. [97] and references therein). In the domain of condensed matter, the basis for the optical trapping is provided by the possibility to modify the energy spectrum of a material system by strong coupling to the high- frequency laser radiation resulting in the dynamic Stark effect. Dramatic modifications of the transport properties in the regime of strong light- matter coupling were reported for semiconductor quantum wells [44, 47–49, 98], carbon nanostructures [12, 59, 60, 102, 138, 139, 141], topological insulators [61–63, 112] and others.

In particular, it was shown that in graphene strongly coupled to circular polarized light the topological bandgap Δ_g opens [103–105] . Its value depends on the intensity I and frequency ω of the driving field and can thus be reversibly changed in a controllable way. In realistic configurations i.e in the infra-red scale, a bandgap up to 1 meV can be open.

This effect can be exploited for the trapping of Dirac electrons in graphene. Indeed, consider the case when the intensity of the driving field is not homogeneous and has a minimum in real space at $r = 0$, having for example a reverse Gaussian profile. In this situation the effective bandgap induced by light- matter coupling will be minimal in the center of the dip and increase if one deviates further from it as is shown in the Fig. 4.1(a). This will confine the low energy electrons in the region around $r = 0$. The mechanism of the confinement is similar to that obtained in semiconductor heterostructures when a layer of narrow band semiconductor is sandwiched between wide gap semiconductors with the only difference being that the band mismatch in our case is produced all optically.

One way to get the desired Gaussian dip is to shine a sample of graphene with a broad Gaussian and another Gaussian beam with a much smaller radius. The latter can be passed through a filter where its phase is shifted by π. Negative interference thus leads to a Gaussian dip on the graphene plane.

In theory, since Maxwell's equations are linear, any superposition of solu-

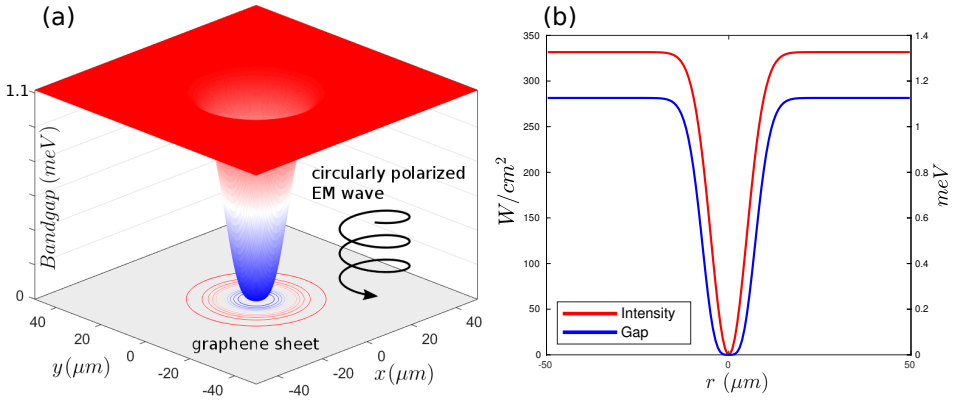

Figure 4.1 – **(a)** The profile of the bandgap in real space induced by an inhomogeneous high-frequency electromagnetic field with the intensity having a Guassian dip. The value of the optically induced gap is proportional to the intensity of the dressing field, so electrons become trapped in the region where intensity is minimal. **(b)** A combined diagram showing the dependence of the illumination intensity on the distance from the minimum ans the bandgap which is opened as a consequence.

tions is also a solution. The beam used here is a superposition of a gaussian and a homogeneous wave so it naturally obeys the Maxwell's equations.

4.1. The model

Let us consider a monolayer of graphene, which lies in the plane $\mathbf{r} = (x, y)$ at $z = 0$ and interacts with an electromagnetic wave propagating along the z-axis. The frequency of the wave ω is assumed to be high enough to satisfy the condition $\omega\tau \gg 1$, where τ is a characteristic relaxation time in the system. In this case, the electromagnetic wave can not be absorbed around the Dirac points and should be considered as a pure dressing field. The low-energy Hamiltonian of the system reads:

$$\hat{\mathcal{H}}(t) = \hbar v_F \left[\xi \sigma_x \left(k_x + \frac{eA_x(t)}{\hbar} \right) + \sigma_y \left(k_y + \frac{eA_y(t)}{\hbar} \right) \right] \tag{4.1}$$

where v_F is the Fermi velocity, ξ the valley index and σ_i, $i = x, y$, are the Pauli matrices and $\xi = \pm 1$ is a valley factor. The interaction with

external electromagnetic radiation was introduced via the minimal coupling substitution, $k_{x,y} \to k_{x,y} + (e/\hbar)A_{x,y}$ where $A_{x,y}$ corresponds to the vector potential of the dressing field. To break time reversal symmetry and open the band gap at the Dirac points we should consider the case of circular polarization, choosing

$$A_x = \frac{cE_0}{\omega} G(r) \sin(\omega t), \tag{4.2}$$

$$A_y = -\frac{cE_0}{\omega} G(r) \cos(\omega t), \tag{4.3}$$

where ω and E_0 are frequency and amplitude of the dressing field, and function $G(r)$ describes its profile in the real space. To be specific, we choose the latter to be represented by a Gaussian dip,

$$G(r) = 1 - \exp\left(-\frac{r^2}{2L^2}\right) \tag{4.4}$$

where parameter L characterizes the lateral size of the intensity dip.

The Hamiltonian in Eq. 5.1 is time-dependent, but in the high frequency limit it can be reduced to a stationary effective Hamiltonian. The mathematical basis for that is provided by Floquet theory of periodically driven quantum systems [38–40, 143]. The homogeneous case of this problem has been deeply studied in the past [103], the following calculation only brings informations about the non homogeneous potential case. The main steps are as follows. The time-dependent Hamiltonian can be expressed as :

$$\hat{\mathcal{H}}(r,t) = \hat{\mathcal{H}}_0 + \hat{V}\exp(i\omega t) + \hat{V}^\dagger \exp(-i\omega t) \tag{4.5}$$

where

$$\hat{\mathcal{H}}_0(t) = \hbar v_F \left[\xi \sigma_x k_x + \sigma_y k_y\right], \tag{4.6}$$

$$\hat{V}(r) = \frac{\hbar\Omega}{2} \left(\xi\sigma_x - i\sigma_y\right) G(r). \tag{4.7}$$

and

$$\hbar\Omega = \frac{v_F e E_0}{\omega} \tag{4.8}$$

is a parameter describing the strength of electron- photon coupling which can be referred to as a characteristic Rabi energy. Since the frequency ω is assumed to be high compared to all characteristic frequencies of the system, the electron dynamics is not able to follow the fast time oscillations of the vector potential, and the effective time-independent Hamiltonian can be obtained by Floquet-Magnus expansion [26, 124, 125] in powers of ω^{-1}. Restricting ourselves to the first three terms in the infinite series we get:

$$\begin{aligned}\hat{\mathcal{H}}_{\text{eff}} \approx \hat{\mathcal{H}}_0 + \frac{\left[\hat{V}, \hat{V}^\dagger\right]}{\hbar\omega} + \frac{\left[\left[\hat{V}, \hat{\mathcal{H}}_0\right], \hat{V}^\dagger\right] + \text{H.c.}}{2(\hbar\omega)^2} \approx \\ \approx \hbar\widetilde{v}_F(r)(\xi\sigma_x k_x + \sigma_y k_y) - \xi\frac{\Delta_g(r)}{2}\sigma_z \\ + i\frac{\hbar v_F \Omega^2}{\omega^2 L^2}\left(\xi\sigma_x x + \sigma_y y\right)\exp\left(-\frac{r^2}{L^2}\right) G\left(r\right),\end{aligned} \tag{4.9}$$

In this equation $\Delta_g(r) = 2\hbar\Omega^2 G^2(r)/\omega$ is the position- dependent gap, which is a monotonously increasing function of r with $\Delta(0) = 0$ and

$$\Delta(\infty) = \frac{2\hbar\Omega^2}{\omega} = \frac{4v_F^2 e^2 I}{\hbar\epsilon_0 c\omega^3} \tag{4.10}$$

where $I = \epsilon_0 c E_0^2/2$ is the intensity of the dressing field. The corresponding term the Eq. 5.7 is responsible for the trapping of particles with energies $E < \Delta(\infty)$. The position- dependent renormalized Fermi velocity $\widetilde{v}_F(r) = v_F(1 - \Omega^2\omega^{-2}G^2(r))$. The last term in Eq. 5.7 appears due to the energy-momentum non-commutativity. It is small with respect the other terms but should be nevertheless retained in order to keep the effective Hamiltonian Hermitian.

To make the trapping most efficient, one would wish to produce deep traps with small lateral size, minimizing L and maximizing $\Delta(\infty)$. Unfortunately, these two parameters are not completely independent. Indeed, according to

Eq. 4.10, the value of the gap equal to the depth of the trap is inversely proportional to the cube of the frequency of the dressing field. Therefore, if one wants to keep the intensity I moderate one can not use very high frequencies. On the other hand, for a given frequency the lateral size of the trap can not be done arbitrary small because of the diffraction limit and its minimal size can be estimated as

$$L_{min} \approx \lambda = \frac{2\pi c}{\omega} \tag{4.11}$$

In principle, this size can be further reduced by using the methods of sub-wavelength optics, but this will need metallic patterning of the sample and consideration of this case goes beyond the scope of the present work. Our estimations show that there is an optimal range of frequencies corresponding to THz and far infrared for which the traps with a depth of about one meV with lateral size of tens of microns can be achieved for realistic values of the dressing intensities not exceeding several kW/cm^2. In Fig. 4.1(b), we have produced a combined 2D plot showing the illumination intensity and the bandgap as a function of distance from the trap center for higher clarity.

4.2. Results and discussion

To demonstrate the effectiveness of the proposed trapping scheme, we study numerically the dynamics of the electronic wavepacket initially located around $r = 0$. We use the following parameters of the dressing field; intensity $I = 330$ W/cm^2, dressing field frequency $\omega = 15$ THz, and intensity dip radius $L = 7$ μm. The width of the initial wavepacket was taken to be $d = 5$ μm so that it has energy distribution of $\hbar v_F/d \approx 0.13$ meV around the Fermi energy $E_F = 0$ meV. The initial wavepacket is composed of equal contributions from the two equivalent valleys (K and K') in the band structure of graphene. The results are shown in the Fig. 4.2. As it is clear from the panels (b)-(d), for the case of the electromagnetic dressing the electrons stay around $r = 0$ where the gap is smaller and can not

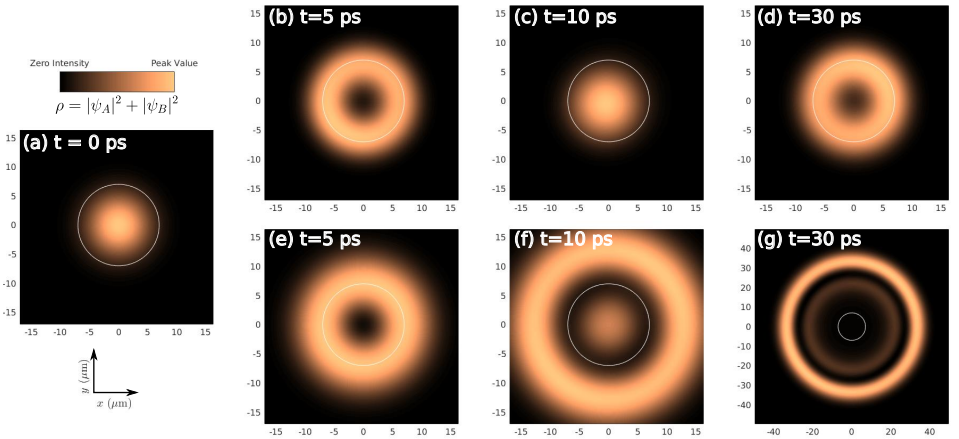

Figure 4.2 – Plots of the total electron density, $\rho = |\psi_A|^2 + |\psi_B|^2$, for several values of the evolution time indicated in each subfigure. Panel **(a)** corresponds to the initial distribution at $t = 0$. Panels **(b)-(d)** correspond to the dynamics in the presence of the optical trap. Panels **(e)-(g)** correspond to the free electron propagation (note that panel (g) includes a larger area of the system). One clearly sees that the presence of the optical trap effectively confines the electronic wavepacket which stays localized around $r = 0$ at all times.

penetrate to the region where the gap reaches its maximal value. Panels (f)-(g) correspond to the case of the freely propagaing wavepacket and are demonstrated for the reasons of comparison. Wavepacket dynamics in this case reproduces well known results studied elsewhere before [107]. We also estimated the position of the energy levels in our trapping potential as it is shown at the Table 4.1. Characteristic separation between the neighboring levels is of the order of magnitude of 0.1 meV which should be possible to observe experimentally.

Table 4.1 – The energies of the lowest confined states for the optical trap in graphene. See main text for the values of the parameters. The energy levels are found by assuming a perfect trap and imposing vanishing boundary conditions on the wavefunction at the radius of the trap.

j	$k_j(\mu\mathrm{m}^{-1})$	E_j (meV)	$E_j - E_{j-1}$ (meV)
1	0.347	0.188	
2	0.547	0.299	0.111
3	0.734	0.401	0.102
4	0.789	0.430	0.030
5	1.002	0.547	0.117

3

As discussed briefly in the introduction, the trapping mechanism is similar to the one encountered in semiconductor heterostructures. In the latter, when a wide-gap semiconductor is sandwiched between two narrow-gap semiconductors, electrons occupying the bottom of the conduction band of the middle semiconductor, are subjected to a potential barrier to the both sides and thus are unable to leave the middle semiconductor. Similarly, in our case, electrons occupying the states around the Fermi energy which lies around the neutral charge point $E = 0$ in the low-bandgap region aren't able to propagate to the region with high intensity illumination because there the bandgap is higher and there are no states to scatter into.

A simple calculation of the local Chern number [108, 109] shows that the gap opened by the electromagnetic field is topological. As a consequence, in the vicinity of the trap, as on the edge of a finite graphene monolayer, edge states may appear depending on the parameters i.e the type of edge in the case of graphene finite monolayer. Using the model presented and under some precise initial conditions, topological edge states can be observed. The precise understanding of their nature and of the necessary conditions to observe them would be a nice topic for further investigations.

4.3. Concluding remarks

In conclusion, in this article we have proposed a scheme for trapping conduction electrons in a single layer of graphene using a monochromatic

beam with a dip in the intensity. This unusual beam opens a gap everywhere on the sheet except in the dip region where electronic states are present around the Fermi energy so electrons occupying these states aren't able to leave the region. We provided numerical simulations showing effective trapping and we also discussed how an optical beam with such a profile can be constructed.

5. Optical valleytronics in gapped graphene

5.1. Introduction

The discovery of graphene, a monolayer of carbon atoms with low energy linear dispersion, and its unique electronic properties still continue to create an increasing interest of the scientific community [1, 3, 66], and initiated a large amount of studies on a new class of nanostructures, the *Dirac materials*. Graphene is characterized by the gapless energy spectrum, which makes difficult its application in modern electronic fields. Therefore many efforts have been dedicated towards the fabrication of gapped Dirac materials. The spectrum of those materials is parabolic near the band edge (located at the so-called Dirac points) but becomes linear far from it. Therefore electronic properties of such materials strongly depend on the value of the band gap and, consequently, they are suitable for potential nanoelectronic applications [68, 127, 128]. Like in bare gapless graphene, the confinement of Dirac electrons in such systems, and the wide range of potential practical applications, are compromised by their ability to perfectly transmit through arbitrary potentials barriers at normal incidence. This effect is well known for Dirac particles as the Klein paradox [129].

Valley transport in graphene has recently become a very active field of research since it is expected that the valley degree of freedom can play the same role as the electron spin in information processing [130–132]. Today this approach is referred as *valleytronics* and it has many similarities with

spintronics. In graphene like systems, the valley degree of freedom exists due to the fact that there are two inequivalent edges of the Brillouin zone in the honeycomb lattice labbelled as K and K'. Due to the large distance between those two valleys in the reciprocal space, only scatterers with a range smaller that the lattice constant can induce intervalley scattering, for that reason it is usually considered very weak and can be neglected in clean samples. Therefore, the valley index is a quantum number that can be considered as conserved for electron transport. A lot of proposals in the literature were put forward to generate valley-polarized currents by using graphene nanoribbons [132, 133], electromagnetic or optical field [134, 135] and lattice strain [136, 137].

In the present letter, we propose a way to achieve valley dependent optical trapping of Dirac electrons in gapped Dirac systems and to create a valley router. In the framework of condensed matter physics, the basis for optical trapping is provided by the possibility to locally modify the energy spectrum of the particles by strong coupling to high frequency electromagnetic field resulting in the dynamic Stark effect. Strong modifications of the transport properties in the regime of strong light-matter couplig have been recently reported for semiconductor quantum well [44, 45, 47–49], carbon nanostructures [12, 54, 59, 138–140] and topological insulators [61, 62, 112].

Particularly, it has been shown that in gapped Dirac systems strongly coupled to circularly polarized light the value of the band gap Δ_g is either increased or decreased valley dependently [141]. This modification depends on the intensity I and the frequency ω of the driving field. Therefore, this mechanism offers a reversible way to control the electronic properties of the system. Indeed, let us consider the case of a non-homogeneous intensity of the driving field i.e. a simple Gaussian shaped beam (see figure 1). In this case, the band gap is modified in the vicinity of the beam and it will be unchanged away from it. Therefore, an electron located inside the illuminated area, will not be able to escape since there is no available propagating states. This mechanism has been described before for bare graphene [142]

and is similar to the electron confinement in semiconductor heterostructures when a layer of narrow band semiconductor is sandwiched between wide gap materials with the only difference being that the band mismatch in this case is produced all optically. In gapped Dirac systems, the valley dependence of the band gap has to be taken into account, since the gap increases in one valley and decreases in the other one, the shined area will respectively be a forbidden area for low energy electrons or a trapping one. Moreover, since the energy spectrum is locally changed, electrons propagating towards the illuminated area feel it as a potential barrier, and therefore valley dependent scattering will occur. In this letter we propose and describe a system, based on this principle, which traps electrons valley dependently and filters electrons moving towards the shinned area.

5.2. Model

Let us consider an infinite single layer of graphene which lies in the plane $\mathbf{r} = (x, y)$ at $z = 0$, grown between two 3 nm thick layers of SiO_2. We locally add a circular metallic resonator with a $R = 2\ \mu m$ radius, centred at $(x, y) = 0$, the top SiO_2 layer is directly stuck below the top gold plate while on the other side a thick silicon layer is grown [see Fig 5.1 (a)]. The resonator is added in order to break through the diffraction limit and to obtain micrometer scale trap/filter in the infra-red range. This system interacts with an electromagnetic wave propagating along the z-axis. The influence of the resonator on the effective distribution of the electromagnetic field is modeled numerically. The in-plane component of the field is displayed in Fig 5.1 (b).

The frequency of the wave ω is assumed to be high enough to satisfy the condition $\omega\tau \gg 1$, where τ is a characteristic relaxation time in the system. In this case, the electromagnetic wave can not be absorbed around the Dirac points and should be considered as a pure dressing field. The low- energy Hamiltonian of the system reads:

$$\hat{\mathcal{H}}(t) = \hbar v_F \left[\xi\hat{\sigma}_x\left(k_x + \frac{eA_x}{\hbar}\right) + \hat{\sigma}_y\left(k_y + \frac{eA_y}{\hbar}\right)\right] + \frac{\Delta_g}{2}\hat{\sigma}_z \qquad (5.1)$$

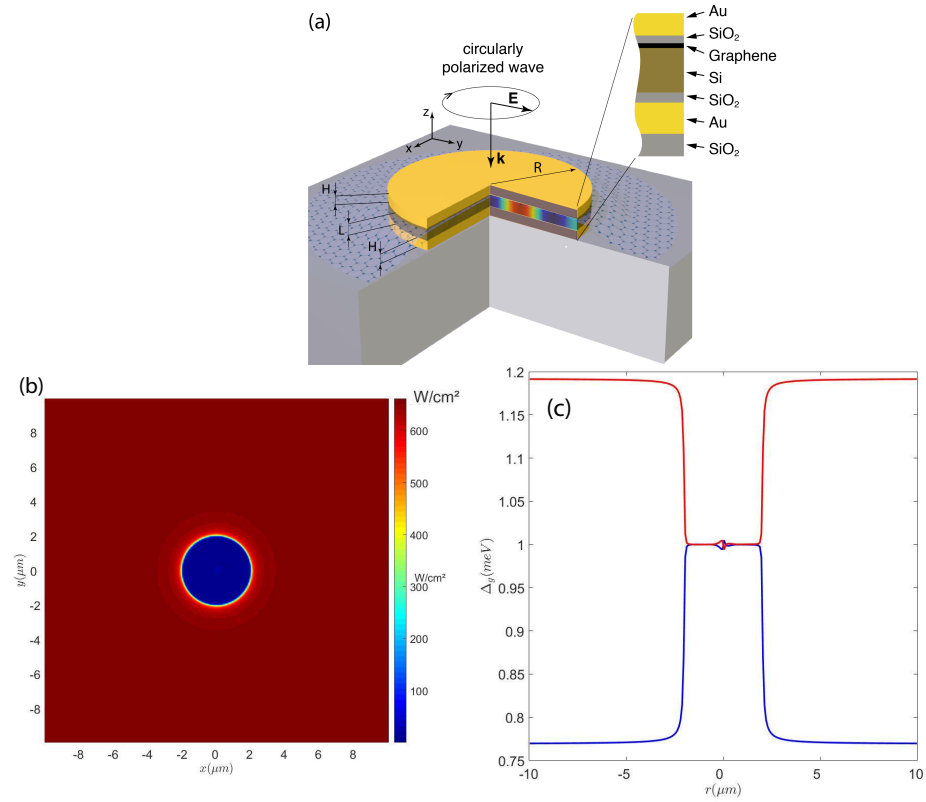

Figure 5.1 – (a) Sketch of the considered system. The presence of a micro- scale metallic resonator allows to focus high frequancy electromagnetic field at subwavelength scale (b) Spacial profile of the intensity of the field (c) Spacial dependence of the gap on the radial distance form the center of the beam in K (red) valley and K' (blue) valley.

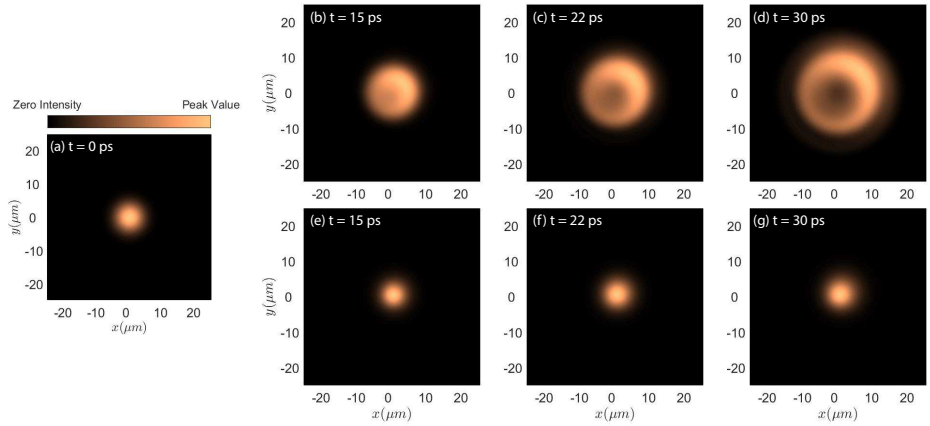

Figure 5.2 – Plots of the total electron density, $\rho = |\psi_A|^2 + |\psi_B|^2$, for several values of the evolution time indicated in each subfigure. Panel **(a)** corresponds to the initial distribution at $t = 0$. Panels **(b)-(d)** correspond to the dynamics in the K valley. Panels **(e)-(g)** correspond to the dynamics in the K' valley. One clearly sees that while electrons located in the K valley escape the trap, those located in K' valley remain confined in it.

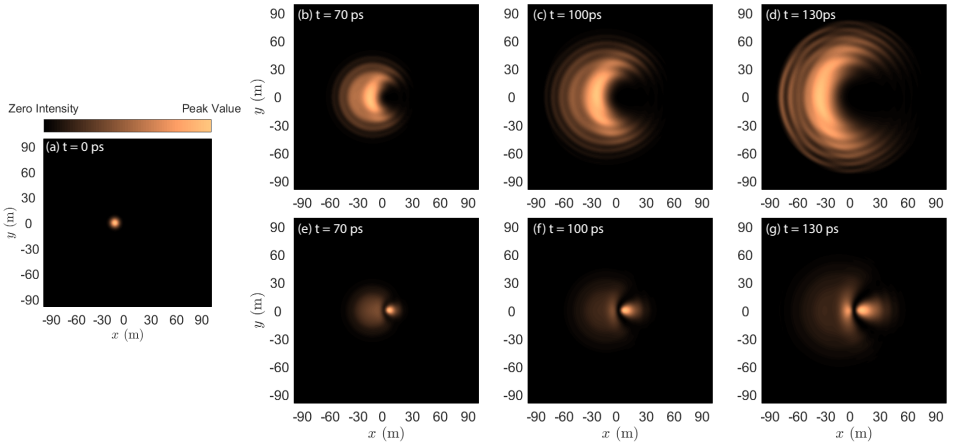

Figure 5.3 – Plots of the total electron density, $\rho = |\psi_A|^2 + |\psi_B|^2$, for several values of the evolution time indicated in each subfigure. Panel **(a)** corresponds to the initial distribution at $t = 0$. Panels **(b)-(d)** correspond to the dynamics in the K valley. Panels **(e)-(g)** correspond to the dynamics in the K' valley. One clearly sees different scattering patterns for electrons in K and K' valleys.

where v_F is the Fermi velocity, $\xi = \pm 1$ the valley index and σ_i, $i = x, y$, are the Pauli matrices. The interaction with external electromagnetic radiation is introduced via the minimal coupling substitution, $k_{x,y} \to k_{x,y} + (e/\hbar)A_{x,y}$ where $A_{x,y}$ corresponds to the vector potential of the dressing field. To break time reversal symmetry and open the band gap at the Dirac points we should consider the case of circular polarization, choosing

$$A_x = \frac{E_x(r,\theta)}{\omega}\cos(\omega t), \tag{5.2}$$

$$A_y = \frac{E_y(r,\theta)}{\omega}\sin(\omega t), \tag{5.3}$$

where ω and $E_{x,y}$ are frequency and amplitudes of the dressing field.

The Hamiltonian in Eq 5.1 is time-dependent, but in the high frequency limit it can be reduced to a stationary effective Hamiltonian. The mathematical basis for that is provided by the Floquet theory of periodically driven quantum systems [26,38,39,143]. The main steps are as follows. The time-dependent Hamiltonian can be expressed as :

$$\hat{\mathcal{H}}(r,t) = \hat{\mathcal{H}}_0 + \hat{V}\exp(i\omega t) + \hat{V}^{\dagger}\exp(-i\omega t) \tag{5.4}$$

where

$$\hat{\mathcal{H}}_0(t) = \hbar v_F(\xi\hat{\sigma}_x k_x + \hat{\sigma}_y k_y) + \frac{\Delta_g}{2}\hat{\sigma}_z, \tag{5.5}$$

$$\hat{V}(r) = \frac{e v_F}{2\omega}(\xi E_x\hat{\sigma}_x - iE_y\hat{\sigma}_y). \tag{5.6}$$

Since the frequency ω is assumed to be high compared to all characteristic frequencies of the system, the electron dynamics is not able to follow the fast time oscillations of the vector potential, and the effective time-independent Hamiltonian can be obtained by Floquet-Magnus expansion [26,27,125] in powers of ω^{-1}. Restricting ourselves to the first three terms in the infinite

series we get:

$$\hat{\mathcal{H}}_{\text{eff}} \approx \hat{\mathcal{H}}_0 + \frac{\left[\hat{V}, \hat{V}^\dagger\right]}{\hbar\omega} + \frac{\left[\left[\hat{V}, \hat{\mathcal{H}}_0\right], \hat{V}^\dagger\right] + \text{H.c.}}{2(\hbar\omega)^2}$$

Using this expression, one can find out the renormalization of the band parameters of the system [141], the modified band-gap can be expressed as:

$$\tilde{\Delta}_g = \Delta_g \left(1 - \left(\Omega_x^2 + \Omega_y^2\right)\right) - 2\xi\hbar\omega\Omega_x\Omega_y \tag{5.7}$$

where

$$\Omega_{x,y} = \frac{v_F e E_{x,y}}{\hbar\omega^2} \tag{5.8}$$

This term is responsible for the valley dependent trapping of electrons with energy below the bare gap value and for the valley dependent scattering of electrons. The position-dependent renormalized Fermi velocity $\tilde{v}_{x,y} = v_F(1-\Omega_{x,y}^2)$. One should note that since the distribution of the field is space dependent, non-commutative terms appear in the effective Hamiltonian due to the canonical commutation relation. Those terms are small with respect to the other terms but are retained in the following simulations in order to keep the effective Hamiltonian Hermitian.

It should be noted that Eq.(5.7) is derived under the condition $\hbar\omega \gg \Delta_g$. The gap in such system can be tuned in the broad range $\Delta_g = 1 - 60$ meV [70, 144]. Therefore, assuming the gap to be of meV scale, and the field to be in the far infrared range, we can easily satisfy this condition.

5.3. Results and discussion

In order to demonstrate the valley dependence of the electron dynamic and its consequences on the optical trapping of electrons in gapped Dirac systems, we first study numerically the dynamic of an electronic wave packet

initially located around $r = 0$. We use the following parameters of the dressing field; intensity $I = 300$ W/cm^2, dressing field frequency $\omega = 33$ THz. The width of the initial wavepacket is taken to be $d = 4$ μm. The initial average wave vector is null. The simulation is run for K and K' independently i.e. the electron wave packet is injected in one valley at a time. The conservation of the global intensity has been checked and is verified up to $10^{-6}\%$. The results are shown in FIG. 5.2. From this simulation one can conclude that, in the valley where the gap in the area between the metallic plates is lower than elsewhere, described by panes (b) to (d) electrons cannot find any possible state to propagate to, and therefore stay in the vicinity of $r = 0$. This mechanism has already been described in recent studies [142]. In the other valley, described by panels (e) to (g), when the gap is smaller, propagating states with not zero k vectors exist, and depending on the energy at which the electron is injected, not zero velocity can be observed. Also, this valley dependence can be optically controlled using the polarization of the field. Namely, switching form a clockwise to a counterclockwise circular polarization will switch the effect to its opposite in each valley [141].

In order to study the interaction between a propagating electron wave packet and the light induced valley and space dependent modification of the gap, it is now introduced at $x = -15\mu$m , $y = 0$ with the same characteristics as the previous study. The results are shown in Fig.5.3. From this simulation one can conclude that in both valleys, the dynamic of the propagation wave packet is strongly affected by the modification of the gap. In the K valley, described by panels (b) to (d), where the gap is decreased, part of the total intensity is transmitted and will continue to propagate to the right. The appearance of a "fan" pattern is due to the radial symmetry of the light induced effective potential. In the K' valley, the wave packet is scattered in every direction but the Ox one. Simulations with different initial energies of the wavepacket have been run, this effect subsists up to an initial energy of the packet close to the value of the modified band gap. As in the case of the valley dependent trapping, the valley can be switched by changing the

polarization.

5.4. Conclusion

In conclusion, in this work we have proposed a scheme that can both behave as a valley dependent trap for electrons and as a valley router, on a scale lower than the one usually allowed by the diffraction limit. The basis on which this results lies on is the all optical valley dependent modification of the band gap. This modification of the band parameters changes the position of the electronic propagating states and therefore electrons can be either trapped, reflected or transmitted. Numerical simulations supporting the prediction of the trap and filter behaviour of the system are provided. This findings open the routes to the all-optical manipulation of the valley transport in 2d materials with the subwavelength resolution.

Conclusions

Among the original work described in this thesis, the following has been achieved. The strong coupling of a bilayer graphene system to a dressing electromagnetic field has been shown to be a all optical tool to control the topology of the Fermi surface of bilayer graphene. Moreover using the polarization degree of freedom the field can induce the Lifshitz transition with different possible outputs for the low energy dispersion. Therefore a dressing electromagnetic field can be used as an in-situ tool to control the electronic properties of bilayer graphene bases structure.

Also, the dressing field is able to control various electronic properties of gapped Dirac material such as the band gap and the spin splitting. For instance, they can be closed all optically with the right set of frequency, polarization and intensity of the dressing field. The polarization is also in this case a degree of freedom than can be used to control the band parameters, but not only. The circular polarization brings an additional effect due to the break of the time reversal symmetry it induce, the equivalence between the valleys is broken, allowing the creation of valleytronic systems based on this phenomena. As a consequence, a gapped Dirac system strongly coupled to a dressing electromagnetic field is a good candidate for the creation of electronic, spintronic and valleytronic devices.

Using the principle just described, a device allowing to trap electrons in a Dirac material can be designed. Using a monochromatic beam with a dip in the intensity, the gap can be engineered space dependently. The gap is therefore opened everywhere besides in the dip region. Electrons in this area

will therefore be in states not present anywhere else and will therefore not be able to leave the trap. Using this principle, the idea has been extended to gapped Dirac material, where as described before the valley symmetry can be broken. Therefore since the band gap can be, on the same area, open in one valley and closed in the other one, the electrons will be trapped depending on their valley index. This phenomena gives access to the design of many all optical valleytronics devices .

List of publications

Relevant to this thesis

- O.V. Kibis, K. Dini, I.V. Iorsh, I.A. Shelykh, "All-optical band engineering of gapped Dirac materials", Phys. Rev. B **95**, 125401 (2017).

- I.V. Iorsh, K. Dini, O.V. Kibis, I.A. Shelykh, "Optically induced Lifshitz transition in bilayer graphene" Phys. Rev. B **96**, 155432 (2017).

- S. Morina, K. Dini, I.V. Iorsh, I.A Shelykh, "Optical trapping of electrons in graphene" ACS Photonics **5** , 1171-1175 (2018).

- K Dini, IV Iorsh, A Bogdanov, IA Shelykh, "Optical valleytronics in gapped graphene" arXiv preprint arXiv:1807.01228.

Other Publication

- O.V. Kibis, S. Morina, K. Dini, I.A. Shelykh, "Magnetoelectronic properties of graphene dressed by a high-frequency field", Phys. Rev. B **93**, 115420 (2016).

- K. Dini, O.V. Kibis, I.A. Shelykh, "Magnetic properties of a two-dimensional electron gas strongly coupled to light", Phys. Rev. B **93**, 235411 (2016).

- H. Sigurdsson, O. Kyriienko, K. Dini, T.C.H. Liew, "Polaritonic networks as classical analog simulators", arXiv preprint arXiv:1804.02446 (2018).

Bibliography

[1] A.K. Geim, K.S. Novoselov, "The rise of graphene". *Nature Mater.* **6**, 183–191 (2007).

[2] O. Klein, "Die Reflexion von Elektronen an einem Potentialsprung nach der relativistischen Dynamik von Dirac". Zeitschrift für Physik. **53** (3–4): 157 (1929).

[3] A. H. Castro Neto, F. Guinea, N. M. R. Peres, K. S. Novoselov, and A. K. Geim, "The electronic properties of graphene", Rev. Mod. Phys. **81** (2009).

[4] S. Das Sarma, S. Adam, E. H. Hwang, and E. Rossi, Electronic transport in two-dimensional graphene. Rev. Mod. Phys. **83** (2011).

[5] P. E. Trevisanutto, C. Giorgetti, L. Reining, M. Ladisa, and V. Olevano, Ab Initio GW Many-Body Effects in Graphene, Phys. Rev. Lett. **101**, 226405 (2008).

[6] M. Calandra and F. Mauri, Electron-phonon coupling and electron self-energy in electron-doped graphene: Calculation of angular-resolved photoemission spectra, Phys. Rev. B **76**, 205411 (2007).

[7] G. Giovannetti, P. A. Khomyakov, G. Brocks, P. J. Kelly, and J. van den Brink, "Substrate-induced band gap in graphene on hexagonal boron nitride: Ab initio density functional calculations" Phys. Rev. B **76**, 073103 (2007).

[8] M. Kindermann, B. Uchoa, D. L. Miller, "Zero-energy modes and gate-tunable gap in graphene on hexagonal boron nitride", Phys. Rev. B **86**, 115415 (2012).

[9] G. Cocco, E. Cadelano and L. Colombo, "Gap opening in graphene by shear strain", Phys. Rev. B **81**, 241412R (2010).

[10] I. I. Naumov and A. M. Bratkovsky, "Gap opening in graphene by simple periodic inhomogeneous strain", Phys. Rev. B **84**, 245444 (2011).

[11] O. V. Kibis, "Metal-insulator transition in graphene induced by circularly polarized photons" Phys. Rev. B **81**, 165433 (2010).

[12] K. Kristinsson, O. V. Kibis, S. Morina, I. A. Shelykh, "Control of electronic transport in graphene by electromagnetic dressing", Sci. Rep. **6**, 20082 (2016).

[13] P. Allain and J. N. Fuchs, "Klein tunneling in graphene: optics with massless electrons", Eur. Phys. J. B. **83**, 301-317 (2011).

[14] E. McCann and M. Koshino, "The electronic properties of bilayer graphene", Rep. Prog. Phys. **76**, 056503 (2013)

[15] E. McCann and V. I. Fal'ko, "Landau-Level Degeneracy and Quantum Hall Effect in a Graphite Bilayer", Phys. Rev. Lett. **96**, 086805 (2006).

[16] K. Yan, H. Peng, Y. Zhou, H. Li, and Z. Liu, Formation of Bilayer Bernal Graphene: "Layer-by-Layer Epitaxy via Chemical Vapor Deposition", Nano Lett. 11, 3, 1106-1110.

[17] J. M. B. Lopes dos Santos, N. M. R. Peres, and A. H. Castro Neto, "Graphene Bilayer with a Twist: Electronic Structure", Phys. Rev. Lett. **99**, 256802 (2007).

[18] S. Predin, P. Wenk, and J. Schliemann, "Trigonal warping in bilayer graphene: Energy versus entanglement spectrum", Phys. Rev. B **93**, 115106 (2016).

[19] I.S. Grant, W.R. Phillips, Electromagnetism (2nd Edition), Manchester Physics, John Wiley & Sons, 2008.

[20] Y.B. Zeldovich, "The Quasienergy of a Quantum-mechanical System Subjected to a Periodic Action", Sov. Phys. JETP **24**, 1006 (1967)

[21] J.H. Shirley, "Solution of the Schrödinger Equation with a Hamiltonian Periodic in Time", Phys. Rev. **138B**,(1965).

[22] H. Sambe, "Steady States and Quasienergies of a Quantum-Mechanical System in an Oscillating Field", Phys. Rev. A **7**, 2203 (1973).

[23] W.R. Salzman, "Quantum mechanics of systems periodic in time", Phys. Rev. A **10**, 461 (1974).

[24] F. Gesztesy and H. Mitter, "A note on quasi-periodic states", J. Phys. A **14**, L79 (1981).

[25] T. P. Grozdanov and M. J. Raković, "Quantum system driven by rapidly varying periodic perturbation", Phys. Rev. A **38**, 1739 (1988).

[26] N. Goldman and J. Dalibard, "Periodically Driven Quantum Systems: Effective Hamiltonians and Engineered Gauge Fields" Phys. Rev. X **4**, 031027 (2014).

[27] S. Rahav, I. Gilary and S. Fishman, "Effective Hamiltonians for periodically driven systems", Phys. Rev. A **68**, 013820 (2003).

[28] Schroedinger E 1930 Sitzungsber. Preuss. Akad. Wiss. Phys. Math. Kl. **24** 418.

[29] W. Zawadzki, in Optical Properties of Solids, edited by E. D. Haidemenakis (Gordon and Breach, New York, 1970à, p. 179.

[30] W. Zawadzki, in High Magnetic Fields in the Physics of Semiconductors II, edited by G. Landwehr and W. Ossau World Scientific, Singapore, 1997, p. 755.

[31] J. Schliemann, D. Loss, and R. M. Westervelt, "Zitterbewegung of Electronic Wave Packets in III-V Zinc-Blende Semiconductor Quantum Wells", Phys. Rev. Lett. **94**, 206801 (2005).

[32] J. Schliemann, D. Loss, and R. M. Westervelt, "Zitterbewegung of electrons and holes in III-V semiconductor quantum wells", Phys. Rev. B 73, 085323 2006.

[33] M. I. Katsnelson, "Zitterbewegung, chirality, and minimal conductivity in graphene", Eur. Phys. J. B **51**, 157-160 (2006)

[34] J. Cserti and G. David, "Unified description of Zitterbewegung for spintronic, graphene, and superconducting systems", Phys. Rev. B **74**, 172305 (2006).

[35] J.A. Lock, "The Zitterbewegung Of A Free Localized Dirac Particle", Am.J.Phys. **47** (1979) 797-802.

[36] O. V. Kibis, How to suppress the backscattering of conduction electrons?, EPL **107**, 5 (2014).

[37] Zheng Liu, Kazu Suenaga, Peter J. F. Harris, and Sumio Iijima, "Open and Closed Edges of Graphene Layers", Phys. Rev. Lett. **102**, 015501 (2009).

[38] P. Hänngi, Driven quantum systems, in Quantum Transport and Dissipation edited by T. Dittrich, P. Hänggi, G.-L. Ingold, B. Kramer, G. Schön, and W. Zwerger (Wiley, Weinheim, 1998).

[39] S. Kohler, J. Lehmann, P. Hänggi, Driven quantum transport on the nanoscale, Phys. Rep. **406**, 379 (2005).

[40] M. Holthaus, "Floquet engineering with quasienergy bands of periodically driven optical lattices", J. Phys. B **49**, 013001 (2016).

[41] F. Meinert, M.J. Mark, K. Lauber, A.J. Daley, and H.-C. Nägerl, Floquet Engineering of Correlated Tunneling in the Bose-Hubbard Model with Ultracold Atoms, Phys. Rev. Lett. **116**, 205301 (2016).

[42] M. O. Scully and M. S. Zubairy, Quantum Optics (Cambridge University Press, Cambridge, 2001).

[43] C. Cohen-Tannoudji, J. Dupont-Roc, and G. Grynberg, Atom- Photon Interactions: Basic Processes and Applications (Wiley, Weinheim, 2004).

[44] M. Wagner, et al., Observation of the intraexciton Autler-Townes effect in GaAs/AlGaAs semiconductor quantum wells, Phys. Rev. Lett. **105**, 167401 (2010).

[45] M. Teich, M. Wagner, H. Schneider, and M. Helm, "Semiconductor

quantum well excitons in strong, narrowband terahertz fields", New J. Phys. **15**, 065007 (2013).

[46] O. V. Kibis, "How to supress the backscattering of conduction electrons?", Europhys. Lett. **107**, 57003 (2014).

[47] S. Morina, O. V. Kibis, A. A. Pervishko, and I. A. Shelykh, "Transport properties of a two-dimensional electron gas dressed by light", Phys. Rev. B **91**, 155312 (2015).

[48] A. A. Pervishko, O. V. Kibis, S. Morina, I. A. Shelykh, "Control of spin dynamics in a two-dimensional electron gas by electromagnetic dressing", Phys. Rev. B **92**, 205403 (2015).

[49] K. Dini, O. V. Kibis, I. A. Shelykh, Magnetic properties of a two-dimensional electron gas strongly coupled to light, Phys. Rev. B **93**, 235411 (2016).

[50] O. V. Kibis, O. Kyriienko, I. A. Shelykh, "Persistent current induced by vacuum fluctuations in a quantum ring", Phys. Rev. B **87**, 245437 (2013).

[51] H. Sigurdsson, O. V. Kibis, I. A. Shelykh, Optically induced Aharonov-Bohm effect in mesoscopic rings, Phys. Rev. B **90**, 235413 (2014).

[52] F. K. Joibari, Ya. M. Blanter, G. E. W. Bauer, "Light-induced spin polarizations in quantum rings", Phys. Rev. B **90**, 155301 (2014).

[53] K. L. Koshelev, V. Yu. Kachorovskii, M. Titov, "Resonant inverse Faraday effect in nanorings", Phys. Rev. B **92**, 235426 (2015).

[54] T. Oka, H. Aoki, Photovoltaic Hall effect in graphene, Phys. Rev. B **79**, 081406 (2009).

[55] O. V. Kibis, O. Kyriienko, I. A. Shelykh, Band gap in graphene induced by vacuum fluctuations, Phys. Rev. B **84**, 195413 (2011).

[56] S. V. Syzranov, Ya. I. Rodionov, K. I. Kugel, F. Nori, "Strongly anisotropic Dirac quasiparticles in irradiated graphene", Phys. Rev. B **88**, 241112 (2013).

[57] P. M. Perez-Piskunow, G. Usaj, C. A. Balseiro, L. E. F. Foa Torres, Floquet chiral edge states in graphene, Phys. Rev. B **89**, 121401(R) (2014).

[58] M. M. Glazov, S. D. Ganichev, "High frequency electric field induced noinlinear effects in graphene", Phys. Rep. **535**, 101 (2014).

[59] O. V. Kibis, S. Morina, K. Dini, I. A. Shelykh, "Magnetoelectronic properties of graphene dressed by a high-frequency field", Phys. Rev. B **93**, 115420 (2016).

[60] M. Ezawa, Photoinduced Topological Phase Transition and a Single Dirac-Cone State in Silicene, Phys. Rev. Lett. **110**, 026603 (2013).

[61] G. Usaj, P. M. Perez-Piskunow, L. E. F. Foa Torres, C. A. Balseiro, Irradiated graphene as a tunable Floquet topological insulator, Phys. Rev. B **90**, 115423 (2014).

[62] L. E. F. Foa Torres, P. M. Perez-Piskunow, C. A. Balseiro, G. Usaj, "Multiterminal Conductance of a Floquet Topological Insulator", Phys. Rev. Lett. **113**, 266801 (2014).

[63] H. L. Calvo, L. E. F. Foa Torres, P. M. Perez-Piskunow, C. A. Balseiro, G. Usaj, "Floquet interface states in illuminated three-dimensional topological insulators", Phys. Rev. B **91**, 241404(R) (2015).

[64] T. Mikami, S. Kitamura, K. Yasuda, N. Tsuji, T. Oka, H. Aoki, Brillouin-Wigner theory for high-frequency expansion in periodically driven systems: Application to Floquet topological insulators, Phys. Rev. B **93**, 144307 (2016).

[65] K. S. Novoselov, et al., "Electric field effect in atomically thin carbon films", Science **306**, 666 2014.

[66] S. Das Sarma, S. Adam, E. H. Hwang, E. Rossi, "Electronic transport in two-dimensional graphene", Rev. Mod. Phys. **83** 407 (2011).

[67] A. Ferrari, et al. Science and technology roadmap for graphene, related two-dimensional crystals, and hybrid systems, Nanoscale **7**, 4598 (2014).

[68] Yu. D. Lensky, J. Song, P. Samutpraphoot, L. S. Levitov, "Topological Valley Currents in Gapped Dirac Materials", Phys. Rev. Lett. **114**, 256601 (2015).

[69] K. S. Novoselov, A. Mishchenko, A. Carvalho, A. H. Castro Neto, "2D materials and Van der Waals heterostructures", Science**353**, 9439 (2016).

[70] B. Sachs, T. O. Wehling, M. I. Katsnelson, A. I. Lichtenstein, "Adhesion and electronic structure of graphene on hexagonal boron nitride substrates", Phys. Rev. B **84**, 195414 (2011).

[71] J. Jung, A. M. DaSilva, A. H. MacDonald, S. Adam, "Origin of band gaps in graphene on hexagonal boron nitride", Nature Commun. **6**, 6308 (2014).

[72] Q. H. Wang, K. Kalantar-Zadeh, A. Kis, J. N. Coleman, M. S. Strano, "Electronics and optoelectronics of twodimensional transition metal dichalcogenides", Nature Nanotechnol. **7** 699 (2012).

[73] S. Z. Butler, et. al., "Progress, challenges, and opportunities in two-dimensional materials beyond graphene", ACS Nano **7**, 2898 (2013).

[74] K. Kosmider, J. Gonzalez, A. Fernandez-Rossier," Large spin splitting in the conduction band of transition metal dichalcogenide monolayers", Phys. Rev B **88**, 245436 (2013).

[75] A. Kormányos, et. al., "K·p theory for two-dimensional transition metal dichalcogenide semiconductors", 2D Mater. **2**, 022001 (2015).

[76] K. Mak, K. McGill, J. Park, P. McEuen, "The valley Hall effect in MoS_2 transistors", Science **344**, 1489 (2014).

[77] P. Rakyta, A. Kormányos, J. Cserti," Trigonal warping and anisotropic band splitting in monolayer graphene due to Rashba spin-orbit coupling", Phys. Rev. B **82**, 113405 (2010).

[78] L. Chirolli, M. Polini, V. Giovannetti, A. H. MacDonald, DrudeWeight, "Cyclotron Resonance, and the Dicke Model of Graphene Cavity QED", Phys. Rev. Lett. **109**, 267404 (2012).

[79] F. M. D. Pellegrino, L. Chirolli, R. Fazio, V. Giovannetti, M. Polini, "Theory of integer quantum Hall polaritons in graphene", Phys. Rev. B **89**, 165406 (2014).

[80] G. Bir, E. Pikus, "Symmetry and Strain-induced Effects in Semiconductors" (New York, Wiley, 1974).

[81] E. J. Sie, J. W. McIver, Y.-H. Lee, L. Fu, J. Kong, N. Gedik, "Valley-selective optical Stark effect in monolayer WS_2", Nature Mater. **14**, 290 (2015).

[82] I. I. Ryzhov, et al., "Spin noise explores local magnetic fields in a semiconductor", Sci. Rep. **6**, 21062 (2016).

[83] P. S. Pershan, J. P. Van Der Ziel, L. D. Malmstrom, "Theoretical discussion of the inverse Faraday effect, Raman scattering, and related phenomena", Phys. Rev. **143**, 574 (1966).

[84] K. He, et al., "Tightly bound excitons in monolayer WSe_2", Phys. Rev. Lett. **113**, 026803 (2014).

[85] A. Chernikov, et al., "Exciton binding energy and nonhydrogenic rydberg series in monolayer WS_2", Phys. Rev. Lett. **113**, 076802 (2014).

[86] M. Joffre, D. Hulin, A. Migus, A. Antonetti, "Dynamics of the Optical Stark Effect in Semiconductors", J. Mod. Optics **35** 1951 (1988).

[87] M. Joffre, et al., "Coherent effects in pump-probe spectroscopy of excitons", Optics Lett. **13**, 276 (1988).

[88] S. G. Lee, et al.," Femtosecond excitonic bleaching recovery in the optical Stark effect of $GaAs/Al_xGa_{1-x}As$ multiple quantum wells and directional couplers", Phys. Rev. B **43** 1719 (1991).

[89] Dombey, N.; Calogeracos, A. Seventy years of the Klein paradox. *Phys. Rep.* **1999**, *315* , 41–58.

[90] Withers,F.; Dubois, M.; Savchenko, A.K.; Electron properties of fluorinated single-layer graphene transistors. *Phys. Rev. B* **2010**, *82*, 073403.

[91] Balog R.; & al. Bandgap opening in graphene induced by patterned hydrogen adsorption. *Nat. Mater.* **2010**, *9*, 315–319.

[92] Brey L.; Fertig, H.A. Electronic states of graphene nanoribbons studied with the Dirac equation. *Phys. Rev. B* **2006**,*73*, 235411.

[93] Ni, Z.H.; Yu, T.; Lu, Y.H.; Wang, Y.Y.;Feng,Y.P.; Shen, Z.X. Uniaxial Strain on Graphene: Raman Spectroscopy Study and Band-Gap Opening. *ACS Nano* **2008**, *2* 2301.

[94] Cocco, G.; Cadelano, E.; Colombo, L. Gap opening in graphene by shear strain. *Phys. Rev. B* **2010**, *81*, 241412(R).

[95] Morsch, O.; Oberthaler, M. Dynamics of Bose-Einstein condensates in optical lattices. *Rev. Mod. Phys.* **2006**, *78*, 179.

[96] Dholakia, K.; Zemanek, P. Colloquium: Gripped by light: Optical binding. *Rev. Mod. Phys.* **2010**, *82*, 1767.

[97] Marago, O.M.; Jones P.H.; Gucciardi, P.G.; Volpe, G.; Ferrari, A.C. Optical trapping and manipulation of nanostructures. *Nat. Nanotechnol.* **2013**, *8*, 807–819.

[98] Teich, M.; Wagner, M.; Schneider, H.; Helm M. Semiconductor quantum well excitons in strong, narrowband terahertz fields *New J. Phys.* **2013**, *15* 065007.

[99] Vega Monroy, R.; Salazar Cohen, G. Photon-Induced Quantum Oscillations of the Terahertz Conductivity in Graphene. *Nano Letters* **2016**,*16*, 6797–6801.

[100] Kibis, O.V.; Dini, K.; Iorsh, I.V.; Shelykh, I.A. All-optical band engineering of gapped Dirac materials. *Phys. Rev. B* **2017**, *95*, 125401.

[101] Iorsh, I.V.; Dini, K.; Kibis, O.V.; Shelykh, I.A. Optically induced Lifshitz transition in bilayer graphene. *Phys. Rev. B* **2017**, *96*, 155432.

[102] Iurov, A.; Gumbs, G.; Roslyak, O.; Huang, D. Photon dressed electronic states in topological insulators: tunneling and conductance. *J. Phys.: Condens. Matter* **2013**, *25*, 135502.

[103] Oka, T.; Aoki, H. Photovoltaic Hall effect in graphene. *Phys. Rev. B* **2009**, *79*, 081406(R) .

[104] Kibis, O.V. Metal-insulator transition in graphene induced by circularly polarized photons. *Phys. Rev. B* **2010**, *81*, 165433.

[105] Usaj, G.; Perez-Piskunow, P.M.; Foa Torres, L.E.F.; Balseiro, C.A. Irradiated graphene as a tunable Floquet topological insulator. *Phys. Rev. B.* **2014**, *90*, 115423.

[106] Bukov, M.; D'Alessio, L.; Polkovnikov, A. Universal High-Frequency Behavior of Periodically Driven Systems: from Dynamical Stabilization to Floquet Engineering. *Adv. Phys.* **2015**, *64*; 139–226.

[107] Maksimova, G.M.; Demikhovskii, V.Ya.; Frolova, E.V. Wave packet dynamics in a monolayer graphene. *Phys. Rev. B* **2008**, *78*, 235321.

[108] Kitagawa, T.; Oka, T.; Brataas, A.; Fu, L.; Demler, E. Transport properties of nonequilibrium systems under the application of light: Photoinduced quantum Hall insulators without Landau levels. *Phys. Rev. B* **2011**, *84*, 235108.

[109] Xiao, D.; Chang, M.; Niu, Q. Berry phase effects on electronic properties. *Rev. Mod. Phys.* **2010**, *82*, 1959.

[110] M. Bukov, L. D'Alessio, and A. Polkovnikov, Universal High-Frequency Behavior of Periodically Driven Systems: from Dynamical Stabilization to Floquet Engineering, Adv. Phys. **64**, 139–226 (2015).

[111] O. V. Kibis, K. Dini, I. V. Iorsh, and I. A. Shelykh, All-optical band engineering of gapped Dirac materials, Phys. Rev. B **95**, 125401 (2017).

[112] D. Yudin, O. V. Kibis, and I. A. Shelykh, "Optically tunable spin transport on the surface of a topological insulator", New J. Phys. **18**, 103014 (2016).

[113] E. McCann and M. Koshino, The electronic properties of bilayer graphene, Rep. Prog. Phys. **76**, 056503 (2013).

[114] C. J. Tabert, E. J. Nicol, "Dynamical conductivity of AA-stacked bilayer graphene", Phys. Rev. B **86**, 075439 (2012).

[115] A. Varlet, D. Bischoff, P. Simonet, K. Watanabe, T. Taniguchi, T. Ihn, K. Ensslin, M. Mucha-Kruczyński, and V.I. Fal'ko, Anomalous

Sequence of Quantum Hall Liquids Revealing a Tunable Lifshitz Transition in Bilayer Graphene, Phys. Rev. Lett. **113**, 116602 (2014).

[116] A. Varlet, M. Mucha-Kruczyński, D. Bischoff, P. Simonet, T. Taniguchi, K. Watanabe, V. Fal'ko, T. Ihn, and K. Ensslin, Tunable Fermi surface topology and Lifshitz transition in bilayer graphene, Synthetic Metals **210**, 19-31 (2015).

[117] A. Shtyk, G. Goldstein, and C. Chamon, Electrons at the monkey saddle: A multicritical Lifshitz point, Phys. Rev. B **95**, 035137 (2017).

[118] C. Dutreix, E. A. Stepanov, and M. I. Katsnelson, "Laser-induced topological transitions in phosphorene with inversion symmetry", Phys. Rev. B **93**, 241404(R) (2016).

[119] D. S. L. Abergel and T. Chakraborty, Generation of valley polarized current in bilayer graphene, Appl. Phys. Lett. **95**, 062107 (2009).

[120] D. S. L. Abergel and T. Chakraborty, Irradiated bilayer graphene, Nanotechnology **22**, 015203 (2011).

[121] E. Suarez Morell, and L. E. F. Foa Torres, Radiation effects on the electronic properties of bilayer graphene, Phys. Rev. B **86**, 125449 (2012).

[122] W.S. Cheung and K.S. Chan, Creation of Quasi-Dirac Points in the Floquet Band Structure of Bilayer Graphene, J. Phys.: Condens. Matter **29**, 215503 (2017).

[123] G. P. Mikitik and Yu. V. Sharlai, Electron energy spectrum and the Berry phase in a graphite bilayer, Phys. Rev. B **77**, 113407 (2008).

[124] F. Casas, J. A. Oteo, and J. Ros, "Floquet theory: exponential perturbative treatment", J. Phys. A **34**, 16 (2001).

[125] A. Eckardt and E. Anisimovas, "High-frequency approximation for periodically driven quantum systems from a Floquet-space perspective" , New J. Phys. **17**, 093039 (2015).

[126] M. I. Amanti, M. Fischer1, G. Scalari, M. Beck, and J. Faist, "Low-divergence single-mode terahertz quantum cascade laser", Nat. Photonics **3**, 586–590 (2009).

[127] M. J. Zhu, A. V. Kretinin, M. D. Thompson, D. A. Bandurin, S. Hu, G. L. Yu, J. Birkbeck, A. Mishchenko, I. J. Vera-Marun, K. Watanabe, T. Taniguchi, M. Polini, J. R. Prance, K. S. Novoselov, A. K. Geim and M. Ben Shalom, Nature Communications **8**, 14552 (2017).

[128] A. Kundu, H.A. and B. Seradjeh, "Floquet-Engineered Valleytronics in Dirac Systems", Phys. Rev. Lett. **116**, 016802 (2016).

[129] M. I. Katsnelson, K. S. Novoselov and A. K. Geim, Nature Physics **2**, 620–625 (2006).

[130] D. Pesin and A. H. MacDonald, Nature Materials **11**, 409–416 (2012).

[131] J. J. Wang, S. Liu, J. Wang and J. Liu, Sci. Rep. **7**, 10236 (2017).

[132] A. Rycerz, J. Tworzydlo and C. W. J. Beenakker, Nature Physics **3**, 172–175 (2007).

[133] A. R. Akhmerov, J. H. Bardarson, A. Rycerz and C. W. J. Beenakker, Phys. Rev. B **77**, 205416 (2008).

[134] L. E. Golub, S. A. Tarasenko, M. V. Entin and L. I. Magarill, Phys. Rev. B **84**, 195408 (2011).

[135] H. Zeng, J. Dai, W. Yao, D. Xiao and X. Cui, Nat. Nanotechnol. **7**, 490 (2012).

[136] Q. Wu, Z. Liu, A. Chen, X. Xiao and Z. Liu, Sci. Rep **6**, 21590 (2016).

[137] T. Fujita, M. B. A. Jalil1, and S. G. Tan, Appl. Phys. Lett. **97**, 043508 (2010).

[138] R. Vega Monroy and G. Salazar Cohen, Nano Lett. **16**, 6797–6801 (2016).

[139] I. V. Iorsh, K. Dini, O. V. Kibis and I. A. Shelykh, Phys. Rev. B **96**, 155432 (2017).

[140] V. Dal Lago, E. Suárez Morell and L. E. F. Foa Torres, Phys. Rev. B **96**, 235409 (2017).

[141] O. V. Kibis, K. Dini, I. V. Iorsh and I. A. Shelykh, Phys. Rev. B **95**, 125401 (2017).

[142] S Morina, K Dini, IV Iorsh and IA Shelykh arXiv preprint arXiv:1711.07313 (2017).

[143] M. Bukov, L. D'Alessio, A. Polkovnikov, Adv. Phys. **64**, 139–226 (2015).

[144] J. Jung, A. M. DaSilva, A. H. MacDonald and S. Adam Nat. Com. **6**, Article number: 6308 (2015).